

Evaluating Acoustic Technologies to Monitor Aquatic Organisms at Renewable Energy Sites

Final Report



U.S. Department of the Interior
Bureau of Ocean Energy Management
Headquarters

Evaluating Acoustic Technologies to Monitor Aquatic Organisms at Renewable Energy Sites

Final Report

Authors

John K. Horne
Dale A. Jacques
Sandra L. Parker-Stetter
Hannah L. Linder
Jennifer M. Nomura

June 2013

Prepared under BOEM Contract
M10PC00093 by
University of Washington
School of Aquatic and Fishery Sciences
College of the Environment
Seattle, Washington 98105

Published by

U.S. Department of the Interior
Bureau of Ocean Energy Management
Headquarters

Cooperative Agreement
School of Aquatic and Fishery Sciences
University of Washington

DISCLAIMER

This report has been reviewed by the Bureau of Ocean Energy Management and approved for publication. Approval does not signify that the contents necessarily reflect the views and policies of the Management, nor does mention of trade names or commercial products constitute endorsement or recommendation for use.

REPORT AVAILABILITY

Copies of this report may be obtained from the Environmental Studies Program Information System (ESPIS) at

http://www.data.boem.gov/homepg/data_center/other/espis/espismaster.asp?appid=1

CITATION

Suggested Citation:

Horne, J. K., D. A. Jacques, S. L. Parker-Stetter, H. L. Linder, and J. M. Nomura. 2014. Evaluating Acoustic Technologies to Monitor Aquatic Organisms at Renewable Energy Sites. U.S. Dept. of the Interior, Bureau of Ocean Energy Management. BOEM 2014-057

ACKNOWLEDGEMENTS

The coauthors thank the Captains and crews of the University of Washington's R/V Centennial from Friday Harbor Laboratories for their navigational efforts and humor during the field sampling program. Personnel from vendor partners at BioSonics, Sound Metrics, and Teledyne Reson are thanked for adapting acoustic instruments for autonomous operation on very short notice, and for discussions related to sampling and survey design. Jeff Condiotty from Konsberg Fisheries is thanked for his loan of the net monitoring system and demonstration of the multibeam sonar. Jim Thomson (UW-Applied Physics Laboratory) and Brian Polagye (UW-Mechanical Engineering) were instrumental in the design, deployment, and retrieval of autonomous acoustic instruments packages. David Barbee (UW-School of Aquatic and Fishery Sciences) is thanked for assistance in integrating vessel software, field sampling, and data processing. Kurt Fresh and Anna Kagley (NOAA Northwest Fisheries Science Center) are thanked for biological sampling during the mobile surveys. Adam Ü is acknowledged for his capable work as the marine mammal and seabird observer.

ABSTRACT

Marine renewable energy (MRE) devices potentially impact dynamics of aquatic organisms including macroinvertebrates, fish, seabirds, and marine mammals. Understanding potential impacts of MRE technologies on biological communities requires knowledge of species-specific spatial and temporal density distributions. Acoustic technologies capable of providing images and data for baseline characterizations and operational monitoring are commercially available but configurations and system integration for MRE applications have not been established nor evaluated. Deployment, operation, and retrieval of autonomous acoustic instrument packages are also complicated by extreme water flows at MRE sites. At a proposed tidal energy site in Puget Sound, Washington, USA, an echosounder, multibeam sonar, acoustic camera, and an Acoustic Doppler Current Profiler (ADCP) were deployed on bottom during May and June, 2011. To provide a spatial characterization of the biological community at the site, a vessel-mounted echosounder and pelagic trawl were used to map fish and macrozooplankton densities during day, dusk, and night surveys. Marine mammals and seabirds were identified and counted during surveys. The primary objective of the project was to compare sampling capabilities of surface- and bottom-deployed acoustic instruments.

Our field work confirmed that autonomous instrument sampling is more constrained by power than by data storage; that direct sampling in high flow environments is a challenge; and that limited direct samples constrain acoustic target classification. A suite of metrics successfully characterized vertical distributions of aquatic organisms in the water column. Results showed that surface and bottom deployed echosounders detected horizontal and vertical density changes that were correlated with environmental covariates. Metric values from the acoustic camera and ADCP data were not as sensitive to changes in density.

Current acoustic technologies can be configured and used to characterize aquatic organism distributions at MRE sites. Integrated acoustic instrument systems that include target tracking and impact warning do not exist in autonomous or cabled configurations. Development of algorithms to translate temporal to spatial variance and to scale observed effects from pilot to commercial site domains is needed to complete the ability to monitor change and to detect impacts on biological communities for MRE site monitoring.

TABLE OF CONTENTS

TABLE OF CONTENTS	v
LIST OF TABLES	vii
LIST OF ABBREVIATIONS AND ACRONYMS	viii
1. INTRODUCTION	1
2. METHODS	2
2.1. PROJECT ORGANIZATION	2
2.2. SAMPLING DESIGN	3
2.2.1 <i>Acoustic Instrumentation</i>	4
2.2.2 <i>Mobile Sampling</i>	7
2.3. STATIONARY SAMPLING	9
2.3.1 <i>Deployment and Recovery</i>	9
2.3.2 <i>Instrument Specifications</i>	11
2.4. DATA PROCESSING	13
2.4.1 <i>Data Pre-Processing</i>	13
2.5. DATA ANALYSIS	15
2.5.1 <i>Trawl Catches</i>	15
2.5.2 <i>Water Flow Properties</i>	15
2.5.3 <i>Data Visualization</i>	15
2.5.4 <i>Horizontal binning</i>	16
2.5.5 <i>Vertical Binning</i>	16
2.5.6 <i>Echometrics</i>	17
2.5.7 <i>Characterizing Backscatter Variability</i>	17
2.5.8 <i>Acoustic Technology Comparisons</i>	18
3. RESULTS	19
3.1. TRAWL CATCHES.....	19

3.1.1. <i>North-South Grid</i>	19
3.1.2. <i>Sampling Months</i>	21
3.1.3. <i>Diel Sampling</i>	22
3.1.4. <i>Fish Length Frequency</i>	23
3.2. WATER FLOW PROPERTIES	24
3.3. ACOUSTIC DATA VISUALIZATION.....	24
3.3.1. <i>Acoustic Backscatter Distribution Patterns</i>	24
3.4. ACOUSTIC DATA BIN SIZES	26
3.4.1. <i>Horizontal</i>	26
3.5. ACOUSTIC BACKSCATTER VARIABILITY.....	27
3.5.1. <i>Spatially Indexed</i>	27
3.5.2. <i>Temporally Indexed</i>	29
3.5.3 <i>Backscatter Covariate Distributions</i>	33
3.5.4. <i>Vertical Distributions</i>	36
3.6. ACOUSTIC TECHNOLOGY COMPARISONS	38
3.6.1. <i>Temporally-Indexed</i>	38
3.6.2. <i>Spatial-Temporal Comparison</i>	43
4. DISCUSSION	50
5. CONCLUSIONS	53
6. RECOMMENDATIONS	54
7. LITERATURE CITED	57
APPENDIX A: RESON FINAL REPORT:	60
APPENDIX B: NORTHWEST FISHERIES SCIENCE CENTER FINAL REPORT	93

LIST OF TABLES

Table 1. Characteristics of echosounders, acoustic cameras, and multibeam sonars.	5
Table 2. Operating characteristics of echosounders used during mobile surveys and autonomous package deployments.	12
Table 3. Native vertical data resolution of acoustic instrument classes.	16
Table 4. Summary of acoustic and trawling activity during May and June, 2011	19
Table 5. Significance testing of trends in stationary echosounder survey.....	33
Table 6. Comparison of echometric data from echosounder and acoustic camera or ADCP in 24 second temporal bins. CoM stands for Center of Mass, AI stands for Aggregation Index.	40
Table 7. Comparison of echometric values from comparisons of the acoustic camera or ADCP to the echosounder in 12 minute temporal bins. CoM stands for Center of Mass, AI stands for Aggregation Index.	43

LIST OF ABBREVIATIONS AND ACRONYMS

ADCP	acoustic Doppler current profiler
AMOS	autonomous marine observation system
ANOVA	analysis of variance
APL	Applied Physics Laboratory
AUV	autonomous underwater vehicle
CTD	conductivity temperature depth
dB	decibels
EDSU	elementary distance sampling units
EL	echo level
ESA	Endangered Species Act
FADs	fish aggregating devices
FPGA	field-programmable gate array
GARCH	Generalized Autoregressive Conditional Heteroscedasticity
ICPU	integrated control and processing unit
kHz	kilohertz
MARSS	Multivariate Autoregressive State Space
MHK	marine hydrokinetic
MRE	marine renewable energy
NWFSC	Northwest Fisheries Science Center
PDT	Pacific daylight time
SnoPUD	Snohomish Public Utilities District
S_v	volume backscattering strength
TVG	time varied gain

1. INTRODUCTION

Characterizing biological and physical environments is an integral component of marine renewable energy (MRE) site evaluation, development, operational monitoring, and decommissioning. Prior to installation of any MRE devices, potential energy resources must be quantified and baseline environmental conditions measured. Once devices are installed, device performance and environmental variables must be monitored to detect biological or physical impacts. Environmental impacts may occur during installation, occur seasonally with biological cycles, and/or over longer periods. All marine hydrokinetic (MHK) projects in operation or currently being permitted include monitoring plans (e.g. Ocean Power Technologies 2010, Fundy Ocean Centre for Research 2009, Snohomish Public Utility District [SuoPUD] 2009). While technologies to monitor the physical environment around MRE projects are well-established, techniques to monitor densities and distributions of aquatic animals that may interact directly with or be affected by devices within pilot or commercial scale arrays are less developed. As an example, only limited and variable monitoring procedures are contained in the aquatic species monitoring plans listed in the above references.

Before biological monitoring can be implemented and standardized, it is imperative to quantify the composition and distributions of aquatic organisms associated with MRE sites. Without baseline information on nektonic (i.e. macroinvertebrates and pelagic fish species capable of moving independently of fluid motion within the water column) species, the suitability of sites, and potential impacts, or realized effects of device deployment, operation, and decommission cannot be known. Characterization of nekton at MRE sites can also be used to inform the type and number of monitoring instruments needed, design protocols to adequately monitor trajectories of animals toward devices, and detect changes in the composition and distributions of resident and/or migratory nekton species. Ultimately, understanding how nekton distributions at a MRE site vary in time and space is necessary to define what constitutes an effect (e.g. occurrence of endangered or threatened species within established safety radii around devices) or impact (e.g. device strike or animal entrainment), and then design/implement a warning or trigger mitigation action(s) when effects or impacts appear imminent.

High tidal velocities (~3.5 m/s) at MRE sites necessitate the use of sampling technologies that are both robust and meet sampling requirements. Use of direct sampling technologies such as nets may be limited to periods of low tidal exchanges, and increased water turbidity may reduce optical ranges below minimum requirements. Among remote sensing technologies, energy from optical sensors attenuates three orders of magnitude faster than that of sound (i.e. 30 m optical range compared to 30 km acoustic range), which constrains their use to the vicinity of devices (i.e. near-field monitoring). Acoustic technologies can be used to monitor organisms over ranges extending from a few meters near individual MRE devices to hundreds of meters within commercial site domains. Acoustic technologies are commonly used to map, size, count, and identify pelagic fish and macroinvertebrate species in aquatic environments. With the ability to continuously sample the entire water column over short (<1 second) time periods, acoustics provides a comprehensive, high-resolution snapshot of nekton not possible using nets. Acoustic technologies send short (e.g. 0.2 - 1.0 msec), repetitive (e.g. 3 pulses/s) pulses of high frequency sound (e.g. 12 - 420 kHz) in a conical beam. With each acoustic pulse, the entire water column

is sampled at resolutions of one meter or less. When the sound wave encounters a density different from water (e.g. fish or macroinvertebrate), energy is reflected back to the transducer. This echo is used to derive quantitative measures of target locations, sizes, and densities. Acoustic technologies can be deployed at fixed locations to monitor sites over time, or in mobile surveys to construct continuous, detailed maps of target densities and sizes. The traditional approach to identify species in acoustic data is to combine acoustic measurements with directed samples using midwater trawls. Efforts continue to analytically combine data from multiple acoustic frequencies with biological knowledge, to allow remote identification of acoustic targets.

The overall goal of this project was to evaluate the use of acoustic technologies to characterize nekton spatial and temporal distributions at a proposed MRE site in northern Admiralty Inlet, Puget Sound, Washington. This site was selected by SnoPUD for the deployment of two OpenHydro (<http://openhydro.com/home.html>) hydrokinetic turbines.

Four classes of acoustic technologies – echosounder, multibeam sonar, acoustic camera, and ADCP (Acoustic Doppler Current Profiler) were used to detect, and enumerate pelagic nekton at the site. Data from stationary instrument deployments were compared to data from a mobile acoustic and midwater trawling survey to determine how well each technology detected spatiotemporal variation in nekton distributions. Results of the design, deployment, retrieval, and analysis of data from these instrument classes were used to formulate recommendations for instrument choice, configuration, and monitoring methods to characterize and monitor pelagic nekton at any MRE site.

2. METHODS

2.1. Project Organization

This project was organized in four tasks: planning and mobilization, instrumentation deployment, data analysis, evaluation. Equipment manufacturers were invited to collaborate in the project. Their responsibility was to supply and program an acoustic system that would operate autonomously for a month period at a 10% duty cycle, and to recover and deliver the data. The collaborative partners were: echosounder – BioSonics Inc. (<http://www.biosonicsinc.com>); multibeam sonar – Teledyne Reson (<http://www.teledyne-reson.com>); acoustic camera – Sound Metrics (<http://www.soundmetrics.com>). Acoustic Doppler Current Profiler data from a Nortek (http://www.nortek-as.com/en?set_language=en) instrument was acquired in conjunction with concurrent measurements during the field sampling program.

The objectives for each task included:

Task 1: Planning and Mobilization

- Adapt and mount three acoustic instruments and power supplies on frames

- Design mobile survey (echosounder and midwater trawl) to characterize nekton density distribution variability
- Design sampling duty cycles and identify locations for acoustic packages

Task 2: Instrumentation Deployment

- Deploy acoustic packages
- Conduct mobile surveys

Task 3: Data Analysis

- Process all acoustic data using a common software
- Compute species-specific densities using all acoustic data in common spatial and temporal bins
- Compare stationary to mobile acoustic data

Task 4: Evaluation

- Evaluate the ability of representative instruments to detect, categorize, and enumerate aquatic species
- Compare density distributions measured by stationary instruments to those measured during mobile surveys
- Recommend use of acoustic packages, in conjunction with other monitoring to establish the environmental baseline and monitor for environmental effects of renewable energy project developments.

2.2. Sampling Design

Data acquisition included two acoustic and midwater trawl surveys conducted by a surface vessel, and the deployment/recovery of three autonomous acoustic instrumentation packages on bottom. The ADCP was mounted on a separate platform and recovered at the same time as the autonomous instrument packages for this study. The study location was the SnoPUD proposed Admiralty Inlet tidal renewable energy site (north grid), and an adjacent area south (south grid) of the proposed site (Figure 1). Autonomous acoustic instrumentation packages were deployed approximately 750 meters off Admiralty Head in 55 m depth parallel to the main axis of Admiralty Inlet.

Dates for the mobile and stationary field sampling components of the project were finalized at a PI meeting held November 1, 2010. Timing of the mobile surveys was designed to overlap the deployment and recovery of the stationary acoustic packages. The first mobile survey was conducted from May 3 to May 14, 2011. The autonomous acoustic packages were deployed May 9-10, 2011 and retrieved June 9-10, 2011. The second mobile survey was June 2 through June 14, 2011. The research vessel R/V Centennial from Friday Harbor Laboratories (http://depts.washington.edu/fhl/fac_RVCentennial.html) was used as the platform for mobile surveys, and the R/V Jack Robertson (<http://www.apl.washington.edu/about/vessels.php>) from the Applied Physics Laboratory (APL) was used to deploy and retrieve the autonomous acoustic instrumentation packages.

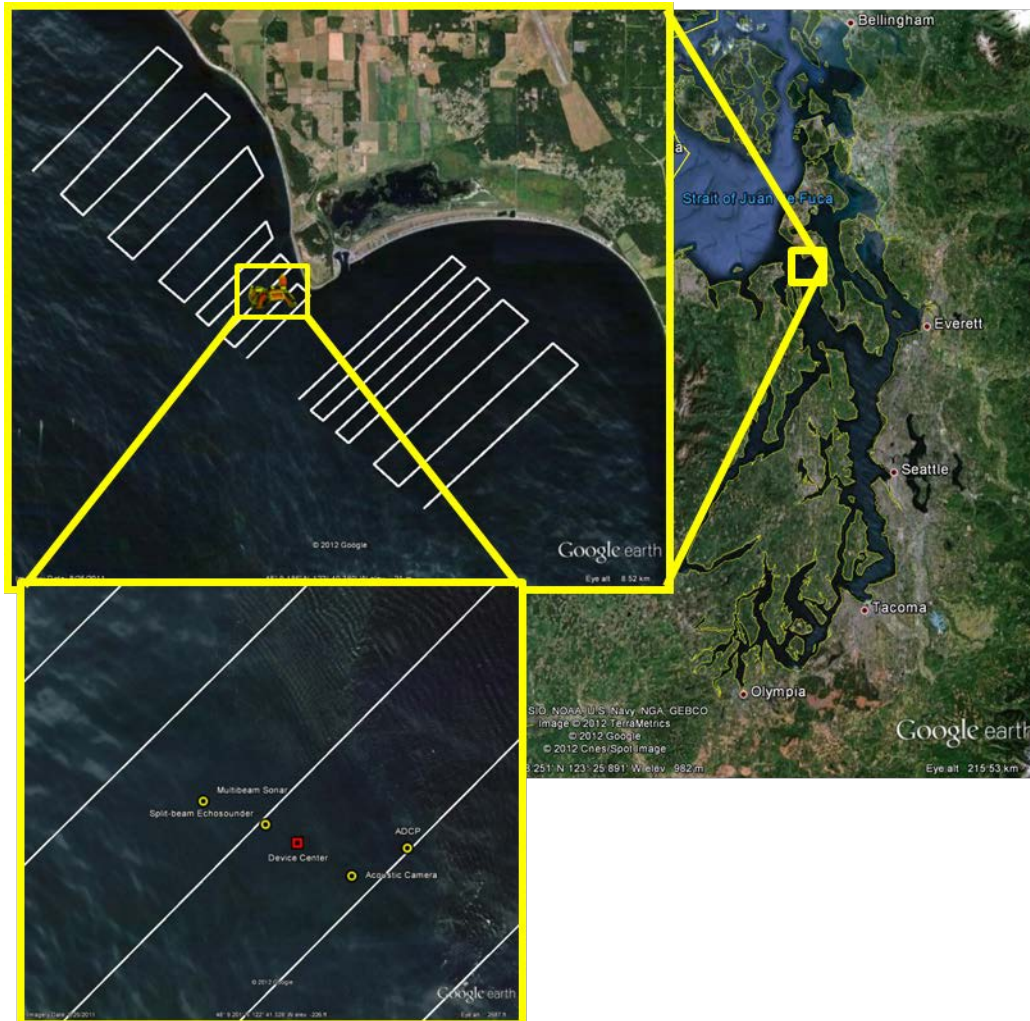


Figure 1. Study location within Puget Sound, Washington (upper right), mobile survey transect layout (upper left) showing north and south grids, and locations of the autonomous acoustic packages (lower left) that correspond to the area of the SnoPUD proposed turbine location.

2.2.1 Acoustic Instrumentation

Hardware characteristics of the four acoustic instruments (ADCP, acoustic camera, multibeam sonar, and echosounder) used in this project determined their ability to meet renewable energy site monitoring objectives. Three important characteristics that vary among instruments are operating frequency, beam angle, and data resolution. Operating frequency determines the range of detection (i.e. how far an animal can be from the instrument and still be detected), but is

limited by power input and energy absorption as a pulse travels through water. Higher operating frequencies have shorter wavelengths, higher absorption rates, and therefore have shorter detection ranges. As an example, a 38 kHz echosounder with 1 kW input power should provide useable data over a range of 800 m or more. A 200 kHz echosounder with 100 W input power should provide useable data up to about 80 m. The beam angle used to transmit and receive sound influences the detection range (due to signal spreading and energy loss) and the amount of water sampled with each transmitted pulse. The swath of multibeam sonars exceeds volumes sampled by echosounders or acoustic cameras by orders of magnitude. Using 100 m depth as an example, an echosounder with a 7° beam insonifies a volume of 3,922 m³ in a single pulse, while a 120° multibeam sonar would insonify a volume of 3,141,771 m³. Typical operating frequencies, beam angles, and maximum power levels for the echosounders, acoustic cameras, ADCPs, and multibeam sonars are summarized in Table 1.

Table 1.

General characteristics of echosounders, acoustic cameras, and multibeam sonars.

Technology	Operating Frequency	Beam Angle	Max Power Requirements
Echosounder	12-400 kHz	Circular: 5° to 15°	60 - 1000 W
Acoustic Camera	700-1800 kHz	Rectangular: 0.3° horz. x 14° vert.	25 – 30 W
Acoustic Doppler Current Profiler	38 kHz - >1 MHz	Circular (3 or 4 beams): 2° to 20°	25 W
Multibeam sonar	120-300 kHz	Rectangular: 90° to 180° horz. x ~2° vert.	45 W

The resolution of acoustic data influences the quality of images from the four instrument classes (Figure 2). Data resolution is influenced by operating frequency, but primarily determined by how reflected echoes are digitized and processed by the instrument. Acoustic cameras produce near optical quality images compared to those from echosounders and multibeam sonars. Acoustic images are used to identify detected targets. Direct comparison of synchronous data was used to quantify instrument attributes and to recommend deployment configurations.

Acoustic echosounders are commonly used to describe density distributions of fish and large invertebrate species distributions within the water column (Simmonds and MacLennan, 2005). Echosounders are deployed from boats at the surface during mobile surveys, or as fixed deployments on midwater platforms or on bottom. Data collected from mobile vessels along acoustic transects, using transducers mounted on the hull, a towed body, or on a pole, are used to map aquatic organism location, and density, and they can be used to compile length frequencies of insonified targets. Transducers deployed at fixed locations are used to monitor the entire

water column or across a channel over time. Transducer deployment choices affect power requirements, data storage, and data acquisition near boundaries at the surface or bottom. Mobile surveys typically utilize ship's power or a portable generator and write data to a computer. Stationary deployments require autonomous power (i.e. battery) and data storage, or have power and communication cable connections to shore.

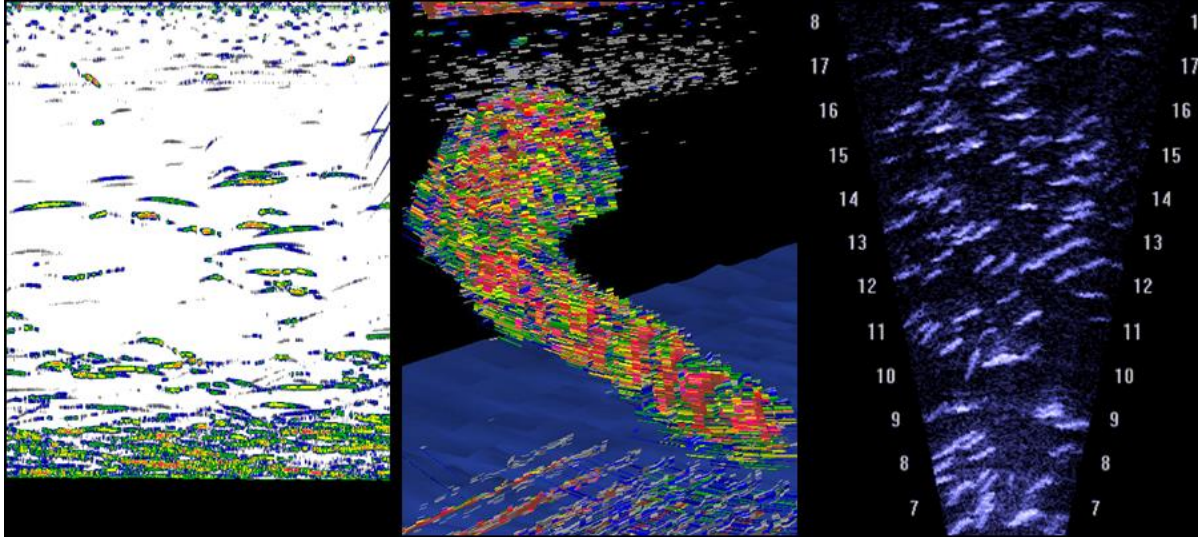


Figure 2. Representative echograms from three of the four acoustic instrument classes: a) echosounder image showing individual fish and zooplankton starting an upward migration at dusk; b) multibeam sonar showing a large fish aggregation above the bottom; c) DIDSON acoustic camera image of individual fish (herring) within an aggregation. Data were obtained independently for each instrument.

Acoustic cameras operate at high frequencies (1.0 to 1.8 MHz) and provide near optical quality images that are used for imaging, navigation, and inspection. This technology provides high resolution images of static structures, but moving objects such as fish, result in blurred or smeared images. These sonars, combined with processing software, rapidly combine images to provide video-like output. Sequential images from two dimensional multi-beam sonars have been used to construct three dimensional images of fish or invertebrate aggregations using sequential transmissions. Stationary acoustic cameras have been used to count migrating salmon (e.g. Burwen et al. 2010) and to track individual targets as they approach a tidal turbine (Viehman, 2012). The primary advantage of acoustic cameras is that, unlike video cameras, they do not require light to acquire images and have a longer operational range compared to equivalent optic instruments. The limitation of the high operating frequencies is that the maximum detection range is restricted (~ 15 to 80 m) depending on the instrument, compared to the 10s or 100s of meters operational range of an echosounder.

The ADCP uses the shift in returned frequency due to the Doppler effect to derive water velocities. Quantitative interpretation of their backscatter data is limited by difficulties with their

calibration (Brierley et al., 1998). Even though not designed to measure backscatter from aquatic organisms, data from ADCP instruments have been used to index biomass variability in the water column over extended periods. Flagg et al. (1994) used ADCPs to measure currents and index biomass in the Mid-Atlantic Bight. Cochrane et al. (1994) used a bottom mounted ADCP to measure temporal variability of the euphausiid (*Meganyctiphanes norvegica*) concentrations over 49 days on the Scotian shelf. Brierley et al. (2006) monitored abundance of Antarctic krill (*Euphausia superba*) over 3 months at South Georgia Island in the Southern Ocean. Radenac et al. (2010) analyzed ADCP data from the TAO/TRITON array in the equatorial Pacific, linking patterns in the acoustic backscatter with environmental forcing. These examples provide a mix of dedicated and opportunistic use of data from ADCPs that are routinely deployed on oceanographic moorings.

Multibeam sonar is an established acoustic technology traditionally used to map bathymetry and to search for objects on or near the seafloor. Multibeam sonars have the widest beam angles of the four active acoustic technology classes, with an array of narrow beams combined to form a swath of up to 180°. The wide swath of multi-beam technologies compared to that of traditional echosounders (~5° to 15°) combined with high sampling rates has increased the use of multibeam sonars to image and count aquatic organisms in large volumes of water (e.g. Gerlotto et al. 1994) at high resolution. Sample volumes of multibeam instruments exceed those sampled by single-beam echosounders by several orders of magnitude. Multibeam sonars designed for fisheries applications do not typically meet federal hydrographic mapping specifications, but a subset of these instruments are used to image and quantify the water column, and/or map the substrate. Depending on the capabilities of the instrument, costs of multibeam sonars range from being comparable, to an order of magnitude higher than a scientific echosounder. Multibeam sonars typically use one or two orthogonal arrays housed in a transducer head that transmits pulses to and receive echoes from the water. If using two arrays, then the transmit array is oriented along-ship and generates a pulse that is wide (typically 120° to 150°) along one axis and narrow (typically 0.5° to 20°) along the orthogonal axis. The receive array is used to form numerous (>100) beams.

2.2.2. Mobile Sampling

The mobile survey consisted of acoustic measurements, midwater trawls, and marine mammal/seabird observations along systematic grids of transects (Figure 3). Each grid had high (0.25 km) and low (0.5 km) resolution transect spacing radiating from the proposed location of the tidal turbines. Acoustic operations during a 12 hour sampling period included running each grid during the day, during the night, and drifting during the crepuscular (i.e. dusk) period. A vessel-mounted echosounder was used to quantify nekton densities and distributions.

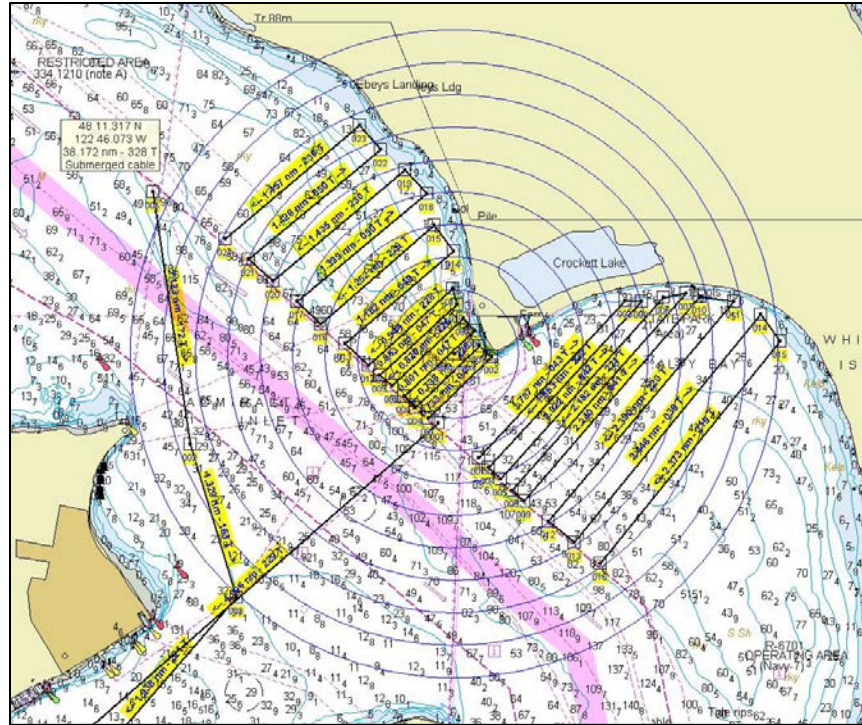


Figure 3. Transect layout for acoustic, trawl, marine mammal, and seabird surveys showing northern and southern grids. A high resolution area with grid spacing of 0.25 nmi overlaid the SnoPUD site with an analogous high-resolution area in the southern grid.

To validate patterns observed on the echosounder and to identify assemblage constituents a midwater trawl was used to sample aggregations or layers in the water column. All trawling was conducted using a Marinovich midwater trawl, a 6 m x 6 m box trawl fished with 4.6 m x 6.5 m (5 ft x 7 ft) steel V-doors. Stretched mesh sizes ranged from 7.6 cm (3 inch) in the forward section of the net to 3.1 cm (1.125 inch) in the cod end. The final third of the cod end was lined with a 0.9 cm (0.375 inch) knotless liner. To monitor and record headrope depth of the trawl a Simrad PI-32 net monitoring system (<http://www.simrad.com/www/01/nokbg0240.nsf/AllWeb/BAE7F29DF0FF9739C12570AD002BD060?OpenDocument>) was used while fishing. The net monitoring system was connected to the EK-60 echosounder to display headrope depth on the echogram and to record headrope depth in the echosounder data record.

Four midwater trawls were planned for each day but tidal velocities were often too strong to fish with the midwater trawl. As a result, trawling was restricted to times when the current was 1 knot or less and dedicated fishing days with low tidal velocities were incorporated into the survey design. Tidal flow predictions were taken from the ADCP data and modeling by Jim Thomson (APL) and Brian Polagye (NNMREC) rather than published tide charts because published tide charts contained inaccurate amplitude and velocity predictions. All trawl samples were identified to the lowest possible taxonomic group, weighed, and measured for length. A

headrope depth monitoring system (Simrad PI-32) was connected to the echosounder so that a line indicating the net depth was visible during trawling. All permits for sampling Endangered Species Act (ESA) listed fish species were held by the Northwest Fisheries Science Center (NWFSC) and ESA listed species caught were tabulated as the survey progressed. At each trawl deployment site, salinity, temperature, and conductivity data were collected using a Seabird SeaCat 19+ (Seabird Inc, Bellevue, WA) Conductivity-Temperature-Depth (CTD) sensor. Along each transect, marine mammals and seabirds were tabulated by a dedicated observer. For each sighting, species identification, number of animals, angle and distance to the sighting, and sea state were recorded for species-specific density estimates (see Appendix B). Observations were not conducted during trawl operations.

2.3. Stationary Sampling

2.3.1. Deployment and Recovery

To ensure that the autonomous acoustic instrument packages were functioning and ready for deployment, a build-up and testing of instrumentation platforms occurred prior to deployment. Instrument platforms used to mount acoustic packages were Ocean Science Sea Spider tripods (<http://www.oceanscience.com/Products/Seafloor-Platforms/Sea-Spiders.aspx>). The University of Washington's Applied Physics Laboratory has previously deployed and recovered autonomous instrument packages (e.g. ADCP, recording hydrophone) on this type of platform in northern Admiralty Inlet. APL engineers under the direction of Dr. Jim Thomson constructed two tripod packages so that the echosounder and the acoustic camera were mounted on its own platform. All Sea Spider tripods had lead ballast weight increased to 364 kg (800 lbs.) and two redundant pop-up buoy systems (Benthos 875-TD) added for tripod recovery. For the autonomous data collections, the sampling strategy was a tradeoff between maximizing temporal resolution and coverage through the duration of the deployment. Periodic cycling of data collection ensured that sampling occurred at all times of the day, during all stages of a tidal cycle, and throughout the month. The goal for autonomous package sampling was a minimum of 10% coverage of the entire deployment period (i.e. 72 hours). Manufacturers were requested to configure instruments to sample at a frequency of 1 Hz for 12 minutes every 2 hour block. Three submersible 12 volt DeepSea batteries (<http://www.deepsea.com/batteries2.php>) were attached to all but the multibeam sonar platforms to supply power for the echosounder and the acoustic camera. A custom built platform was used for the multibeam sonar to enable the housing of 9 marine batteries needed to power the unit during deployment (see Appendix 1 for details).

Autonomous acoustic instrument packages were deployed and recovered by the R/V Robertson. To deploy (Figure 4), Sea Spider tripods were lowered from the gantry A-frame and released using tethering/release and camera techniques developed during previous Sea Spider platform deployments. Autonomous acoustic instrument packages were deployed approximately 100 m apart. Technical difficulties with the RESON multibeam sonar control computer prevented deployment of this package on May 9 and it was not repaired in time for a May 10 deployment. After replacement of the control computer, bench testing, and dockside testing, the package was deployed during an additional cruise on May 25. Continued inconsistencies with software routines on the Micro-Controller computer resulted in some missed data files during bench

testing. It was later determined that the serial/Ethernet converter module had performed inconsistently. In an effort to acquire data, the technician bypassed the sampling control system and set a continuous sample rate of 1 Hz. Available power was predicted to permit continuous data collection for 100 hours. The power to the Micro-Controller was not disconnected, nor was the Ethernet connection. The timing/control system remained functional and shut the system down as it was programmed to do after the first duty cycle. Because of the bypass the system was not restarted and no further data were collected (see Appendix I for further details).



Figure 4. Back deck of R/V Robertson prior to departure from Seattle with acoustic packages being readied for deployment.

As part of a concurrent project, three additional Sea Spider platforms containing ADCPs had been previously deployed to resolve both along and cross current flows within the site (Figure 5).



Figure 5. Target locations of autonomous acoustic instrument package deployment locations and three additional ADCP instrument deployments. The SnoPUD tidal turbine site is outlined with the red triangle and the proposed cable run is outlined in blue, all overlaid on a bathymetric map of the area.

To recover deployed acoustic instrument packages an acoustic signal was used to trigger the Benthos pop-up buoys, and then the attached tether was used to winch each Sea Spider to the surface. Recovery was quick with all packages brought to the surface and loaded on deck during a single slack tide period. No autonomous acoustic instrument packages moved from their deployment locations and all were undamaged when recovered. Sea Spider platforms were transported back to Seattle, instruments were detached from the platforms, and returned to the vendors for data recovery.

2.3.2. Instrument Specifications

2.3.2.1. Echosounders

2.3.2.1.1. Surface Surveys

A Simrad EK-60 echosounder operating at 38 and 120 kHz (between half power points) was used to measure acoustic backscatter during all mobile surveys. Settings for each frequency are listed in Table 2. Transducers were hull mounted on a blister on the starboard side of the keel. The Simrad PI-32 net monitoring output was fed to the echogram display to trace the depth of the midwater trawl headrope during fishing operations.

Table 2

Operating characteristics of echosounders used during mobile surveys and autonomous package deployments.

Attribute	Echosounder (surface)		Echosounder (bottom)
Manufacturer	Simrad	Simrad	BioSonics
Model	EK-60	EK-60	DTX
Frequency (kHz)	38	120	120
Beam Angle (°)	12	7	7
Transmit Power (W)	1000	500	700-1000
Pulse length (ms)	0.512	0.512	0.5
Duty Cycle (Hz)	1	1	5 Hz for 12 minutes every 2 hours

2.3.2.1.2. Bottom Deployed

A BioSonics DTX 120 kHz echosounder and power management modules were configured for autonomous operation at the Admiralty Inlet site. Echosounder settings are listed in Table 2. All power monitoring and operating electronics were housed in an electronics canister with connections to the submersible batteries and the transducer. All data were logged to the operating computer.

2.3.2.2. ADCP

A 1 MHz Nortek Awac with a 25° degree beam angled 20° off-center measured tidal velocities at 1 Hz at 1 m resolution. All data was stored internally and averaged in 10 minute bins.

2.3.2.3. Acoustic Camera

The Sound Metrics DIDSON acoustic camera sampled in long range “detection mode” (operating frequency 700 kHz) over a range from 2.5 m to 42.5 m. The acoustic camera had 48, 0.8° horizontal and 14° vertical beams spaced 0.6° apart. Power consumption when operating was 25 W.

2.3.2.4. Multibeam Sonar

A RESON 7128 SeaBat multibeam sonar operating at 200 kHz was mounted on a custom designed platform for deployment at the Admiralty Inlet site. The multibeam sonar had 27° vertical beam width with 256 1° beams creating a 120° swath. This instrument package did not collect data after deployment (see Appendix I for details).

2.4. Data Processing

Acoustic data from all instruments, except ADCP, were pre-processed using Echoview (<http://www.echoview.com>) software, a suite of descriptive metrics, and matching analytic cell sizes. This approach ensured that data quality was maintained for all data streams, that comparisons among instruments were direct and equivalent, and that the potential for automated processing and warnings of potential impacts from a monitoring system could be evaluated.

If possible, acoustic data processing included four steps: calibration parameter verification, boundary discrimination, noise elimination, and echo integration. Calibration values were used to set instrument operating parameters so that all measurements are consistently scaled to a standard. Boundary discrimination included the bottom for mobile survey data and the surface and turbulence for bottom-mounted autonomous packages. Energy returns from the surface or bottom are orders of magnitude greater than those from aquatic organisms and are not included in summations of echo energy for density calculations (see below). Mechanical or electrical sources can introduce unwanted energy into data. These artificial returns can be eliminated by the use of thresholds, custom algorithms, or by manually excluding data points.

2.4.1. Data Pre-Processing

Mean volume backscattering strength (mean S_v), the mean returned acoustic backscatter per unit volume, was used as a direct metric of biological density. Acoustic energy is proportional to the density of acoustic targets (Foote 1983). Mean volume backscattering strength is independent of depth, allowing for unbiased comparisons even when bad data regions of space/time are excluded from a device. Vertical distributions were measured with respect to the bottom for comparison with the vertical footprint of a bottom mounted turbine. Stationary measurements were constrained to ranges between ~3 to 26 m off bottom, coincident with twice the height of the proposed OpenHydro turbine. Acoustic measurements within 3m of the transducers were excluded to remove nearfield effects and to exclude acoustic ringdown from analysis. Since neither the ADCP nor acoustic camera were calibrated, only bins in which measurements from the calibrated echosounder exceeded its threshold were used for comparison. Data were linked to tidal velocities collected every 10 minutes from the ADCP using a nearest neighbor algorithm. All samples were categorized as day (06:00 – 18:00), night (22:00 – 02:00), or crepuscular (04:00, 20:00) based on naval sunrise/sunset charts. Echosounder data from surface surveys were also categorized as a function of month (May/June) and grid location (North/South).

2.4.1.1. DIDSON

Integrated backscatter was measured in unspecified decibels (dB) at 512 intervals in 48 beams for a total of 24,576 observations per ping. No data threshold was applied to the data in the absence of a noise estimate. A time varied gain (TVG) was manually applied to each beam separately within Echoview to account for dissipation of acoustic strength with range using the equation:

$$\text{EchoLevel (EL)} = \text{Amplitude} + 20\log(\text{range}) + .2584349(\text{range})$$

The absorption coefficient (α) was calculated as 0.2584349 dB/km using Francois and Garrison (1982), and the mean water column depth from a CTD scan on June 3rd, 2011 at 19:35. Data between 15-19m were excluded from analysis to remove a band of noise that varied from the bottom depending on the tidal state and depth of the water column. This was a second echo return from a previous transmit pulse (i.e. ping) reflecting off the surface and bottom and then being received at the transducer. Data were exported in a format readable by the R software language (R Development Core Team 2011) for binning and condensing. Once imported into R, data from all 48 beams were averaged into 1 meter vertical bins and the depths from 15-19m were replaced with the mean density of the remaining bins of that ping to quantify the vertical distribution of backscatter.

2.4.1.2. Autonomous Echosounder

During initial inspection of the BioSonics echosounder data, it was observed that a significant amount of noise was added to the upper half of the water column due to a 3rd surface echo received at the transducer. If a 6 dB signal-to-noise ratio was applied as a filter to the data, then most targets in the upper half of the water column were obscured by the noise, preventing analysis of data from the upper portion of the water column. The location of the 3rd surface echo was a function of water depth, which varied with tide. To preserve as much of the data as possible, an algorithm was developed to exclude the 3rd surface echo using the distance to the surface, sound speed, and ping rate. Data were also examined to manually remove pings that contained noise from passing vessels, and regions of intense backscatter from the surface to the analysis region, consistent with turbulence from strong tidal mixing, which entrained air in the water column. Data were exported using a -75 dB threshold, matching the threshold derived from data acquired during the mobile survey.

2.4.1.3. ADCP

All pre-processing and processing of ADCP data was conducted in R software. Each ping consisted of simultaneous measurements by 3 beams in 25 one meter depth bins for a total of 75 observations per ping. The ADCP wasn't on the same duty cycle as the other two stationary technologies; therefore measurements that were not coincident with the other two technologies (first twelve minutes of even hours) were removed from the analysis. A TVG was calculated for each beam following Nortek (2001). The absorption coefficient used was 358.4 dB/km (Table 2.3 in Simmonds & MacLennan 2005). The ADCP TVG was checked by insuring that the distribution of densities at each depth was approximately similar. Uncalibrated measurements of acoustic backscatter from the three beams were averaged to produce a mean relative density measurement at each depth.

After tabulation of frequencies, tidal velocities were categorized as slack, moderate, and extreme. Categories were chosen to approximate the first and fourth quartile in slack and extreme categories. All samples from autonomous acoustic instrument deployments were categorized as ebb or flood tides based on the dominant tidal direction observed in a frequency distribution histogram.

2.4.1.4. Reson Multibeam

The multibeam sonar failed to collect data during deployment. Appendix 1 contains the manufacturer's report summarizing the data acquisition failure.

2.4.1.5. Surface Echosounder

Echoview's bottom pick algorithm was used to identify the bottom, but additional editing was performed by an analyst to ensure that no echoes from the bottom were included in the acoustic record. A half meter above the bottom was also excluded to remove the acoustic dead zone. A -75 dB filter was used as a data acceptance threshold, providing a 16 dB signal to noise ratio. This threshold also enhanced the algorithm developed to exclude surface turbulence. Surface turbulence was identified using the schools detection algorithm in Echoview (minimum total school length = 5 m, minimum total school height = 3 m, minimum candidate length = 5 m, minimum candidate height = 3 m, maximum vertical linking distance = 10 m, maximum horizontal linking distance = 10 m). Intense acoustic backscatter that intersected the 3 m depth ringdown exclusion was excluded as surface turbulence. In addition to removing the noise from surface turbulence, additional noise from the boat's electronics, cross talk from stationary transducers, and other sources of interference were excluded from the data.

2.5. Data Analysis

The ability of the four acoustic instrument classes (i.e. echosounders, multibeam sonars, acoustic cameras, ADCP) to detect nekton was compared among autonomous instruments and to results from the mobile acoustic surveys. Echometrics, a suite of distribution indices, were used to examine changes in nekton distributions as a function of temporal and environmental covariates.

2.5.1. Trawl Catches

Trawling targeted aggregations observed on the echosounder, but due to high tidal speeds was restricted to times when tidal flows were equal to or less than 1 m/s. All trawl catches were sorted to species, weighed, and measured for length.

2.5.2. Water Flow Properties

Tidal flow (i.e. direction and speed) was quantified using ADCP data binned in 10 minute blocks that corresponded to the even hour, 12 minute measurement periods of the autonomous acoustic instrument packages. Tidal flow was measured at approximately 45 m depth, corresponding to 10 m off bottom.

2.5.3. Data Visualization

To inspect the types of data collected and to visualize the range and potential relationships among data sets, data from all technologies that had sampled on June 7, 2011 between 07:00 to 22:00 were compiled and made available to software engineers who developed the geospatial, data fusion software package Eonfusion (<http://www.eonfusion.com/>). Their objective was to

integrate and visualize all data sets along the timeline of the day in a short, intuitively understandable animation. Data were supplied from an EM3002 multibeam sonar (vessel mounted), an EK-60 echosounder (vessel mounted), a DIDSON acoustic camera (bottom mounted), a DT4 echosounder (bottom mounted), a Seabird 19+ CTD cast (vessel deployed), and tidal velocity data from an ADCP.

2.5.4. Horizontal binning

Horizontal and temporal bin sizes for analyses were determined using autocorrelation functions. The goal to determining an appropriate analytic cell size (i.e. bin size) is to select a cell size large enough to minimize autocorrelation between cells, and at the same time, picking a size small enough to characterize spatial and temporal variability in the data series. Two horizontal analytic cell sizes were used to facilitate comparison among temporally-indexed data series. The first was the minimum autocorrelation distance among bottom-deployed technologies, calculated using area backscattering strength (i.e. depth integrated volume backscattering strength, S_a). Autocorrelation analysis was conducted at the resolution of 1 second, the coarsest temporal sampling grain common to the ADCP and acoustic camera. Among temporally-indexed data series, the echosounder during nighttime slack tides had the largest autocorrelation lag distance (24 seconds). A 24 second analysis cell yielded 30, 24 second bins per 12 minute sampling period. Once the 24 second bins were identified, all measurements from each technology were matched to 24 second bins using a nearest neighbor algorithm. In the second temporal data binning, each 12 minute sampling block was used as a time series resolved at 24 seconds.

Autocorrelation analysis of the spatially-indexed data was conducted at a 10 m resolution using area backscattering strength data. Results showed that 300 m analysis cells ensured that at least 4 data cells would be included in each transect in the North sampling grid, and approximately 10 data cells/transect would result for the South sampling grid.

2.5.5. Vertical Binning

The ADCP had the coarsest vertical resolution at 1 m (Table 3), which was used in the vertical binning of both mobile and autonomous data series.

Table 3.

Native vertical data resolution of acoustic instrument classes.

Technology	Native Vertical Resolution	Vertical Range
ADCP	1 m	25 m
Acoustic Camera	~ 8 cm	43 m
Echosounder	~ 75 cm	Water column

2.5.6. Echometrics

Mean volume backscattering strength (mean S_v ; MacLennan et al. 2004) was used to index nekton densities. An additional three derived metrics were used to characterize the vertical distribution of nekton through the water column from a suite of metrics developed by Burgos & Horne (2008) and further refined by Urmy et al. (2012). Center of mass (units m) is the mean weighted location of backscatter in the water column relative to the bottom. Vertical distributions were measured with respect to the bottom to facilitate comparisons across all tidal states, and between the mobile surveys and autonomous acoustic instrument packages. Inertia (units m^2) indexes dispersion and is analogous to the variance of nekton distribution surrounding the center of mass. The Aggregation Index (units /m) indicates the patchiness of acoustic backscatter through the water column, calculated on a scale of 0 to 1 (with 1 being aggregated). Together, these four metrics compose are referred to as “echometrics.”

2.5.7. Characterizing Backscatter Variability

Mean volume backscattering strength (mean S_v) values at a resolution of 300 m bin sizes were plotted as a function of location and compiled in a frequency histogram. Echometric values from the mobile surveys were indexed by date and tidal speed to illustrate changes through time and tidal currents. Analytic cells were first indexed by date or tidal speed (using 0.1 m/s bins) and then categorized by time of day, location, tidal speed, or month. Metric values within a category were averaged within a specific date or tidal speed.

Mean and variance values of each metric in the data series from each autonomous acoustic instrument package were indexed by date, time of day, and tidal speed. The series were filtered to times when all three technologies were operational. Data plotted by date used the 12 minute blocks ($n = 336$) sampled every two hours, and then smoothed using a six hour, locally-weighted regression (Cleveland 1981). Confidence intervals are cannot be defined for a series in the absence of multiple observations at time. Metric values characterized by time of day and tidal speed used the 24 second temporal bins in the time of day ($n = 10,811$) or tidal speed ($n = 10,130$) series. Mean values are indicated using a black line, and an approximation for the upper 95% confidence interval for a single observation was denoted by the salmon-colored envelope. Significant changes in metric values through time, tidal speed, and time of day were tested using an ANOVA. Date and tidal speed were treated as continuous variables. Day and night were treated as categorical variables in the time of day series. Dusk and dawn observations were not included in the time of day statistical tests.

Box and whisker plots of echometric values were used to illustrate the effect of sampling location, sample month, tidal flow, tidal direction, and time of day on the density and distribution of nekton in the mobile and stationary echosounder data series. Depending if the series was spatially or temporally indexed, observations were a 300 meter or 24 second sample bin, with whiskers extending 1.5 times the interquartile range. The width of a box is proportional to the square root of the number of observations it represents. A total of 5,054 spatially-indexed and 10,811 temporally-indexed samples were used to compute box and whisker plots, with the exception of tidal speed and tidal direction as 681 cells without concurrent tidal measurements

were excluded. If notches in two boxes of a covariate pair do not overlap, then there is strong evidence that the two medians differ (cf. Chambers et al. 1983).

Changes in vertical distributions of acoustic backscatter were also examined using covariates for both the spatially- and temporally-indexed echosounder data series. Vertical distributions observed in the temporally-indexed echosounder were summarized by time of day, tidal speed, and tide status. Twenty four second temporal bins were resolved in 1 m depth bins for each covariate. The mean volume backscattering strength of the entire time series was included as a baseline across all depths, with a 7 dB range between lines. Values to the right of the baseline are greater than the overall mean backscatter.

Operators of MRE devices will need to know the distribution of nekton relative to the vertical footprint of devices in the water. Center of mass and standard deviation echometric values were calculated for each 300 m cell in the spatially-indexed echosounder data series. A cumulative distribution function was used to tabulate the proportion of center of mass values as a function of distance from bottom. Additional cumulative distribution functions were created by subtracting one and two standard deviations from the center of mass to indicate variability in the data series.

2.5.8. Acoustic Technology Comparisons

Coincident backscatter measurements and echometric values from the acoustic camera and ADCP were compared to those from the temporally-indexed echosounder. The echosounder was the only calibrated instrument in the group and was used as the baseline for each comparison. Data were limited to times when all three technologies were actively sampling. Density measurements and/or metric values were compared at a resolution of 24 seconds in 1 m vertical bins, and 24 second ($n = 10,811$) or 12 minute ($n = 358$) bins over the entire water column. Significance differences in values between technologies were tested using an ANOVA on paired observations.

The spatially and temporally indexed data series from the calibrated echosounders were compared using echometrics. The two sets of data contained simultaneous observations at four different times: June 4th, 2011 at 16:00, June 4th, 2011 at 20:00, June 6th at 18:00, and June 7th, 2011 at 10:00. The 12 minute sampling bin from the temporally-indexed data that occurred nearest to the time when the vessel was over the autonomous instrument package was chosen as the coincident time. This 12 minute temporal block was compared to echometric values calculated at three spatial resolutions: the nearest transect, the neighborhood, and the entire grid. A neighborhood consisted of the high resolution, or low resolution section of the grid containing the grid transect. The grid was the northern or southern grid where the neighborhood was located. The depth ranges from the two series were matched when echometric values were calculated. Mean and +/- 2 standard deviation values were calculated for each metric at all three spatial resolutions.

3. RESULTS

3.1. Trawl Catches

The midwater trawl was fished on aggregations observed on the echosounders over a depth range from 7.1 m to 71 m in the adjacent shipping channel. Trawl deployments were timed to coincide with current speeds of approximately 1 knot or less. This constraint may have biased observed species compositions or lengths but numbers and diversity of catches remained consistent between months and grids (see below). Trawling was not conducted near surface or near bottom to avoid ensure proper configuration of the net and to avoid contact with bottom. Trawl samples were nearly evenly distributed between sampling grids and months, with approximately three (north) to five (south) times as many trawls conducted during the day than during the night (Table 4). No trawling was performed during the dusk sampling period.

Table 4.

Summary of acoustic and trawling activity during May and June, 2011.

Month	Activity	Time Period	North Grid	South Grid
May	Acoustic Grids	Day	12	10.5
		Dusk	3	4
		Night	3	3
	Trawling	Day	5	8
		Night	3	2
	June	Acoustic Grids	Day	11
Dusk			4	3
Night			3	4
Trawling		Day	7	8
		Night	1	2

3.1.1. North-South Grid

Fish species composition in the midwater trawl varied with the location and timing of sampling. Overall species diversity and catch composition was similar in both north and south grids (Figure 6). In the north grid, Pacific sand lance (*Ammodytes hexapterus*), northern lampfish (*Stenobranchius leucopsarus*), and Pacific saury (*Cololabis saira*) were the three most common

species. One tow was dominated by Pacific herring (*Clupea pallasii*). Catches in the south grid frequently contained sand lance, copper rockfish (*Sebastes caurinus*), and Pacific herring.

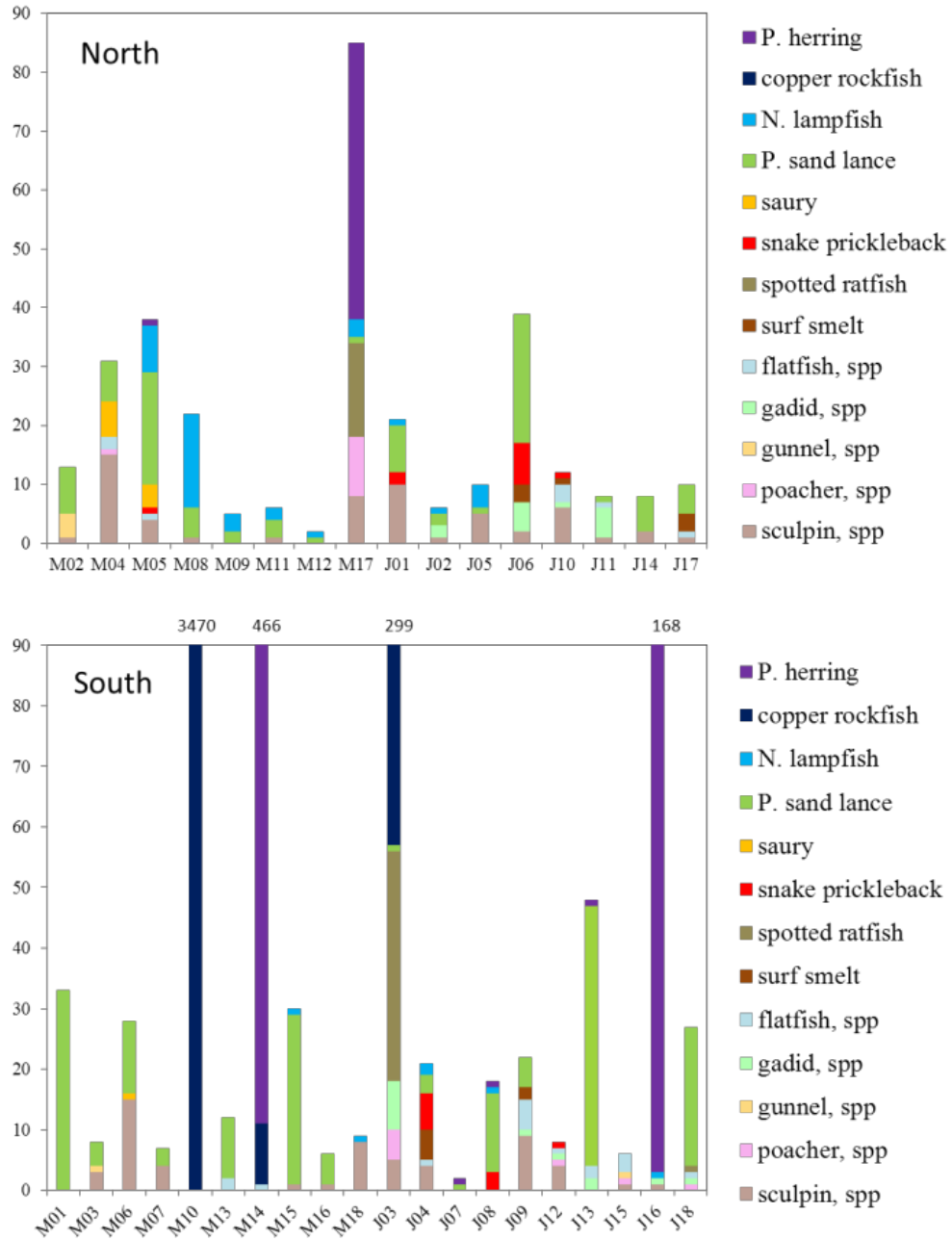


Figure 6. Midwater trawl catch compositions in the north and south grid. Numbers above the upper x-axis indicate total numbers caught.

3.1.2. Sampling Months

Species compositions from the midwater trawls differed between May and June. While Pacific sand lance were present in both months, Pacific saury and northern lampfish were more abundant in May and snake prickleback (*Lumpenus sagittal*) were more abundant in June.

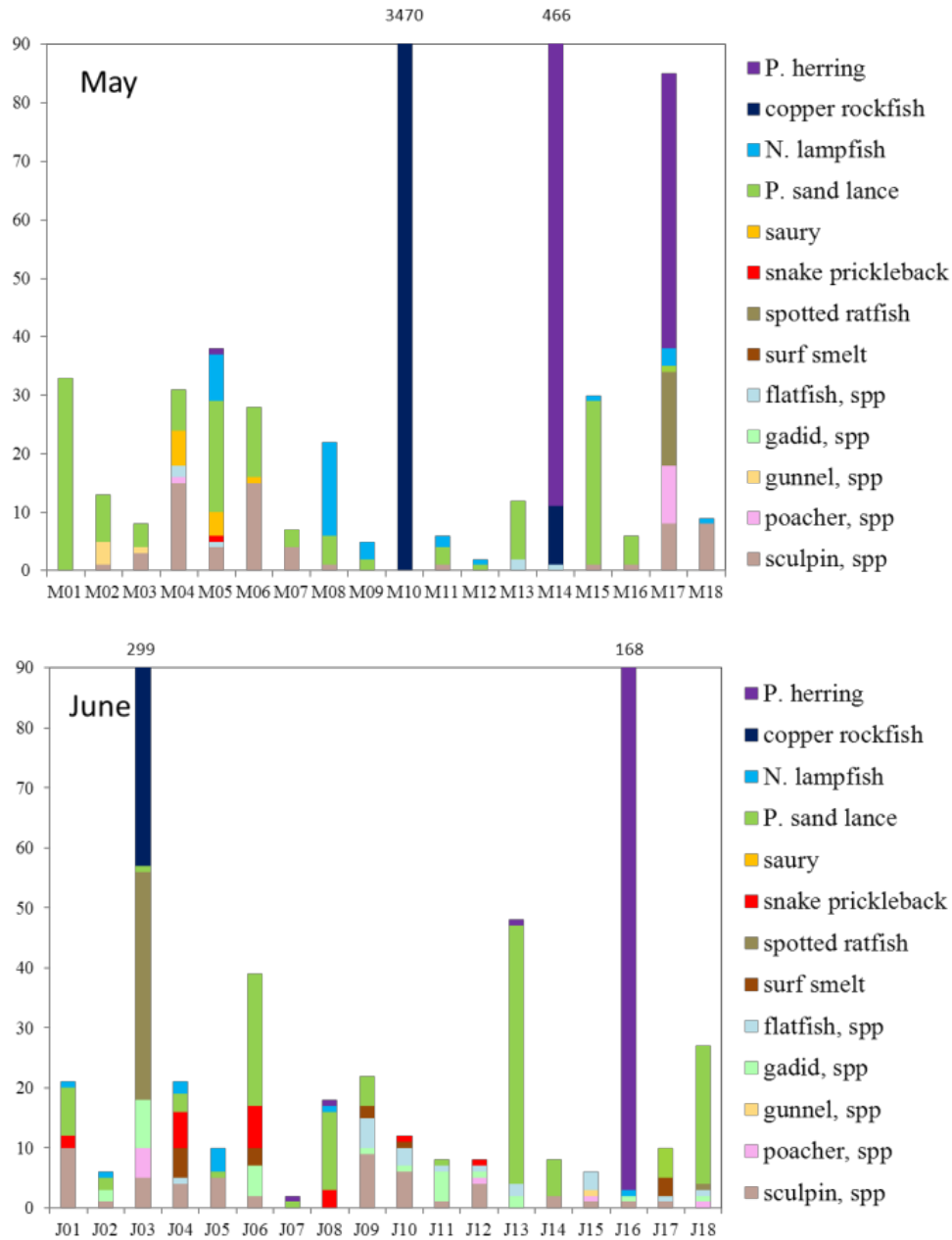


Figure 7. Midwater trawl catch compositions in May (upper panel) and June (lower panel). Numbers above the upper x-axis indicate total numbers caught.

3.1.3. Diel Sampling

Even though midwater trawls targeted large aggregations or layers observed on the echosounder, catch compositions were typically mixed during both day and night. Snake pricklebaks were more common in day catches compared to those at night. Pacific sand lance were caught in all night trawls, despite documented burrowing behavior at low light levels (< 1 lux, Winslade 1974).

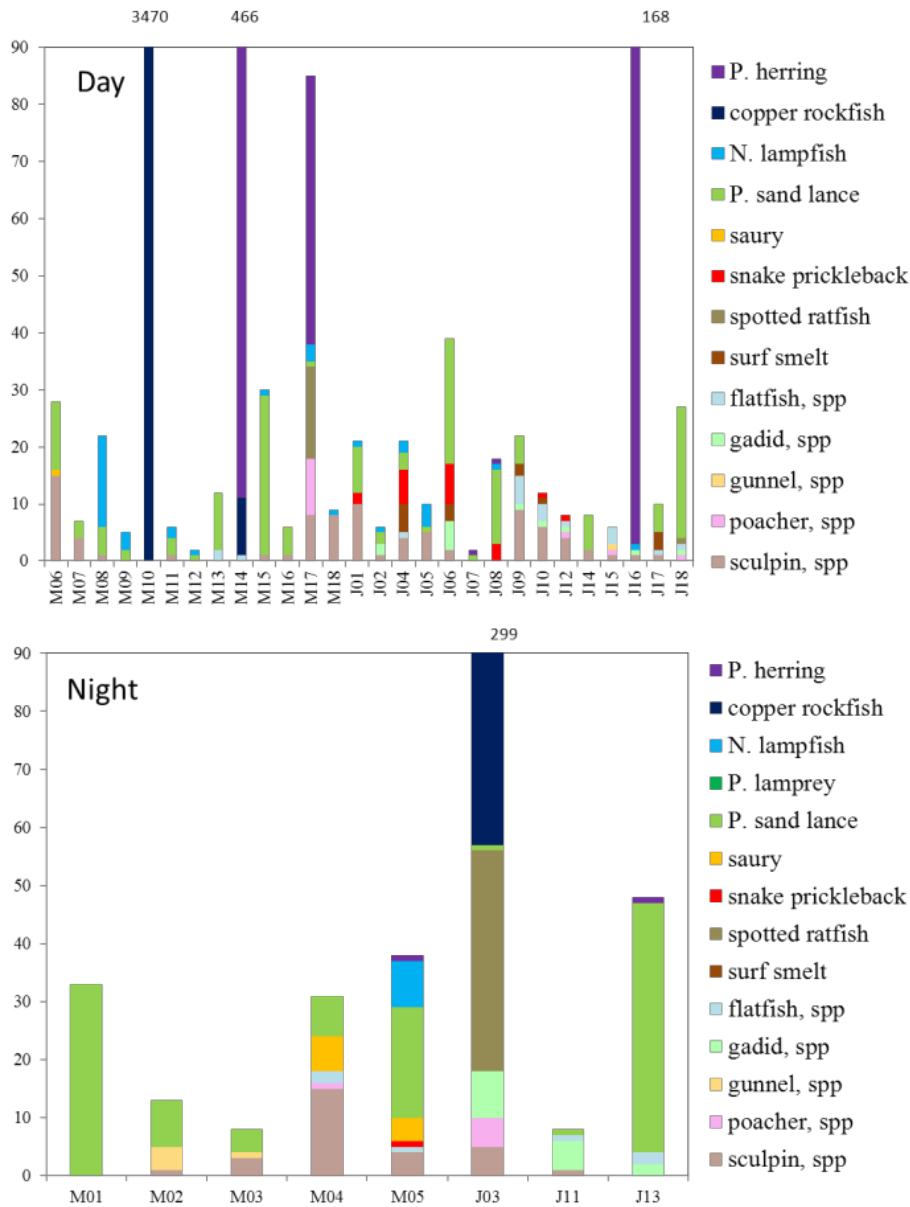


Figure 8. Midwater trawl catch compositions during day (upper panel) and night (lower panel). Numbers above the upper x-axis indicate total numbers caught.

3.1.4. Fish Length Frequency

The midwater trawl caught fish ranging in length from a few millimeters to 675 mm. Seven fish species were caught in sufficient numbers to compile length frequency distributions. Length ranges of fish caught during both May and June were consistent, with the exception of Pacific sand lance which had an increase in the abundance of small fish in June.

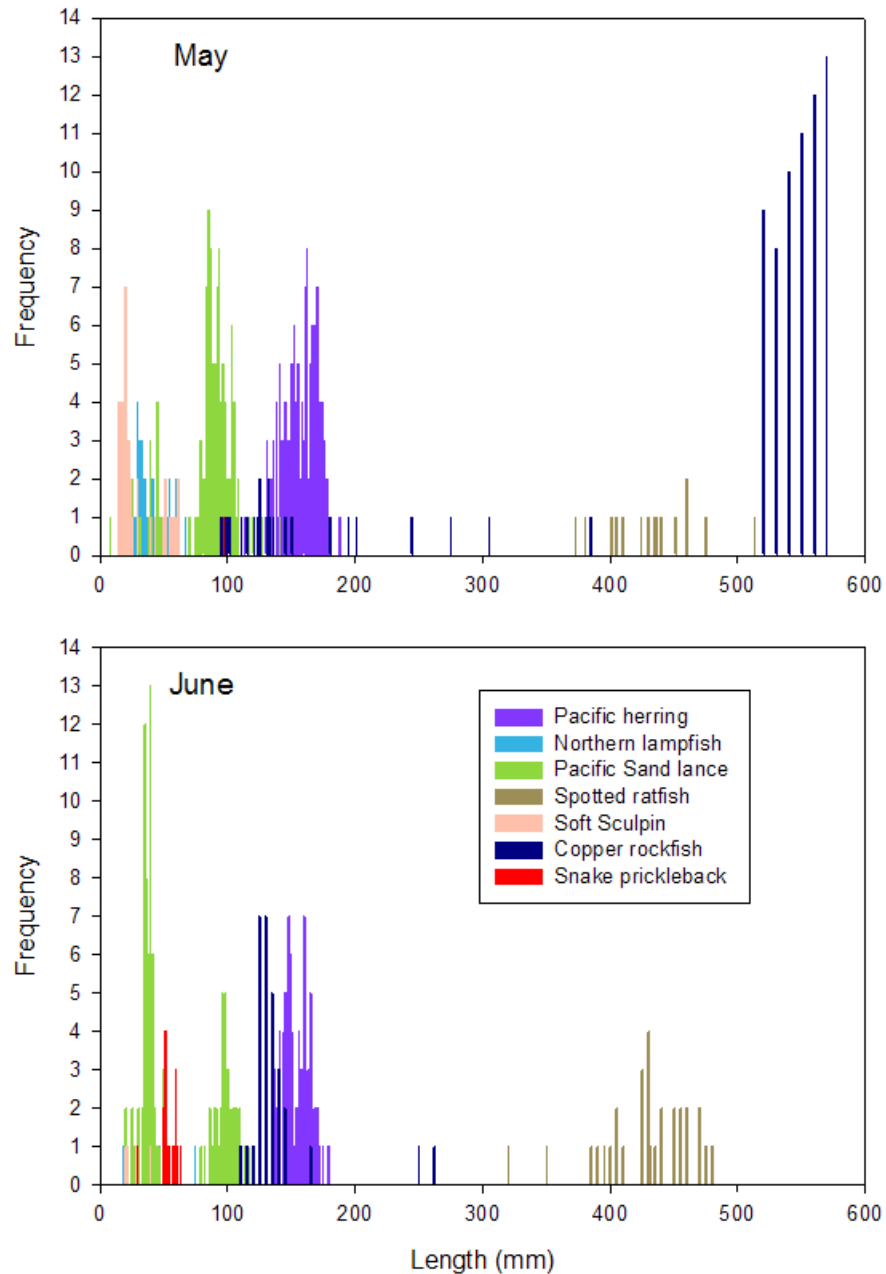


Figure 9. Length frequency distribution of common fish species caught during May (upper panel) and June (lower panel).

3.2. Water Flow Properties

There were 336 ADCP observations that were coincident with the timing of autonomous acoustic backscatter measurements. As expected, the distribution of flow directions was bimodal with peaks centered at 130° and 290° . These directions roughly correspond to the main axis of the channel through Admiralty Inlet. Tidal speeds averaged 1.17 m/s with a median value of 1.07 m/s and a positive standard deviation of 0.657 m/s.

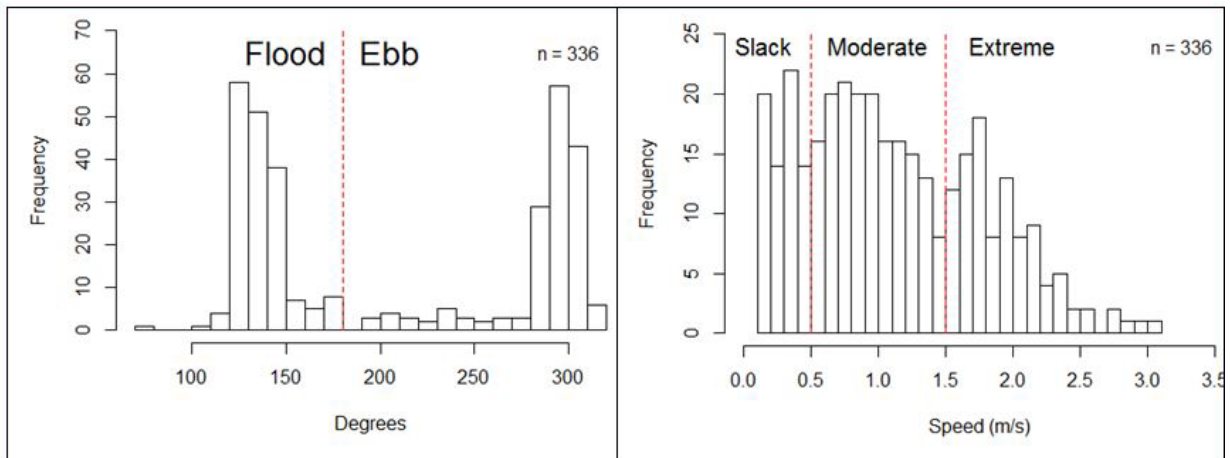


Figure 10. Frequency distribution of tidal direction (left) and tidal speed (right) at the Admiralty Inlet site during May and June 2011.

3.3. Acoustic Data Visualization

3.3.1. Acoustic Backscatter Distribution Patterns

Five different acoustic patterns were observed in the mobile survey data. The dominant feature observed was surface turbulence caused by water motion and small air bubbles becoming entrained by strong tidal mixing (Figure 10a). Surface turbulence was strongest during extreme tidal events and was visible on the surface (Figure 10b). The other four acoustic patterns represented distributions of fish and macrozooplankton. During the day, strong but small midwater targets, consistent with small, densely packed fish, were commonly seen in the water column (Figure 10c). At other times during the day and at night these aggregations dispersed resulting in a “blue fuzz” pattern throughout the water column (Figure 10d). Two types of bottom-associated targets were observed. Large, single targets (Figure 10e) were observed during day and night. These large targets are consistent with bottom-associated piscivorous fish. Finally, bottom-associated aggregations (Figure 10f) were the strongest acoustic targets in the survey. These dense aggregations were meters high and wide, consistent with aggregations of rockfish, Pacific herring, and other small pelagic species.

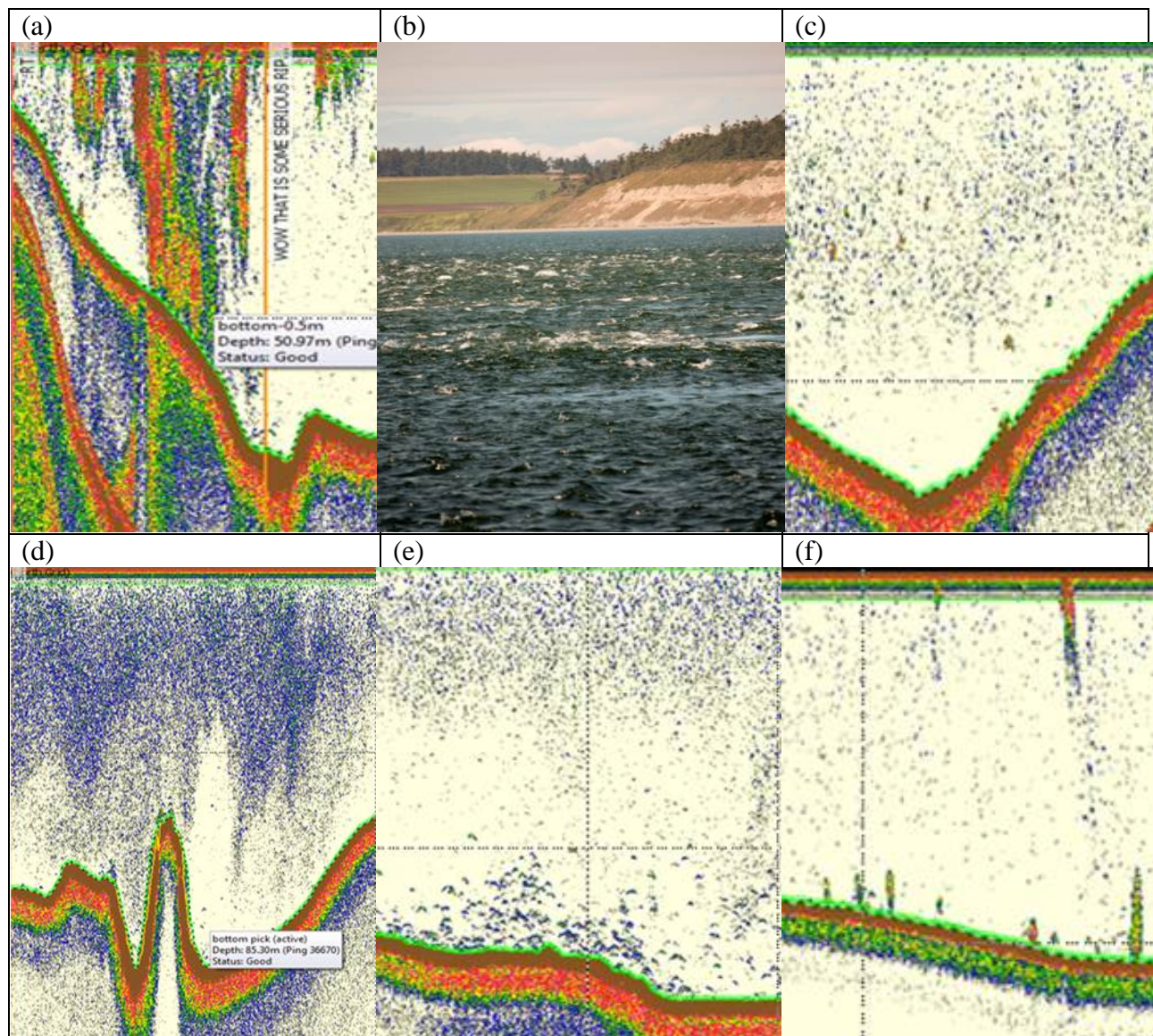


Figure 11. Observed acoustic backscatter patterns within the study location included: (a) turbulence extending from the surface (b) to as deep as 50 m, (c) midwater aggregations of small targets, (d) dispersed individuals forming a “blue fuzz” pattern, (e) single large targets associated with the bottom, and (f) aggregations of small targets associated with the bottom. The seafloor is shown in a and c-f as the neon green line above the dark red region.

The June 7, 2011 data set was integrated and animated in Eonfusion. Time was used to integrate data from each instrument, which differed in format and in the way that data were indexed. The animation (www.acoustics.washington.edu/Eonfusion) was presented as part of an invited oral presentation entitled, “Spatial and Temporal Variability in Pelagic Communities at Marine Kinetic Energy Sites,” at the joint meeting of the European Conference of Underwater Acoustics

(ECUA) and the Acoustical Society of America in Edinburgh, UK held July 2 - 6, 2012. Content of the animation included an overview of the acoustic transects sampled during the sampling period, echosounder and multibeam sonar data used to construct the bathymetry, representations of water column acoustic backscatter and trajectories of single fish, and current velocities through a tidal cycle.

3.4. Acoustic Data Bin Sizes

3.4.1. Horizontal

Autocorrelation plots using echosounder data (Figure 12) indicated that independent horizontal bin sizes occurred at 300 m for mobile survey data and at 24 s for temporally-indexed data based on data categorized as occurring during slack tide. Increased tidal speed in moderate or extreme tidal flows resulted in minor changes in autocorrelation lag distances.

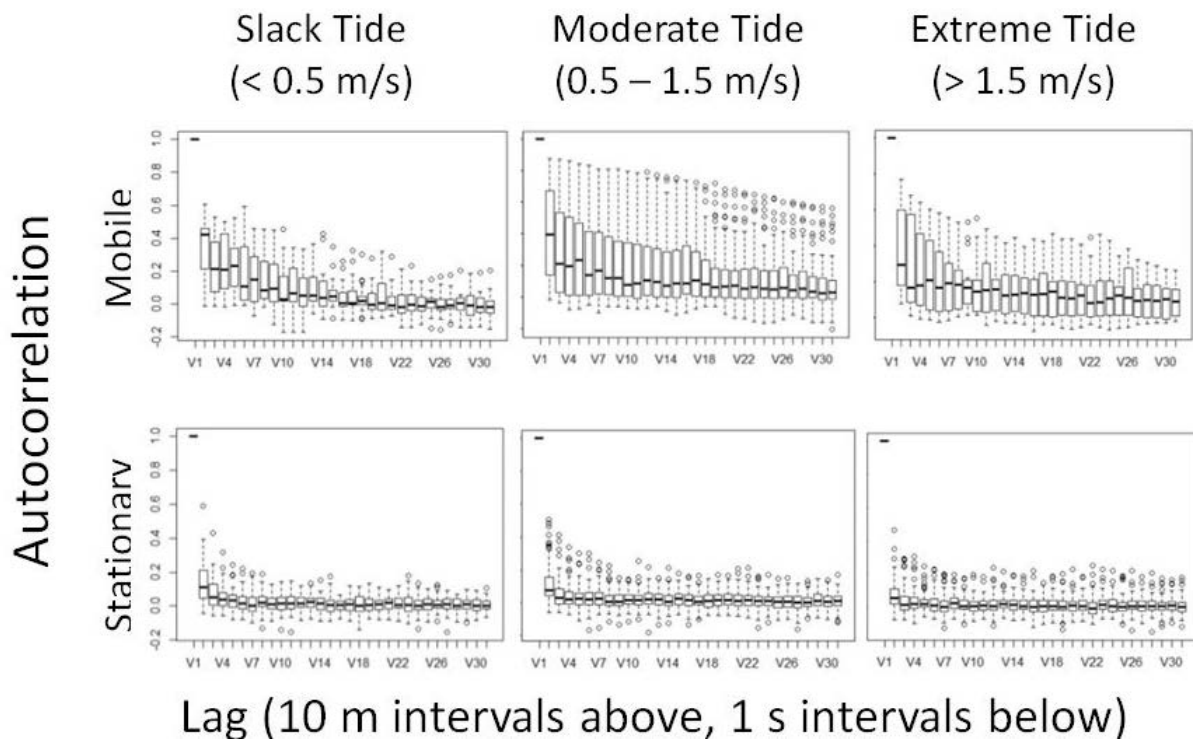


Figure 12. Autocorrelation lag functions of mobile survey (upper panels) and stationary autonomous (lower panels) echosounder data. Arbitrary flow speeds were used to divide data samples into slack, moderate, and extreme tidal flow categories.

3.5. Acoustic Backscatter Variability

3.5.1. Spatially Indexed

Mean S_v values were spatially heterogeneous (Figure 13a) with the southwest (offshore) side of the north grid containing higher densities than the northeast side. Higher mean S_v values occurred along the main axis of the southern grid. Overall, mean S_v values were independent of latitude or longitude (Figures 13b, c) and were normally distributed (Figure 13d).

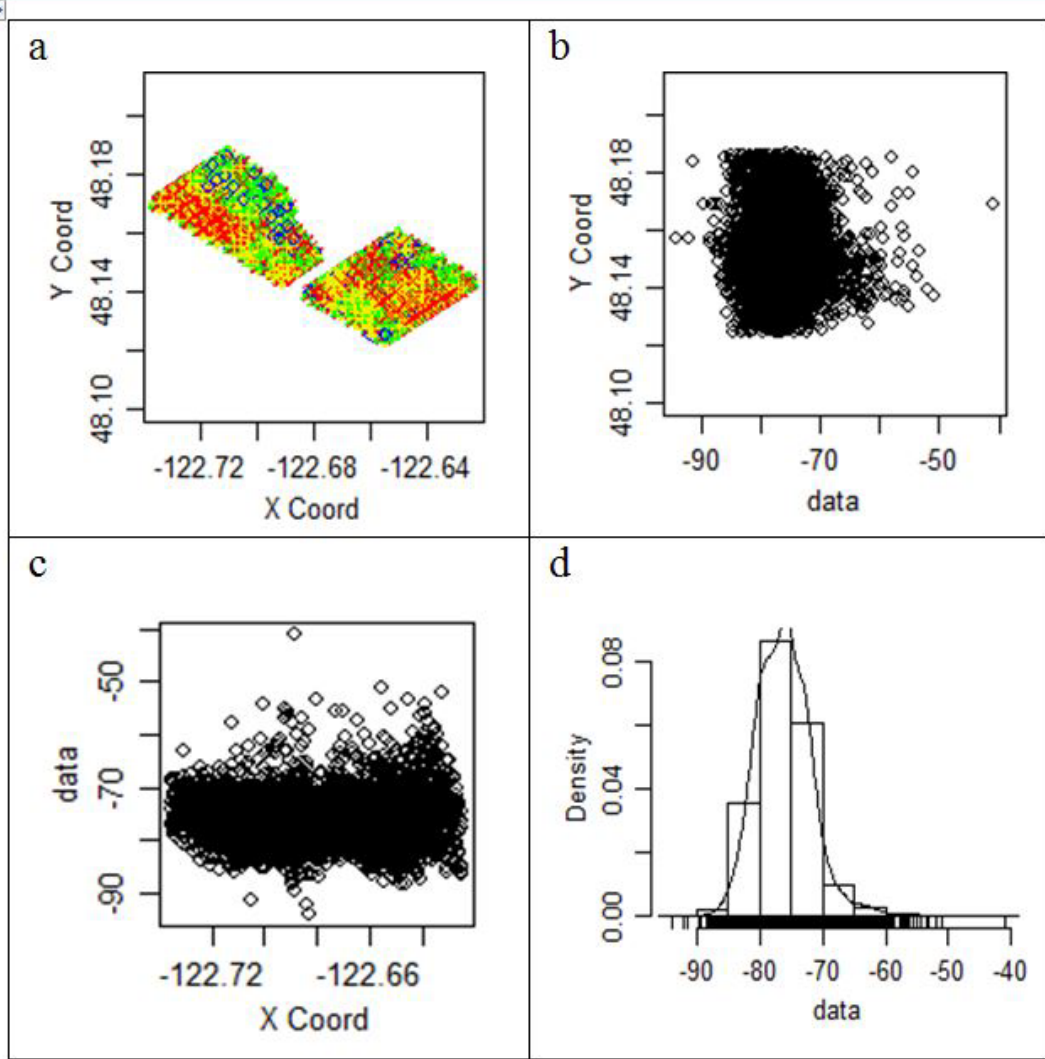


Figure 13. Distributions of aquatic organism density (i.e. mean volume backscattering strength, mean S_v units dB) from mobile survey transects at a horizontal bin resolution of 300 m. (a) Mean S_v along survey transects. (b) Distribution of mean S_v values as a function of latitudinal position. (c) Distribution of mean S_v as a function of longitudinal position. (d) Frequency distribution of mean S_v values.

Echometric values were calculated using mobile echosounder data categorized by grid location, tidal speed, and diel period. Mean S_v increased through the survey with lower values observed at night and in the south grid (Figure 14a, b). Backscatter amplitude and variability was similar across tidal state categories (Figure 14c). Little change in center of mass values was observed between day and night sampling periods (Figure 14a). Center of mass was consistently further from the bottom in the north grid compared to the south (Figure 14b), reflecting deeper mean water depths in the north (31.59 m) compared to the south (23.61 m). No distinct differences were observed in center of mass values between tidal states.

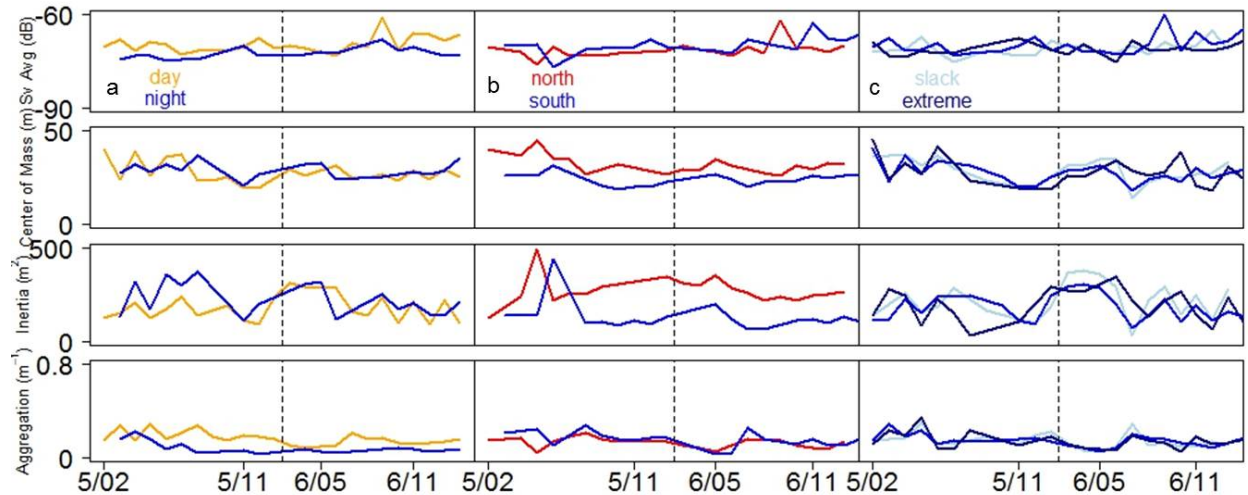


Figure 14. Distribution of echometric values from mobile echosounder data as a function of survey date, categorized by (a) light period (i.e. day/night), (b) grid location (i.e. north/south), and (c) tidal state (slack/moderate/extreme).

Biomass was typically more dispersed through the sampling domain during night in May compared to June (Figure 14a). In parallel, aggregations were more compact during day in both months sampled (Figure 14a). Lower dispersion was observed in the north grid compared to the south with little difference in the patchiness of aggregations. The distribution and patchiness of biomass through the sampling domain did not depend on tidal state.

Given the lack of change in echometric values due to tidal state, it was valid to examine changes in biomass distribution as a function of tidal speed (Figure 15). Mean S_v remained higher in the north grid independent of tidal speed. Mean backscatter values did not differ between months sampled. Center of mass values were independent of tidal speed in three categories, averaging approximately 30 m. After an initial change when tidal speeds were greater than zero, inertia and aggregation index values were essentially independent of tidal speed (Figure 15).

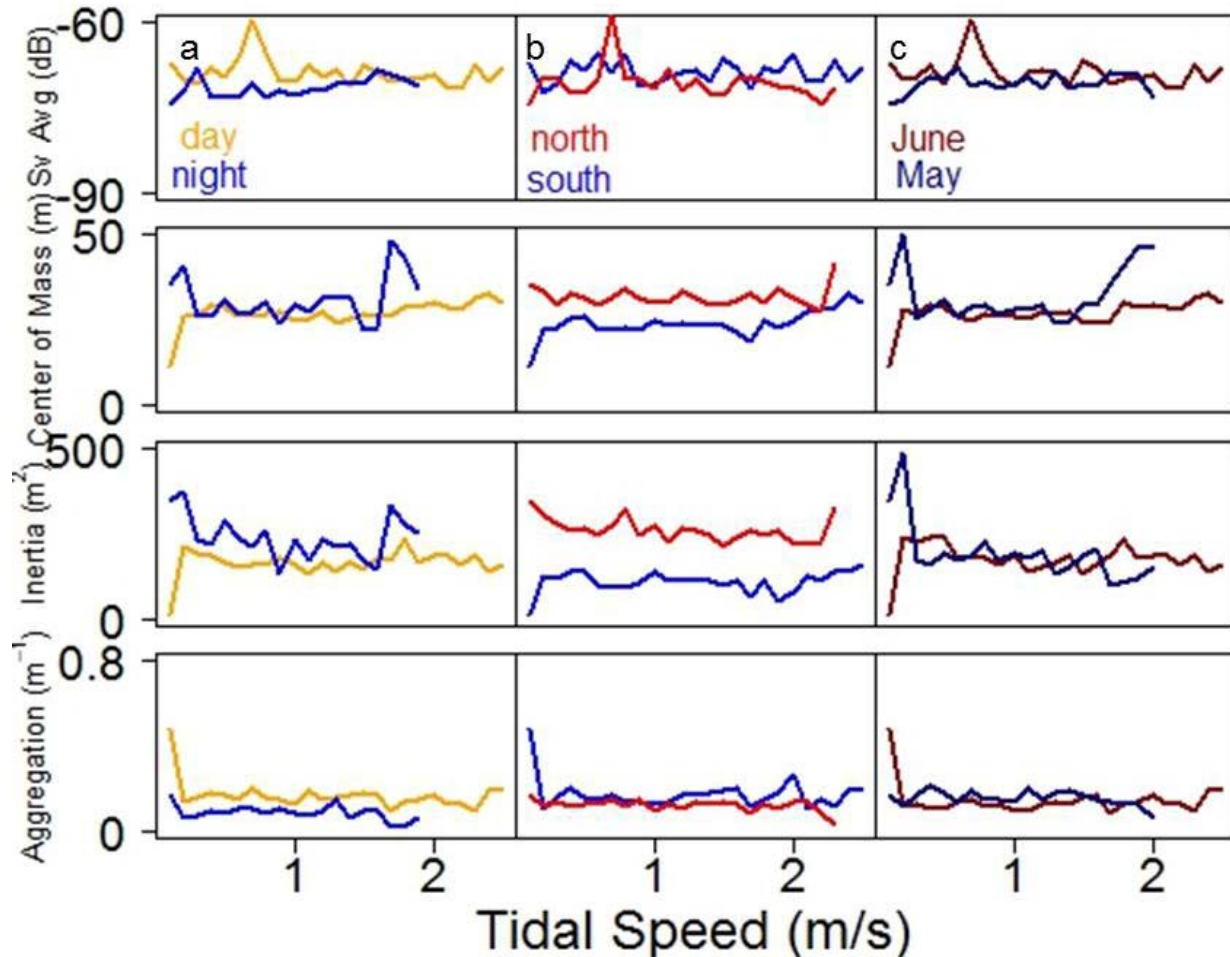


Figure 15. Distribution of echometric values from mobile echosounder data as a function of tidal speed, categorized by (a) light period (i.e. day/night), (b) grid location (i.e. north/south), and (c) date sampled (i.e. May/June).

3.5.2. Temporally Indexed

A saw-tooth, diel pattern dominated values in all four echometric series in the stationary echosounder data (Figure 16). Amplitudes of S_v ranged from -89.67 dB to -63.92 dB, significantly increasing 2 dB through the time series ($n = 336$, $m = 0.006171$ dB/2 hours, $p = 0.0069$, $R^2 = 0.01874$, Figure 16a, Table 5). A 2 dB increase equates to a 58% increase within the month deployment. The center of mass increased almost 3 m higher in the water column through the deployment ($m = 0.008761$ m/2 hours, $p < 0.006966$, $R^2 = 0.031$, Figure 16a), and nekton became more dispersed ($m = 0.03939$ m²/2 hours, $p = 0.0081$, $R^2 = 0.01787$, Figure 16a). The aggregation index remained close to zero throughout most of the time series, punctuated by episodic presence of high aggregation values (Figure 16a). Statistical tests were not applied to the aggregation index because the data were not normally distributed.

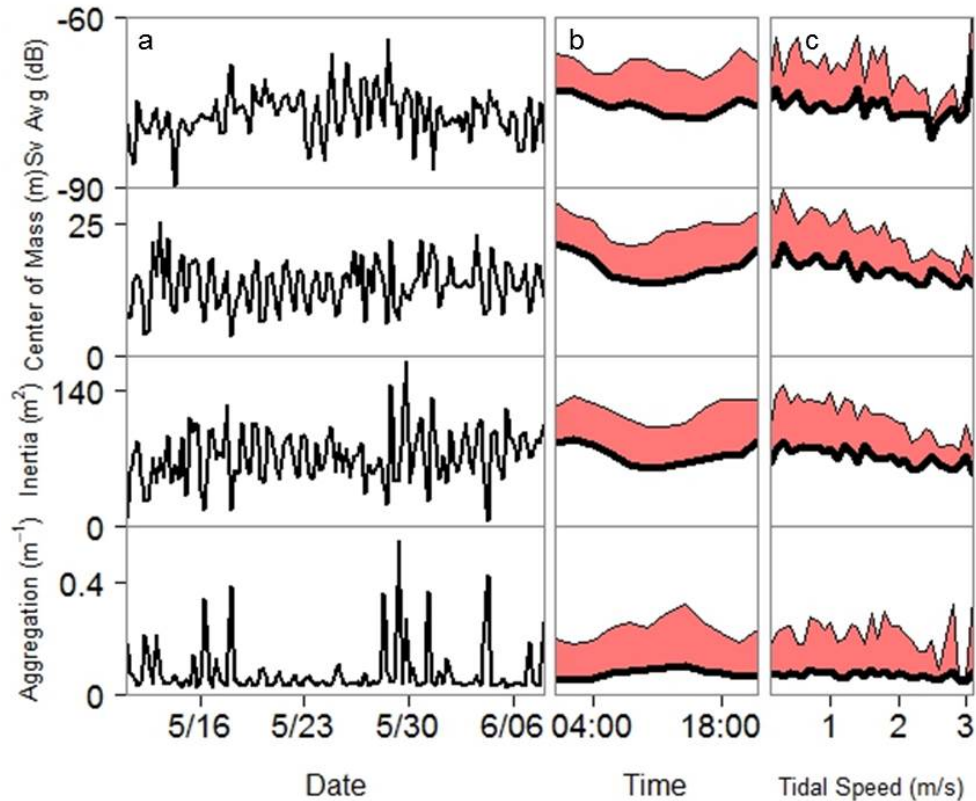


Figure 16. Distribution of echometric values as a function of (a) date, (b) time of day (mean + 2 st. devs.), and (c) tidal speed (mean + 2 st. devs.) for data collected by the autonomous echosounder.

Patterns in the density and distribution of nekton versus time of day were consistent with recognized nekton diel vertical migration patterns (Figure 16b). Acoustic backscatter more than doubled at night (+ 3.5 dB, $p < 0.00001$, $R^2 = 0.1435$) while nekton moved up in the water column (+ 5.6 m, $p < 0.00001$, $R^2 = 0.2604$), and became more dispersed (+ 20.5 m^2 , $p < 0.00001$, $R^2 = 0.1209$). Aggregation index values increased during daylight hours. Variability in all metric values remained relatively consistent through the day.

Echometric values across tidal speed were consistent with observations at other tidal energy sites (NYSERDA 2011). Nekton density decreased as tidal speed increased ($m = -0.69641$ dB/m/s, $p < 0.00001$, $R^2 = 0.0124$, $n = 10,130$, Figure 16c), and moved closer to the bottom ($m = -1.89896$ m/m/s, $p < 0.00001$, $R^2 = 0.07315$, $n = 10,130$) while becoming less dispersed ($m = -8.1284$ $m^2/m/s$, $p < 0.00001$, $R^2 = 0.04466$, $n = 10,130$). Nekton aggregation was independent of tidal speed. In general, variability observed in metric values decreased with tidal speed, but this could be biased due to smaller sample sizes at high tidal speeds (see Figure 9).

Echometric series for the acoustic camera (Figure 17) and ADCP (Figure 18) did not contain the same variability as echometric values in the echosounder series, but did reflect similar patterns in

nekton density and distribution. Both the acoustic camera and ADCP observed an increase in nekton density through time, although only the ADCP was statistically significant (slope = 0.002635 dB/2 hours, $p = 0.0347$, $R^2 = 0.01874$) and the magnitude of change was smaller than in the echosounder (0.006171 dB/2 hours, Figure 17). In general, the acoustic camera and ADCP echometric series measured similar nekton density and distributions as a function of time of day and tidal speed, but the relative magnitude of changes were consistently lower than those in the echosounder echometric series.

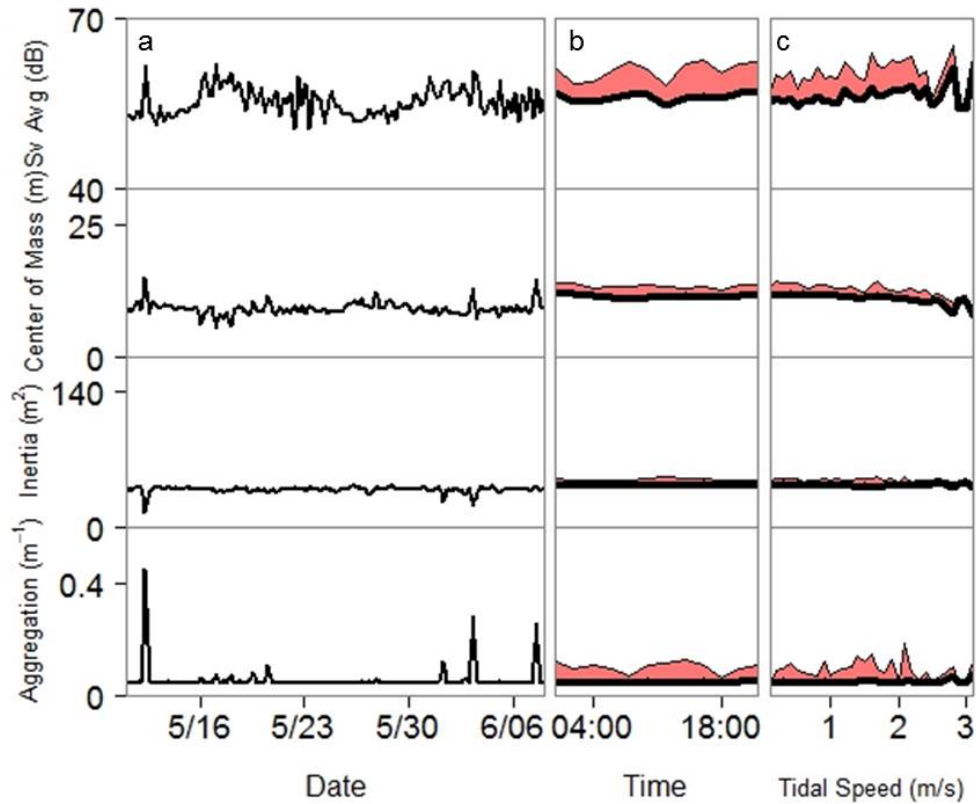


Figure 17. Distribution of echometric values as a function of (a) date, (b) time of day (mean + 2 st. devs.), and (c) tidal speed (mean + 2 st. devs.) for data collected by the acoustic camera.

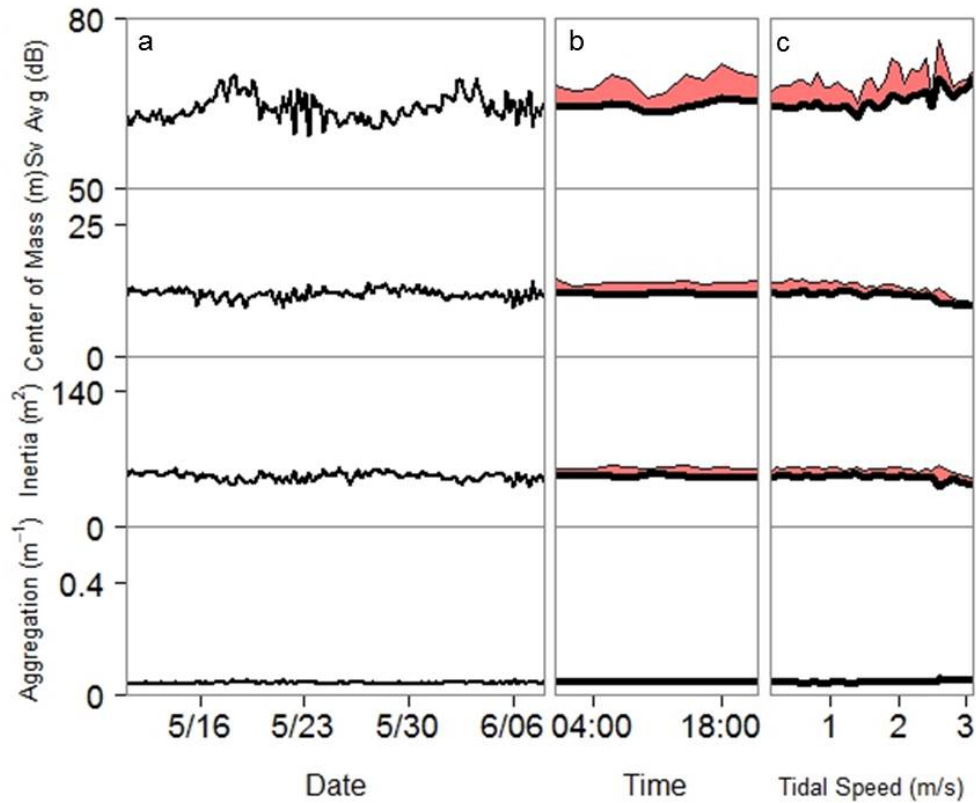


Figure 18. Distribution of echometric values as a function of (a) date, (b) time of day (mean + 2 st. devs.), and (c) tidal speed (mean + 2 st. devs.) for data collected by the ADCP.

At night, both the acoustic camera and ADCP characterized significant increases in nekton density (acoustic camera: + 0.5673 dB at night, $p < 0.00001$, $R^2 = 0.01026$, $n = 10,811$, Figure 17b; ADCP: + 0.45314 dB at night, $p < 0.00001$, $R^2 = 0.009428$, $n = 10,811$, Figure 18b) and center of mass (acoustic camera: + 0.56152 m, $p < 0.00001$, $R^2 = 0.05178$, $n = 10,811$, Figure 17b; ADCP: + 0.36039, $p < 0.00001$, $R^2 = 0.01897$, $n = 10,811$, Figure 18b), but not the same magnitude as the echosounder (+ 3.50823 dB/2 hours, + 5.61108 m). Both the acoustic camera and ADCP observed lower dispersions of nekton at night, which contrasts with the pattern in the echosounder echometric series.

In contrast to the echosounder, nekton density (i.e. mean S_v) increased with tidal speed in the acoustic camera (slope = 0.86751 dB/m/s, $p < 0.00001$, $R^2 = 0.05285$, $n = 10,130$) and ADCP data (slope = 0.69635 dB/m/s, $p < 0.00001$, $R^2 = 0.04121$, $n = 10,130$). Yet, both technologies observed significant decreases in nekton center of mass (acoustic camera: slope = -0.55357 m/m/s, $p < 0.00001$, $R^2 = 0.1144$, $n = 10,130$; ADCP: slope = -0.30274 m/m/s, $p < 0.00001$, $R^2 = 0.03266$, $n = 10,130$) and dispersion (acoustic camera: slope -0.20193 $m^2/m/s$, $p < 0.00001$, $R^2 = 0.001544$, $n = 10,130$; ADCP: slope = -0.49962 $m^2/m/s$, $p < 0.00001$, $R^2 = 0.005057$), consistent with the echosounder.

Table 5:

Significance testing of trends in stationary echosounder survey

Index	Technology	Metric	Slope	N	p	R ²	
Time Series	Echosounder	Mean S _v	0.006171	336	0.006874	0.01874	
		Center of Mass	0.008761	336	0.0006966	0.031	
		Inertia	0.03939	336	0.008099	0.01787	
	Acoustic	Mean S _v	0.002499	336	0.0687	0.0069	
		Camera	Center of Mass	0.0006441	336	0.34	< 0.00001
			Inertia	0.0001924	336	0.922	< 0.00001
	ADCP	Mean S _v	0.002635	336	0.0347	0.01033	
		Center of Mass	-0.0003192	336	0.587	< 0.00001	
		Inertia	-0.008128	336	0.000432	0.03358	
Time of Day	Echosounder	Mean S _v	+3.50823	10,811	< 0.00001	0.1435	
		Center of Mass	+5.61108	10,811	< 0.00001	0.2604	
		Inertia	+20.6315	10,811	< 0.00001	0.1209	
	Acoustic	Mean S _v	+0.56153	10,811	< 0.00001	0.01026	
		Camera	Center of Mass	+0.56152	10,811	< 0.00001	0.05178
			Inertia	-0.61438	10,811	< 0.00001	0.007972
	ADCP	Mean S _v	+0.45314	10,811	< 0.00001	0.009428	
		Center of Mass	+0.36039	10,811	< 0.00001	0.01897	
		Inertia	-0.16706	10,811	0.112216	0.0009646	
Tidal Speed	Echosounder	Mean S _v	-0.69641	10,130	< 0.00001	0.0124	
		Center of Mass	-1.89896	10,130	< 0.00001	0.07315	
		Inertia	-8.1284	10,130	< 0.00001	0.04466	
	Acoustic	Mean S _v	0.86751	10,130	< 0.00001	0.05285	
		Camera	Center of Mass	-0.55357	10,130	< 0.00001	0.1144
			Inertia	-0.20193	10,130	< 0.00001	0.001544
	ADCP	Mean S _v	0.69635	10,130	< 0.00001	0.04121	
		Center of Mass	-0.30274	10,130	< 0.00001	0.03266	
		Inertia	-0.49962	10,130	< 0.00001	0.005057	

3.5.3 Backscatter Covariate Distributions

Mean S_v in the mobile survey ranged from -94.01 dB to -41.06 dB with a median of -76.28 dB (Figure 19). Median densities were consistent between sampling grids, between slack and moderate tidal speeds, while increasing during extreme tidal speeds. Median density increased from May to June and at night compared to day. As median density increased from May to June, the center of mass moved higher in the water column, became more dispersed, and less aggregated.

Spatial differences were apparent in nekton distribution between the north and south sampling grids (Figure 19). Nekton were centered higher in the water column, and were more dispersed in the north grid. Anecdotally, the north grid was deeper than the south grid, possibly exaggerating distribution metrics. The north grid was also in the main channel and wasn't protected from strong tidal currents like parts of the south grid. Median nekton densities more than doubled (118% increase) during night compared to the day (median density -75.8 dB to -79.2 dB, Figure 19a). As expected, nekton moved higher in the water column (median center of mass 20.6 m to 14.6 m, Figure 19b), became more dispersed (median inertia 86.5 m² to 63.7 m², Figure 19c), and less aggregated (median aggregation index 0.04 /m to 0.06 /m, Figure 19d) at night compared to day. This is consistent with nekton diel vertical migration, providing evidence that the mobile survey was able to identify changes in nekton vertical distribution.

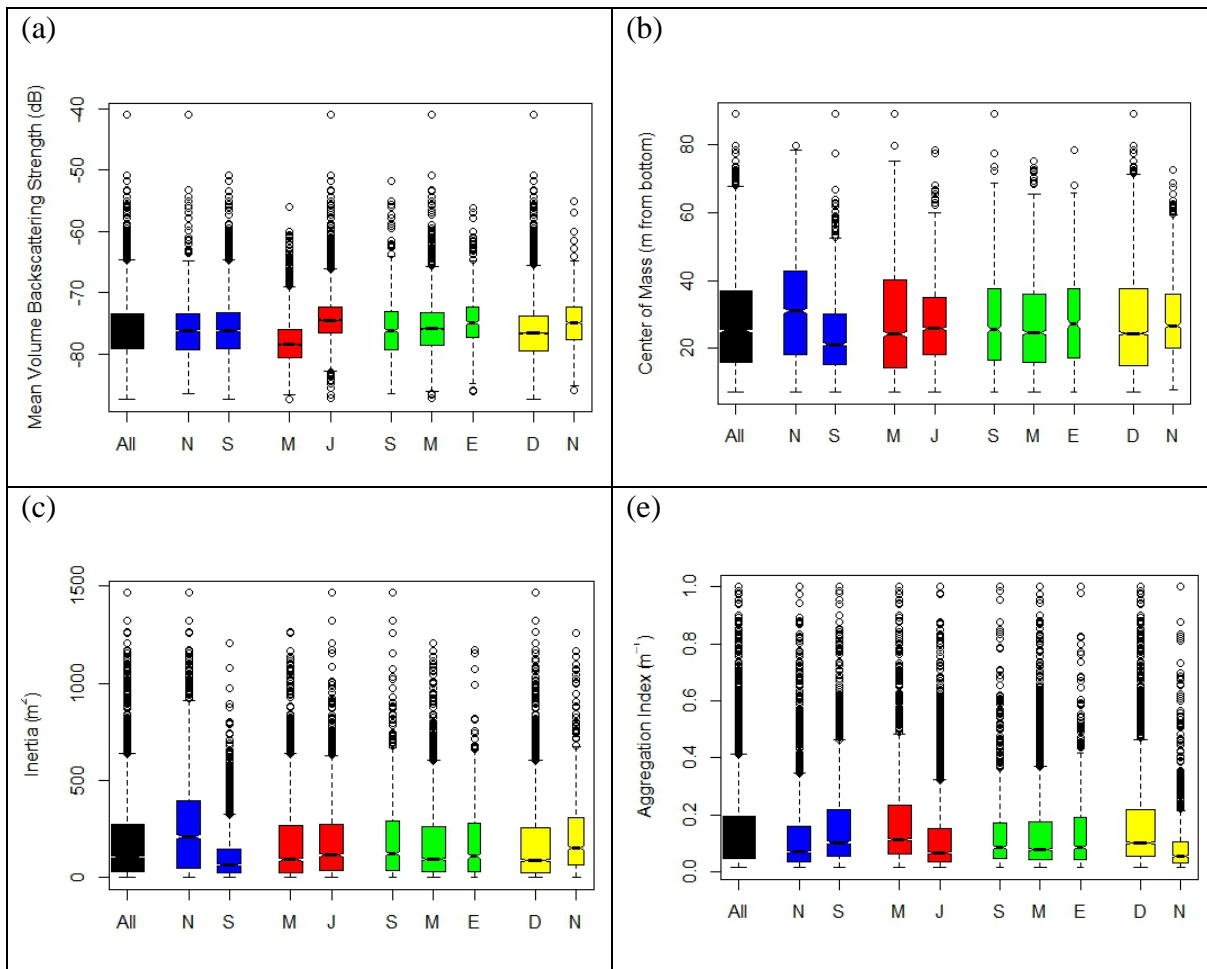


Figure 19. Box and whisker plots visualizing the distribution of echometric values ((a) mean volume backscatter, (b) center of mass, (c) inertia, and (d) aggregation index) for categorical variables grid location (blue; N = north, S = south), month (red; M = May, J = June), tidal speed (green; S = slack (< 0.5 m/s), M = moderate (0.5 < moderate < 1.5 m/s), E = extreme (> 1.5 m/s)), and diel period (yellow, D = day, N = night) for mobile echosounder data.

Within the autonomous echosounder data (Figure 20), nekton density and distribution changed through tidal cycles. Nekton became less dense (median density -76.5 dB at slack tide, -77.2 dB at moderate tidal speeds, and -78.3 dB at extreme tidal speeds, Figure 20a) and moved closer to the bottom (18.2 m to 17.7 m to 15.2 m, Figure 20b) as tidal speed increased. Tidal speed did not affect nekton dispersion at slack or moderate tidal speeds (77.3 m^2 to 79 m^2), but nekton became less dispersed during extreme tidal events (66 m^2 , Figure 20c). Small differences between flood and ebb tides were observed in nekton density (-77.8 dB to -77.2 dB, Figure 20a), center of mass (16.9 m to 16.7 m, Figure 20b), and dispersion (74.8 m^2 to 73.7 m^2 , Figure 20c). Across echometrics, mean S_v values increased slightly during ebb tides while the center of mass and dispersion slightly increased.

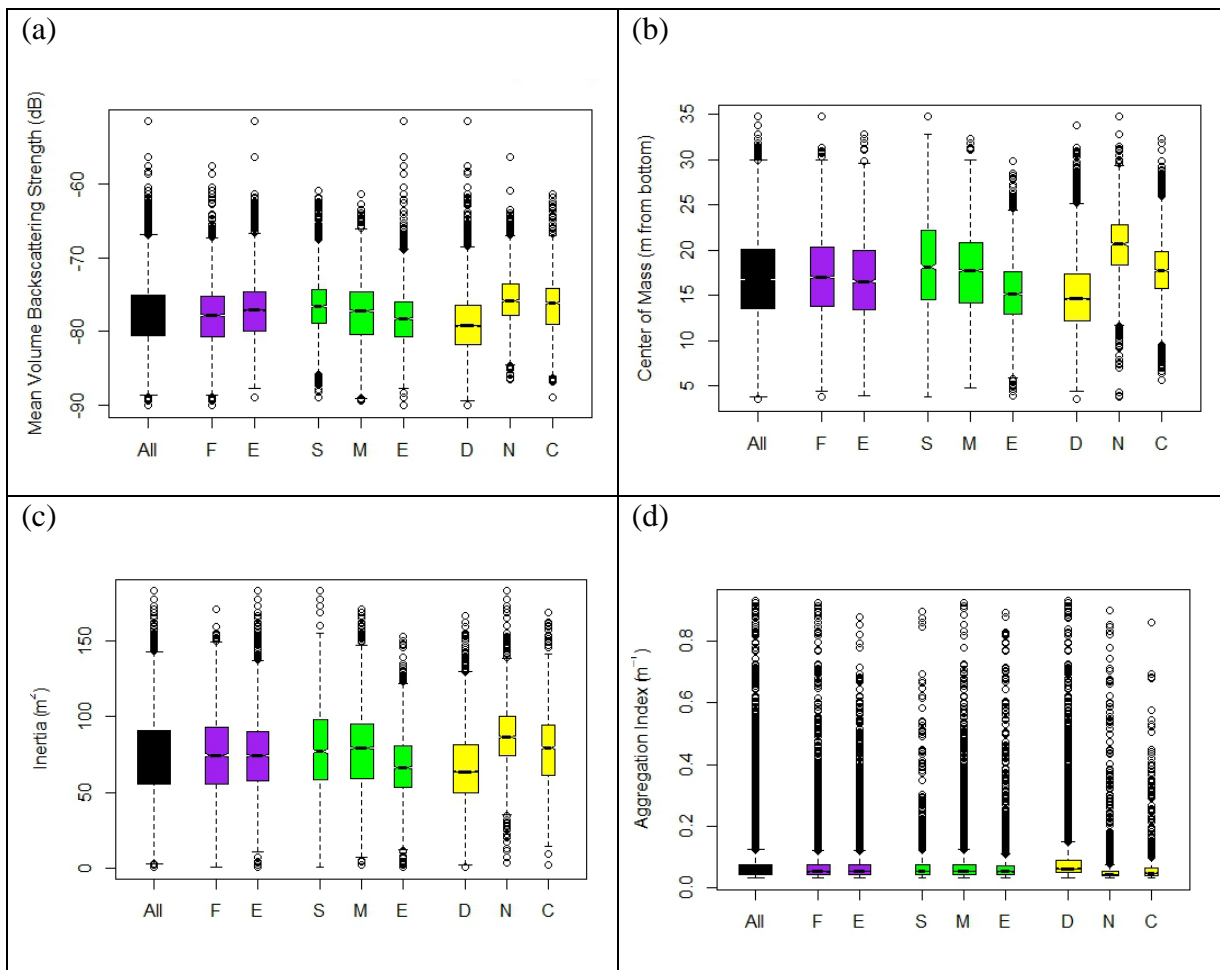


Figure 20. Box and whisker plots visualizing the distribution of echometric values ((a) mean volume backscatter, (b) center of mass, (c) inertia, and (d) aggregation index) for categorical variables tidal state (purple; F = flood, E = Ebb), tidal speed (green; S = slack ($< 0.5 \text{ m/s}$), M = moderate ($0.5 < \text{moderate} < 1.5 \text{ m/s}$), E = extreme ($> 1.5 \text{ m/s}$)), and diel period (yellow; D = day, N = night, C = crepuscular) for autonomous echosounder data.

3.5.4. Vertical Distributions

3.5.4.1. Temporal: Water Column

Mean S_v values increased closer to the bottom (Figure 21a), a trend that was amplified at slack and extreme tidal speeds (Figure 21b), and further exaggerated during ebb compared to flood tides (Figure 21c). The average acoustic backscatter was near uniform through the water column at a moderate tidal speed. In general, the mean S_v within the vertical footprint of the proposed turbine was consistently greater than the mean S_v above.

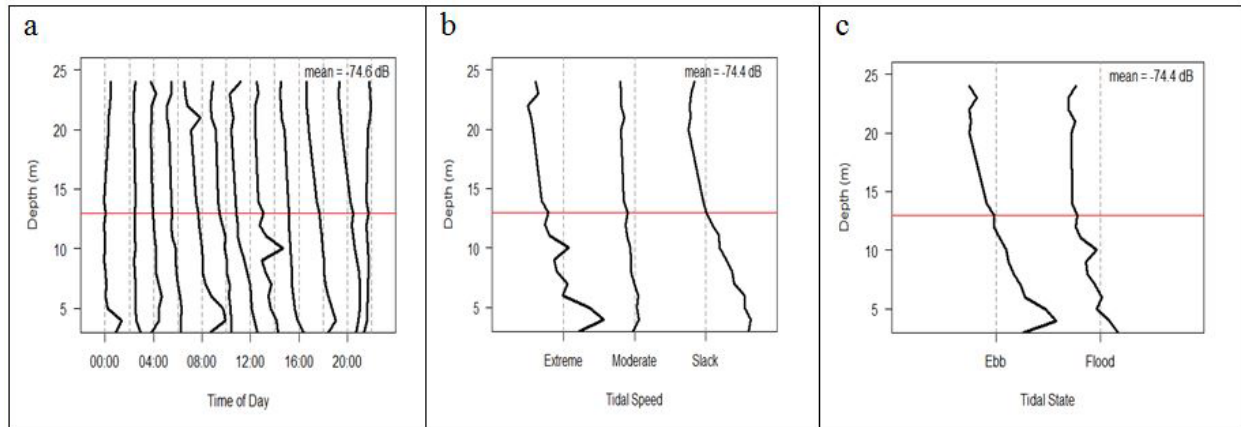


Figure 21. Vertical distribution of mean S_v from the stationary echosounder as a function of (a) time of day, (b) tidal speed, and (c) tidal state. The grey vertical line indicates the mean S_v for the entire time series. The black line indicates the average deviation from the mean for each category at each 1 m depth bin. Grey lines are separated by 7 dB. If nekton were randomly distributed, each black line would match the grey line in each plot.

3.5.4.2. Spatial: Relative to MKH Turbine

Approximately 30% of mobile survey bins had center of mass values at or below the vertical footprint (i.e. 13 m off bottom) of the proposed turbine (Figure 22a). The center of mass minus a standard deviation fell within the vertical footprint of the proposed turbine in ~65% overall, ~60% during the day and ~70% of the night. When proportions were increased to the mean plus two standard deviations, all three categories contained more than of 90% of the center of mass values.

Qualitatively, the percentage of depth bins that overlapped with the vertical footprint of the proposed turbine did not change when data were categorized by day (Figure 22b) or night (Figure 22c).

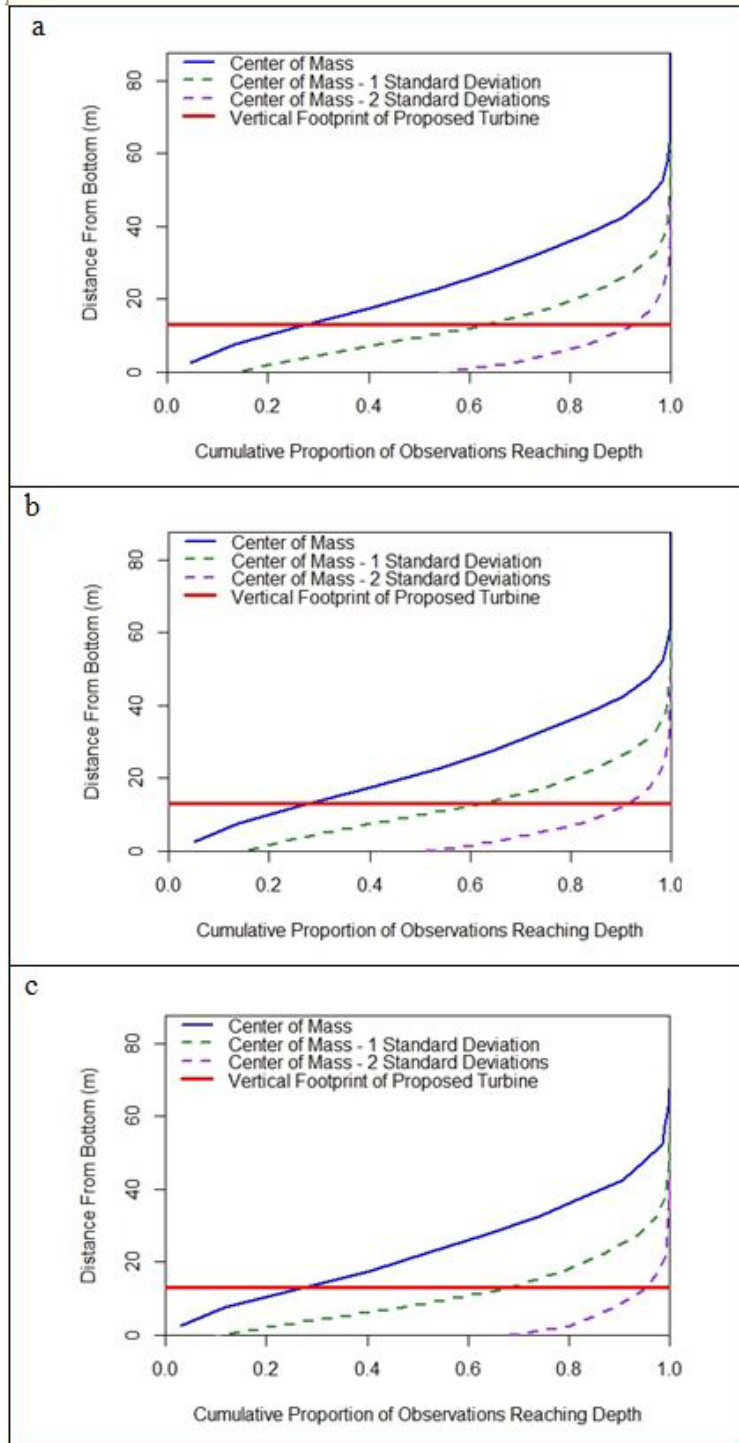


Figure 22. Cumulative proportion of center of mass values from mobile echosounder data as a function of distance from bottom for (a) all, (b) day, and (c) night in 300 m horizontal bins. A reference line of 13 m was added to the plots indicating the vertical height of the proposed turbine. Dotted lines indicate the center of mass minus one (green) and two (purple) standard deviations.

3.6. Acoustic Technology Comparisons

3.6.1. Temporally-Indexed

At the finest resolution (24 s period, 1 m vertical bins), mean S_v measured by the echosounder was positively related to the relative mean S_v measured by the acoustic camera ($p < 0.00001$, $R^2 = 0.01632$, Figure 23 left panel) and the ADCP ($p < 0.00001$, $R^2 = 0.008154$, Figure 23 right panel). Variance in mean S_v increased in both the acoustic camera and ADCP measurements as the echosounder mean S_v measurements increased.

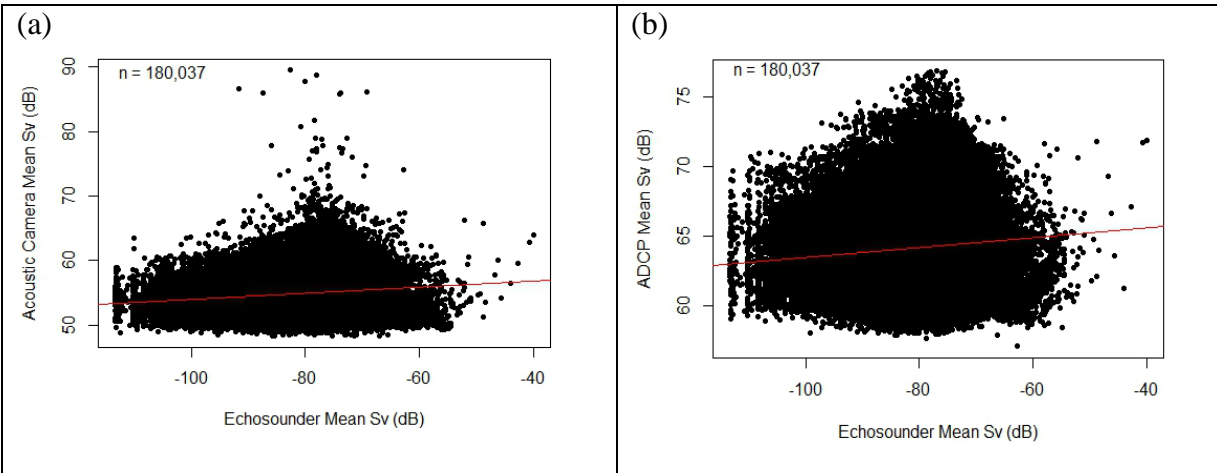


Figure 23. Temporally indexed mean S_v values from the echosounder compared to relative mean S_v values collected by the (a) acoustic camera and (b) ADCP at a resolution of 24 seconds temporal and 1 m vertical bins.

The relative ability of the stationary acoustic technologies to characterize vertical distributions of nekton through the water column at a given time was examined by comparing pairs of echometric values between the echosounder and the acoustic camera (Figure 24) or the ADCP (Figure 25) at a resolution of 24 s temporal and 1 m vertical bins. A significant and positive relationship between coincident measures of density ($p < 0.00001$, $R^2 = 0.01774$) and center of mass ($p < 0.00001$, $R^2 = 0.02338$) occurred between the echosounder and the acoustic camera. There were no significant ($p > 0.05$) relationships in the inertial and aggregation index values between the echosounder and the acoustic camera (Table 6).

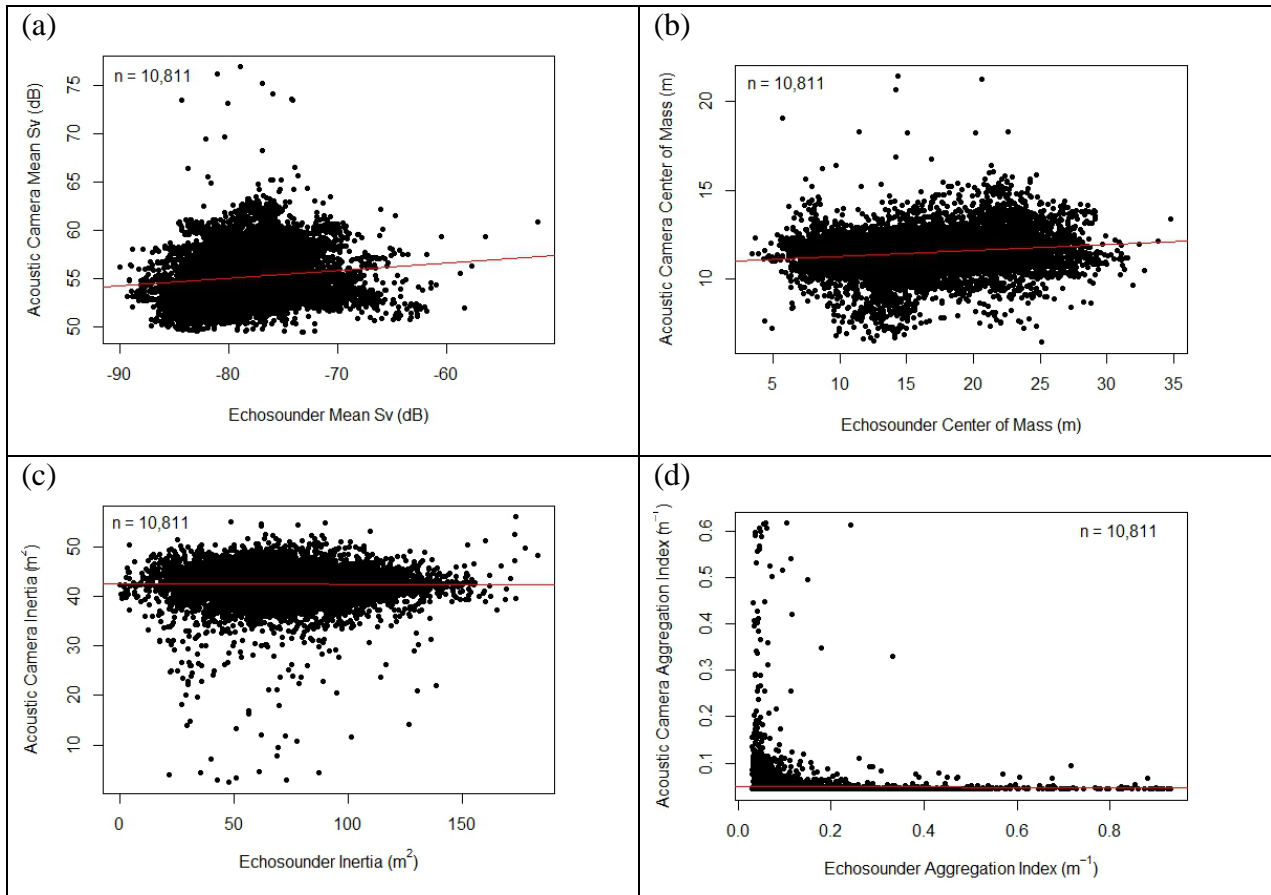


Figure 24. Echometric values ((a) mean volume backscatter, (b) center of mass, (c) inertia, and (d) aggregation index) for the water column at 24 second, 1 m vertical depth resolution, comparing the echosounder to the acoustic camera.

Relationships in echometric values between the echosounder and the ADCP differed depending on the metric (Figure 25). Mean S_v was positively related between the two technologies ($p < 0.00001$, $R^2 = 0.00933$) with the variance increasing with the amplitude of the echosounder. There were no positive relationships in the center of mass, inertia, or aggregation index comparisons (Table 6).

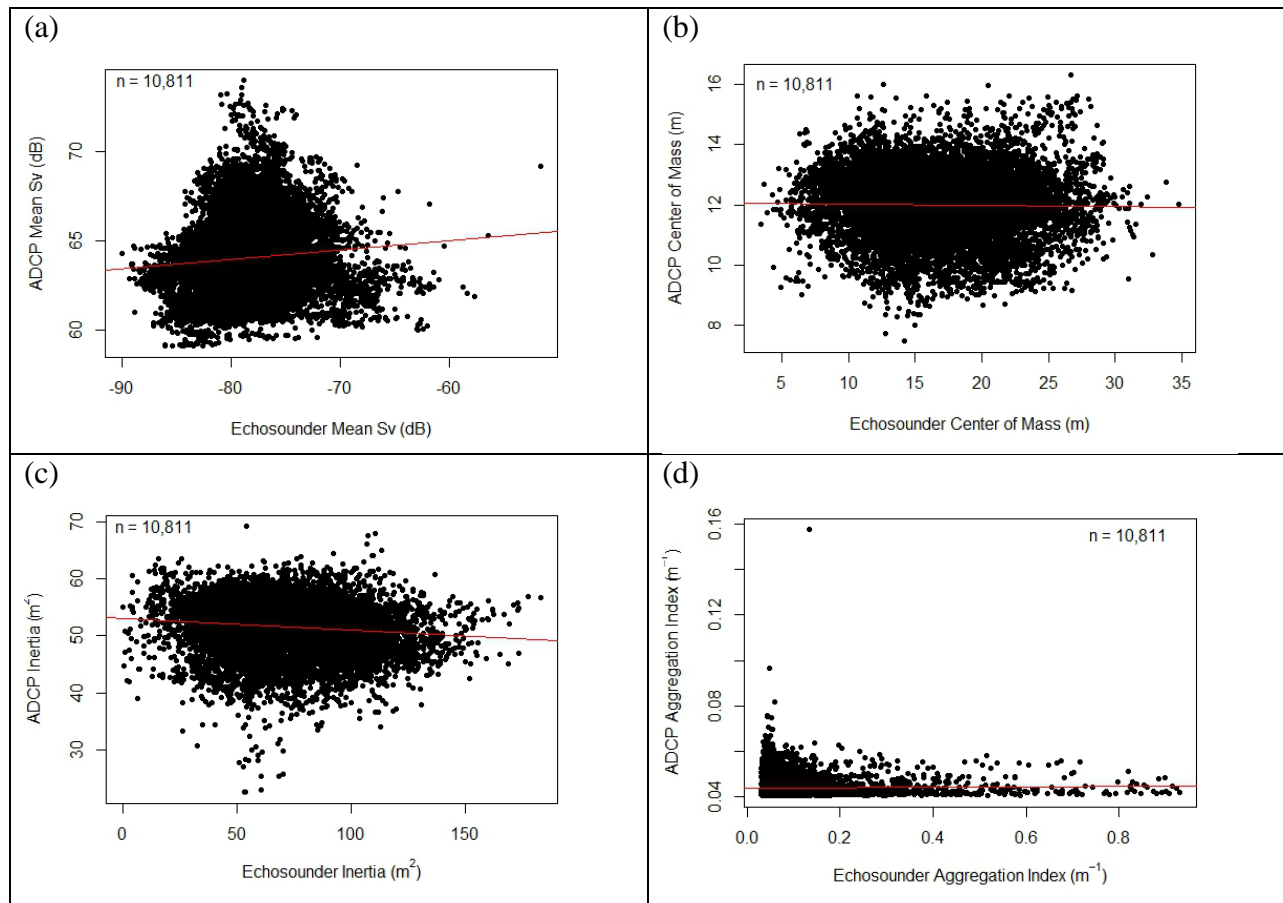


Figure 25. Comparison of echosounder and ADCP echometric ((a) mean volume backscatter, (b) center of mass, (c) inertia, and (d) aggregation index) measurements for the water column at 24 second 1 m vertical bin resolution.

Table 6.

Comparison of echometric data from echosounder and acoustic camera or ADCP in 24 second temporal bins. CoM stands for Center of Mass, AI stands for Aggregation Index.

	Acoustic Camera				ADCP			
Metric	Density	CoM	Inertia	AI	Density	CoM	Inertia	AI
P-value	< 0.00001	< 0.00001	0.3737	0.3006	< 0.00001	0.08708	< 0.00001	0.05199
R ²	0.01774	0.02338	< 0.00001	< 0.00001	0.00933	0.00018	0.01304	0.00026

3.6.1.1. Whole Water Column, 12 min

To examine potential effects of temporal bin size on relationships between acoustic technology pairs, additional comparisons between the echosounder and the acoustic camera (Figure 26) and ADCP (Figure 27) were conducted using 12 minute temporal bins. An increased bin size decreased variability in measurements of nekton density and distribution that may have masked relationships at the higher (i.e. 24 second) temporal resolution. Increasing the temporal bin size reduced the sample to 358 time blocks. When comparing the acoustic camera to the echosounder, there were significant relationships in the mean S_v (Figure 26a; $p = 0.0007124$, $R^2 = 0.02899$) and center of mass (Figure 26b; $p = 0.005048$, $R^2 = 0.01913$) echometrics, but no relationships in the inertia (Figure 26c) or aggregation indices (Figure 26d). Probability and significance values are summarized in Table 7.

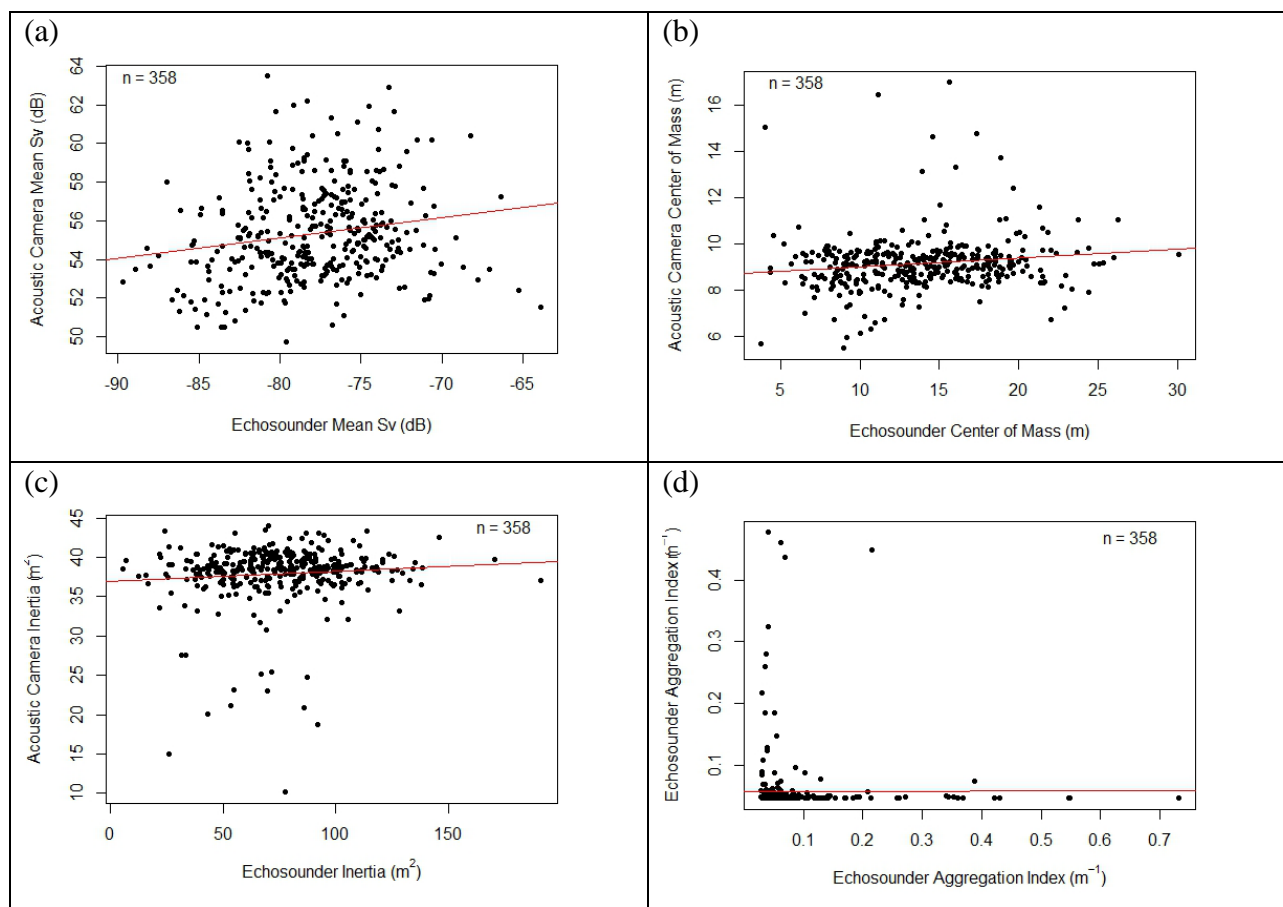


Figure 26. Echometric values ((a) acoustic density, (b) center of mass, (c) inertia, (d) aggregation index) summarizing the entire water column at 12 minute resolution, comparing the echosounder to the acoustic camera.

For the ADCP and echosounder comparison, significant relationships were limited to mean S_v (Figure 27a; $p = 0.03263$, $R^2 = 0.009987$) between the echosounder and ADCP between 12 minute temporal bins. Variance in the ADCP measurement of mean S_v increased as echosounder mean S_v . No trends were significant in the center of mass (Figure 27b), inertia (Figure 27c), or aggregation (Figure 27d) echometric comparisons.

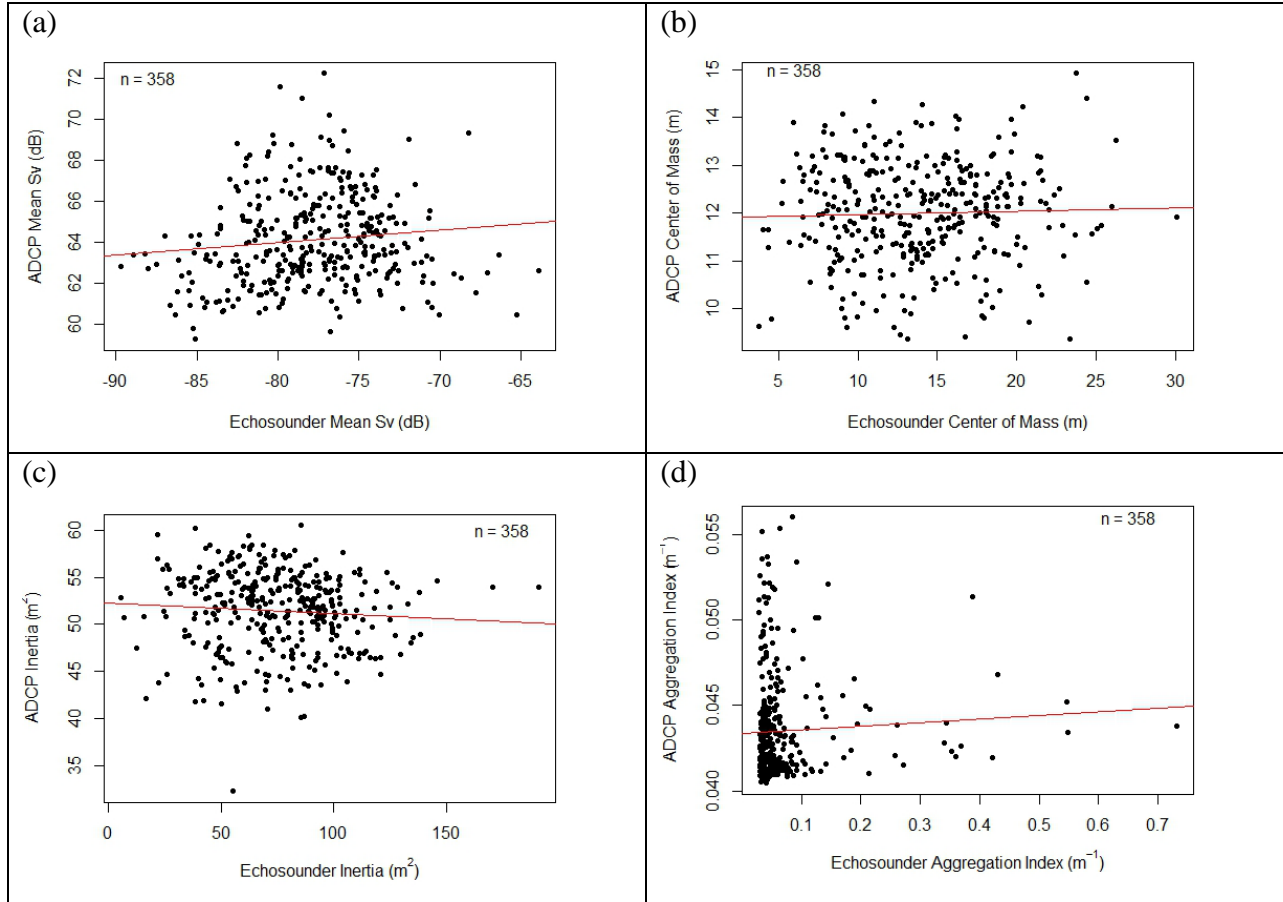


Figure 27. Comparison of echosounder and ADCP echometric values measuring (a) acoustic density, (b) center of mass, (c) inertia, (d) aggregation index summarizing the entire water column at 12 minute temporal resolution

Table 7

Comparison of echometric values from comparisons of the acoustic camera or ADCP to the echosounder in 12 minute temporal bins. CoM stands for Center of Mass, AI stands for Aggregation Index.

	ADCP				Acoustic Camera			
Metric	Density	CoM	Inertia	AI	Density	CoM	Inertia	AI
P-value	0.03263	0.5227	0.1753	0.292	0.00071	0.00505	0.09683	0.9384
R ²	0.00999	< 0.00001	0.00236	0.00038	0.02899	0.01913	0.00494	-0.00279

3.6.2. Spatial-Temporal Comparison

Magnitudes and variability in mobile and stationary echometric values from the echosounder data were compared to examine the relationship between spatially- and temporally-indexed data, and to test the sensitivity of each data set to detect changes in nekton density or distribution. The same trends were present in both the mobile and stationary data for all four echometrics over the periods sampled (Figure 28a), with higher frequency fluctuations observed in the stationary echosounder series. Mean S_v increased over the May and June sampling periods. Mobile inertia values were significantly higher by an order of magnitude than values from the autonomous survey. Inertia values from the south grid were closer to those of the stationary series (Figure 28a), possibly an artifact of the similarity in average depths at the south grid and the locations of the autonomous acoustic instrument packages. Aggregation index values for both mobile and stationary series were low, with the stationary series containing large, irregular spikes that were not observed in the mobile survey.

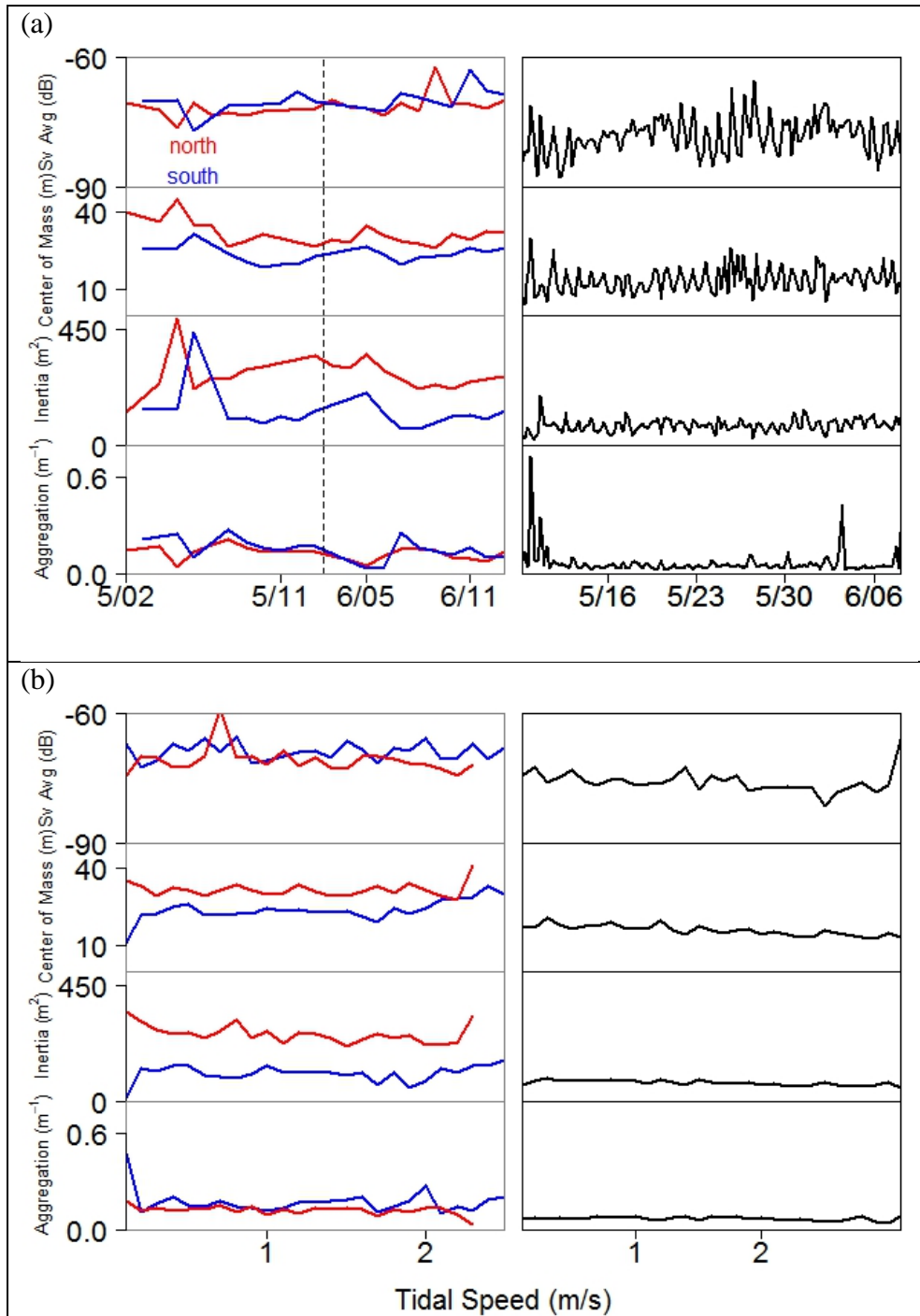


Figure 28. Distribution of mobile (left panel, red = north grid, blue = south grid) and stationary (right panel) echometric values from echosounder data as a function of (a) date and (b) tidal speed. The left panel is taken directly from the middle column in Figure 14(a) and Figure 15(b). The right panel is taken from Figures 16(a, b).

Higher variability was observed in the mobile echometric values when metrics were indexed by tidal speed (Figure 28b). Mean S_v was slightly higher in the mobile survey data than in the stationary data. Echometric values across the range of tidal speeds remained constant in the mobile survey. Center of mass metric values decreased in the stationary survey as tidal speed increased. Inertia values declined slightly in both echosounder series, with the stationary series remaining higher across all tidal speeds. Aggregation index values were low and consistent in both series across all tidal speeds (Figure 28b).

In general, mobile echosounder echometric values suggested that there were spatial differences in center of mass and dispersion by pairing north and south grids, but the metrics did not match the high frequency variability observed in the temporally-indexed series from the stationary echosounder. Both spatial and temporal echometric series detected an increase in nekton density through time (mobile: 0.1115 dB/day, $p < 0.00001$, $R^2 = 0.1787$, $n = 5054$; stationary: 0.074052 dB/day).

3.6.2.1. Acoustic Backscatter Patterns

During mobile surveys, the vessel occasionally passed over the bottom-deployed, autonomous acoustic instrument packages when they were actively sampling. In the two examples below (Figure 29), surface backscatter aggregations occur in the echogram from the mobile survey (top panels), the acoustic camera (middle panels), including the second surface echo that is visible halfway down the echogram, and in the echogram from the bottom-mounted echosounder (bottom panels). The second surface in the echogram from the bottom-mounted echosounder appears as a green band running through the middle of the echogram.

3.6.2.2. Coincident Echosounder Measurements

Three different measurement scopes (i.e. ratio of sample range to resolution) were used to examine if the mobile and stationary echosounders were detecting the same magnitudes and ranges of change in mean S_v . Temporal resolutions were set at the 12 minute sampling bins of the stationary instruments. The spatial sampling range was increased from that of a transect (low scope), to the portion of the grid containing the transect (medium scope), to the entire grid (high scope).

In the low scope plots, a positive, a linear, positive relationship was present in the mean S_v (Figure 30a) although with higher variability in the mobile data. The two series were independent in the center of mass metric (Figure 30b), with comparable ranges in both series. A negative, linear relationship was evident in the inertia plot (Figure 30c), with the stationary series having larger average values. Aggregation index values for the four sampling days were clustered around a value of 0.1 /m for both data sets (Figure 29d).

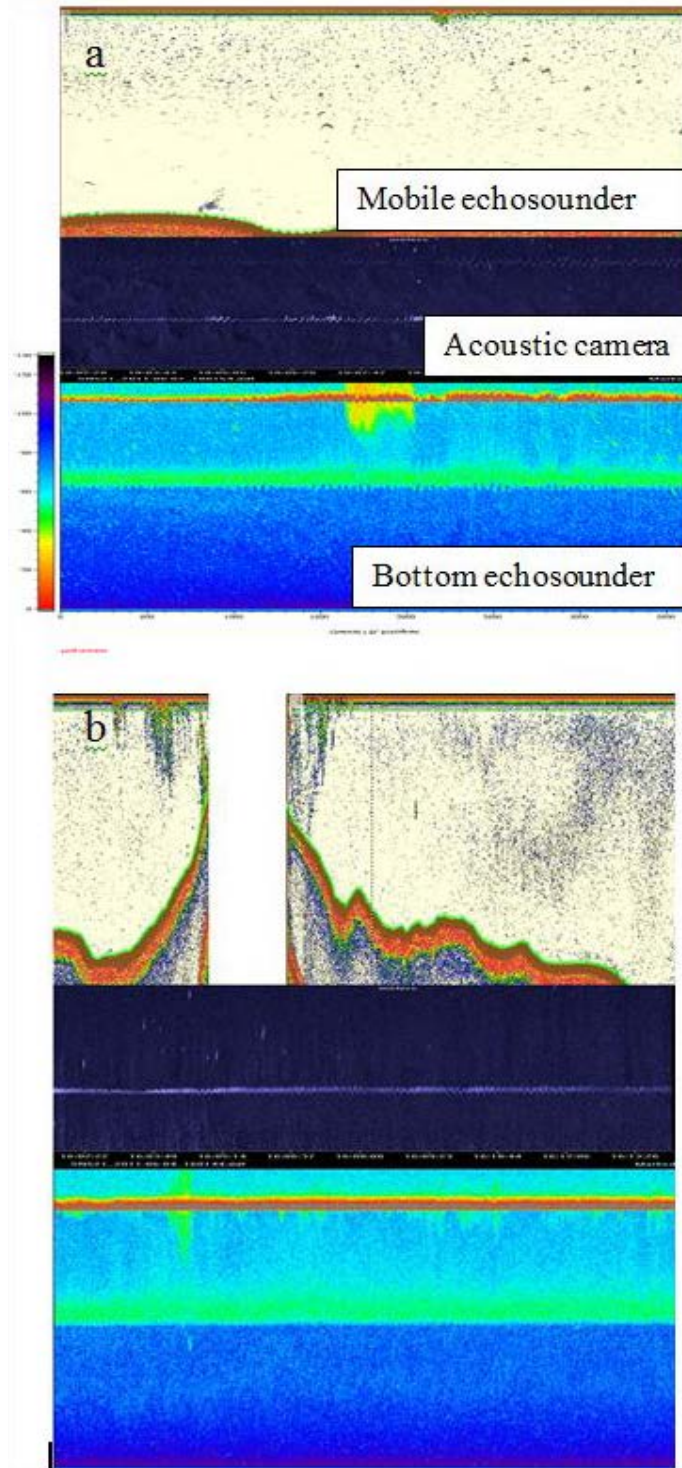


Figure 29. Coincident data collections from the mobile echosounder (top), bottom-mounted acoustic camera (middle), and bottom-mounted echosounder (bottom). Examples are shown from (a) June 7, 2011 at 10:00, and (b) June 4, 2011 at 16:00.

Magnitudes remained consistent in the medium scope plots. Average integrated backscatter (Figure 30a) shifted from a positive linear to an independent relationship.

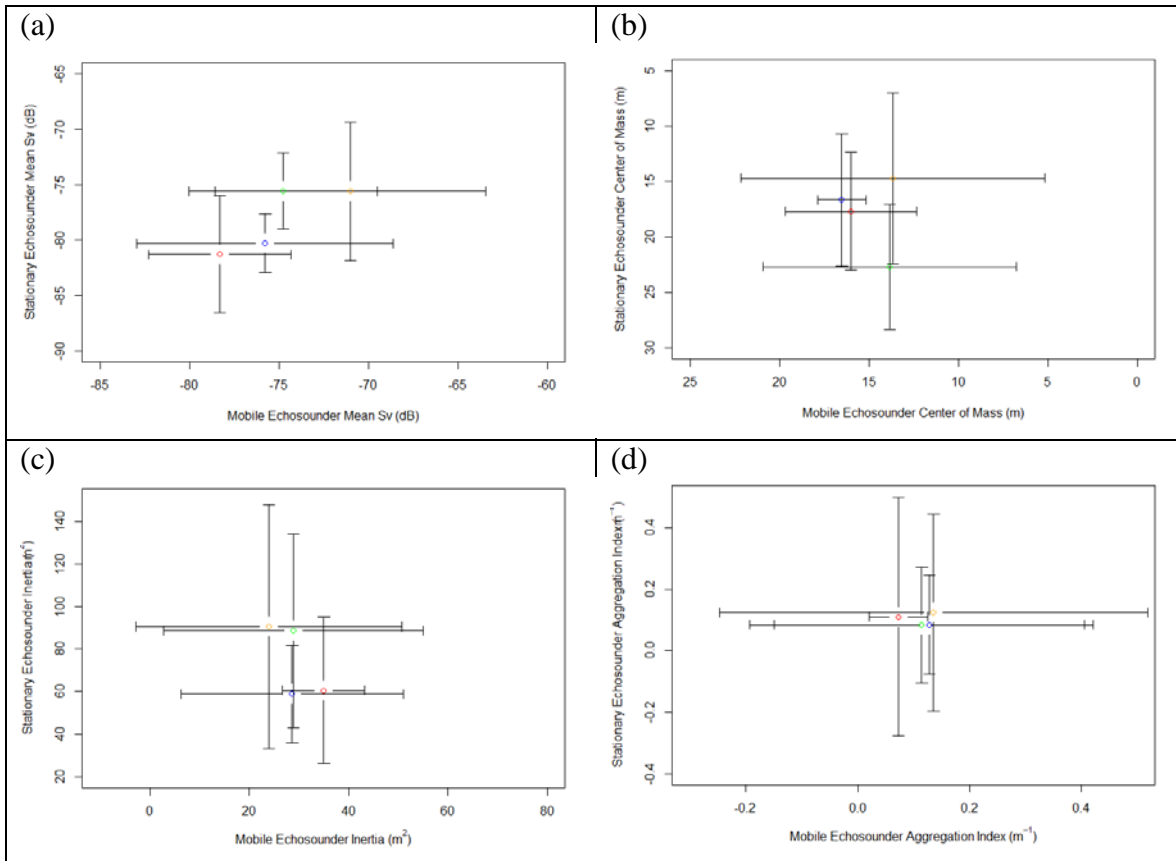


Figure 30. Comparison of coincident mobile and stationary echosounder echometric values of (a) acoustic density, (b) center of mass, (c) inertia, and (d) aggregation index using low scope mobile measurements (single transects compared to 12 min temporal bins).

Center of mass (Figure 30b) values remained independent in the two series. The negative linear relationship in the inertia metric (Figure 30c) was retained at medium scope. Aggregation index (Figure 30d) values remained clustered around the value of 0.1 /m.

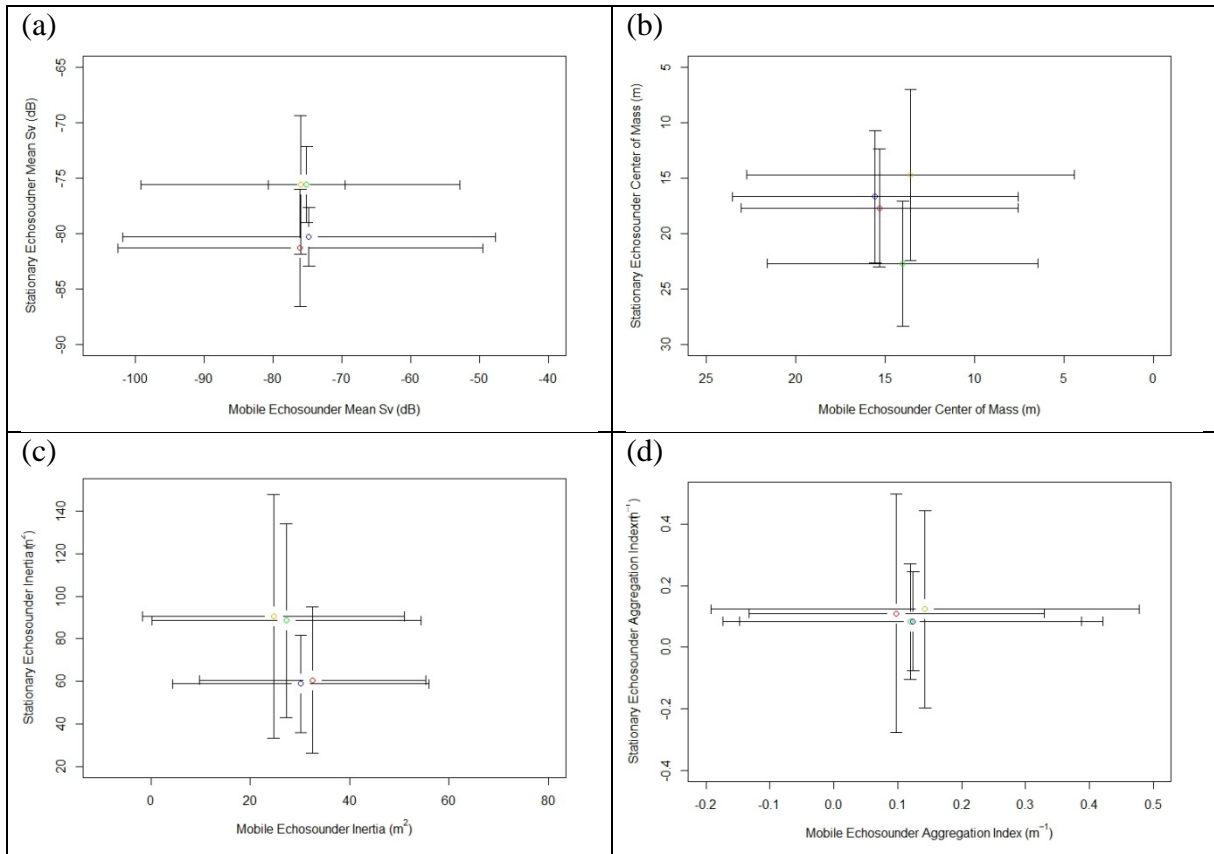


Figure 31. Comparison of coincident mobile and stationary echosounder echometric values of (a) acoustic density, (b) center of mass, (c) inertia, and (d) aggregation index using medium scope mobile measurements (high or low resolution portions of mobile grid compared to 12 minute temporal bins).

Magnitudes and ranges of individual echometric values remained consistent at a high scope. Mean values in the integrated backscatter (Figure 32a) and center of mass (Figure 32b) were independent in the two echosounder data series. The linear relationship previously observed in the inertia echometric comparison shifted to an independent relationship (Figure 32c). Values of the aggregation index remained near 0.1 /m for samples from both echosounders (Figure 32d).

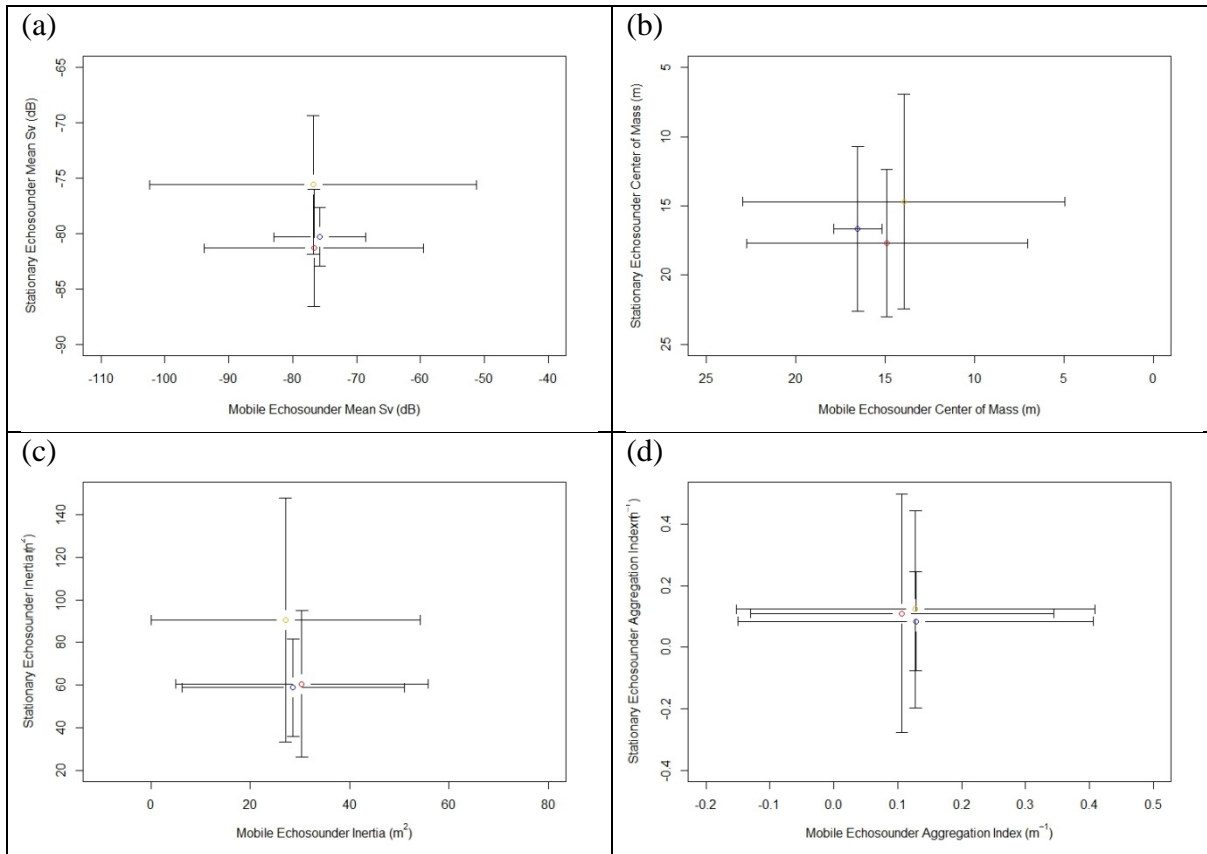


Figure 32. Comparison of coincident mobile and stationary echosounder echometric metric values of (a) acoustic density, (b) center of mass, (c) inertia, and (d) aggregation index using high scope mobile measurements (mobile grid compared to 12 minute temporal bins).

When comparing echometric values across scopes, patterns were not consistent between the mobile and stationary echosounder data. Similar patterns were observed in coincident measures low scope measurements of mean S_v , but these patterns were not consistent when the mobile sampling range increased (i.e. across scopes) or across metrics. The similarity in patterns of mean S_v observed between the low scope mobile measurements and the stationary survey confirmed that the two instruments were calibrated and that detection sensitivities were similar. Positive relationships were not observed in all echometric plots. The negative linear trend observed in the low and medium scope inertia plots suggested that echometric values from the mobile echosounder were roughly 2 times greater than values from the stationary echosounder during the same time frame. The low and medium scope center of mass plots suggested a negative relationship between the two series but similar mean and large standard deviation values masked any trends within or among scope plots. Average values in the aggregation index plots were constant across all scopes.

4. DISCUSSION

Marine renewable energy (MRE) sites are, by definition, dynamic environments that require instrument configurations that can withstand enhanced water flows, and robust technologies to deploy and retrieve instrument packages. When characterizing and monitoring MRE sites, enhanced water flows and associated turbulence are dominant and persistent features that influence sampling efficiency and subsequent data analyses. Acoustic technologies provide a suite of tools that can be used to monitor these sites and are more effective when combined with direct sampling tools such as trawls. A single acoustic instrument will not provide all data needed for baseline measurements or to satisfy the requirements of an operational monitoring program. Combinations of mobile acoustic surveys with bottom-deployed instrument packages are needed to provide an effective solution for MRE site characterization and operational monitoring.

The primary objective of this study was to compare data from all acoustic technologies through the evaluation of mean volume backscatter (S_v) and derived metrics. While this approach provided an apples-to-apples comparison of data, it did not exploit all of the intended uses of each technology. The acoustic camera is designed to provide near optical quality images over relatively short distances. The intended use of ADCPs is to quantify water speed and direction. All acoustic technologies used in the study detected organisms in the water column, but sensitivity and dynamic range was not equal across instruments. Given the rigor used to calibrate scientific echosounders, this technology was used as the baseline in all instrument comparisons. Data from the acoustic camera and ADCP were used as relative indexes of organism density.

The use of derived metrics to describe aquatic organism vertical distributions provides several advantages over traditional backscatter measurements. Calculation of metric values using backscatter data enables a comprehensive yet parsimonious characterization of biomass through the water column. Traditional S_v measures, still part of the echometric suite, are used to quantify density in arbitrary vertical strata. The application of these metrics is also independent of location, time, species composition, species diversity, and type of technology deployed at any potential or operational MRE site. The generic nature of the metric suite facilitates monitoring change in biological conditions over any spatiotemporal scales of interest and the identification of locations or instances when regulatory thresholds have been exceeded. The utility of this approach will be fully realized when echometric calculations are automated in near real time as part of the operating software in monitoring packages.

Variability in S_v values was observed in data from all acoustic technologies across categorizing variables. Both the surface and bottom-mounted echosounders, with higher sensitivity and dynamic range, contained the highest range of backscatter and metric values compared to the other technology classes. The lowest range of echometric values was observed in the ADCP data. The multibeam data could not be examined but given the sensitivity and dynamic range specifications of scientific multibeam sonars, data ranges are expected to match those of echosounders. A caveat for this comparison is that data constraints limited this comparison to the first 26 meters of the water column off bottom. This depth range does not include variability

in near surface waters, but does correspond to twice the vertical height of the OpenHydro turbine proposed for the Admiralty Inlet MRE site. High variability in biomass fluxes increases the complexity of defining effects and impacts of single or multiple MRE device operations on biological communities.

Nekton densities were higher during night observations than during the day, with dominant periodic variability in echosounder data at 6 and 12 hour cycles, consistent with semi-diurnal tides and light cycles in marine environments. Periodic changes in acoustic backscatter are attributed to the diel behavior of fish and macrozooplankton where animals ascend toward surface and disperse during dark hours to feed and to reduce predation risk (Blaxter 1975; Helfman 1993; Pitcher and Parrish 1993). Animals higher in the water column and more dispersed make them more available to all acoustic technologies regardless if they are deployed on the surface or on bottom. Vertical distribution plots of S_v also showed increased densities closer to bottom with increased tidal speeds irrespective of time of day or tide state. This result may have been influenced by data use as tidal speeds at all depths were indexed to the tidal velocity measured 10 m off bottom (corresponding to the height of the center of the proposed turbine). Tidal velocities typically differ through the water column and it may be advantageous to animals wanting to maintain position to be closer to the bottom during high current flows (Vogel 1981). Both the acoustic camera and the ADCP measured increased S_v at higher tidal speeds. It cannot be determined if the observed increase was due to increased densities of organisms, particles, or noise from other sources (e.g. Bassett et al. 2013). Periodic behavior by fish and macroinvertebrates may both aid and hinder MRE developers in their efforts to comply with the biological components of site monitoring plans. Vertical migration by fish and zooplankton to near surface waters reduces the probability of encounter by individuals with tidal devices when visibility is low during dark hours, and increase potential encounters with surface wave devices. Dispersal of aggregations at night also reduces potential encounters of larger groups with submerged or bottom-mounted devices. Vertical migration toward bottom and coalescence into aggregations during light hours may constrain bottom-mounted device operation if aggregation center of mass coincides with device hub heights. Depending on device technology, hub heights may be adjusted to maximize difference between center of mass metric values and hub heights.

Quantification of nekton variability at the proposed SnoPUD demonstration site highlights the requirement for biological baseline studies at all MRE sites. Even though this study was limited in its temporal range (i.e. lack of seasonal or annual sampling), it is not possible to detect change at any specific location if a site characterization is not completed prior to the installation of any device. Differences in echometric values between the north and south grid locations also illustrates that a control site in the vicinity of an MRE installation may not serve as an appropriate control in traditional before-after-control-impact (i.e. BACI) survey designs. At this time, no fixed definitions of change, effect, or impact have been established by regulatory agencies, nor is there a standard set of variables or metrics that are specified to be measured in biological components of monitoring plans.

A combination of mobile and stationary sampling was the best experimental design strategy for acoustic technology comparisons. Mobile surveys were used to map and quantify nekton

densities at the proposed SnoPUD MRE site, and over a comparable area south of the site. A survey grid was sampled in approximately 2.5 hours, approximately one third of a tidal cycle in Admiralty Inlet. Water and passive particles would flow through the region but the maximum sampling lag was approximately a factor of two (based on the distance along the major tidal axis in the north grid was 4.25 km, particle traveling at 1 m/s would take 72 minutes to flow through the grid). Midwater trawling during mobile surveys was used to supplement acoustic samples by providing species composition and length frequency data on targets within aggregations detected by the echosounder. Stationary sampling by autonomous acoustic instrument packages enabled characterization nekton vertical distribution changes over temporal cycles of environmental covariates. Temporally-indexed data can be used to detect lower signal-to-noise patterns as temporal samples do not convolve space with time compared to data from mobile surveys. Spatial coverage of stationary instruments is limited by the footprint of the instrument sampling sensor. Combining the two sampling strategies will enable the scaling of temporally-indexed data to equivalent spatial area (i.e. determining the spatial representativeness of temporal samples). Spatial representativeness is used to determine the density of instrument packages used to monitor MRE commercial scale sites.

Knowledge of acoustic instrument design should be used to guide choice and deployment of any particular technology. Densities and distributions of aquatic organisms at potential MRE sites can be quickly assessed using echosounders deployed from a mobile platform (i.e. vessel). The limited range of acoustic cameras constrains use to characterizing interactions of animals with devices (e.g. Viehman 2012). Data outputs from acoustic cameras were designed to provide near-optic images and the data are not appropriate for traditional echo integration. ADCP's do not contain the dynamic range available in echosounders and are only a viable alternative when no other acoustic technologies are included in the instrument package. The ubiquity of ADCP's in oceanographic moorings/deployments, including those at MRE sites provides a common, albeit very poor, data stream that could be used to index nekton density through the water column. Comments on the utility of multibeam sonars are restricted in this report due to the failure of the instrument package. The availability of quantitative water column data is now common within this technology class. Fast computer processing and algorithm availability has matured to the point where commercial software automates configuration of acoustic beams during processing (i.e. beamforming), reducing the need for custom software. The wide swath, long range, high dynamic range, and high resolution make multibeam sonars an attractive candidate for operational monitoring at MRE sites. Development in data processing, system component integration for autonomous deployment, and power management are needed before there is wide-spread use of this technology for MRE site characterization and monitoring in the near future.

Acoustic technologies can be used to assess and monitor nekton during mobile surveys and through autonomous deployments at MRE sites. But sampling in high flow environments adds challenges to the use of any acoustic instrument. In this study, strong tidal flows augmented by topographic steering affected mobile survey operations and data processing in two ways: limited time windows to fish the midwater trawl; and added noise to the acoustic record from water turbulence. The maximum speed over ground at which the trawl could be fished was 3.5 knots (1.8 m/s). Given an optimal towing speed of 2.5 knots (1.3 m/s), the maximum current speed when trawling restricted fishing to times when water speeds were approximately 1 knot (0.5

m/s). In Admiralty Inlet, low water speeds were as short as 20 minutes and only occurred around slack tides. This short window necessitated adjusting the cruise plan from breaking transects and trawling during slack tides, to dedicated trawling days where the net was fished in quick succession during days with longer tidal slack periods. To increase fishing temporal windows, knotless or high strength-to-weight materials (e.g. High Molecular Density Polyethylene (HMDPE)) will be needed in trawl construction to effectively sample high flow environments. Acoustic sampling in areas of high turbulence increased noise in the acoustic data from the surface to a maximum depth of ~50 m. Distinguishing fish and zooplankton from turbulence was an additional data processing task. The use of the school detection algorithm in Echoview provided a straightforward approach to detecting and eliminating turbulence in the acoustic record.

5. CONCLUSIONS

Existing acoustic technologies can be modified for autonomous deployments in high-flow environments. The biggest challenge was to provide sufficient power to meet demands of the sample design. Supplying power was a bigger constraint than electronic data storage. The physical space needed by marine batteries necessitated additional design and structural modifications to the Sea Spider tripods. A second constraint for autonomous deployments was the inability to verify and monitor data acquisition and data quality during deployments. As prudent examples, failure of the multibeam sonar and the presence of second or third surface echoes in the acoustic camera or echosounder data were not known until instruments were recovered. Given cost and time constraints of field deployments, acoustic modems were not integrated in the autonomous acoustic instrument packages, which would have required additional engineering to integrate communications. Constrained bandwidth of acoustic modems would also limit the amount of data that could be transmitted to the surface. But even limited communications would have been useful. An initial check on operation and data files would have alerted operators to the failure of the multibeam sonar (see Appendix for details) and the presence of second or third surface echoes in the echosounder and acoustic camera.

The temporary nature of biological and environmental sampling for MRE site evaluation ensures continued use of autonomous instrument packages. Increased experience with instrument and power integration for autonomous deployment will reduce failure rates of instruments such as the multibeam sonar used in this study. It was not the instrument itself that failed, but the power system that regulated start and stop sampling times that failed. Additional pre-deployment testing and standardized parameter settings will ensure high quality data acquisition by all instruments. For example, reductions in the pulse rate and power settings of the bottom-mounted echosounder would have reduced or eliminated multiple surface returns and data saturation in the upper water column. Similarly a very small shift in the angle of the acoustic camera transducer would have eliminated the second surface return. These examples illustrate the lack of vendor and research community experience in instrument setup and component integration of these acoustic technologies for MRE site sampling. Additional research and development are needed for MRE and other ocean observing applications that require extended autonomous instrument deployments. At pilot or commercial scale sites, the ultimate solution is to provide

communication and power from shore or MRE devices to all monitoring packages. This may be convenient for near-field monitoring at device locations, but would require cabling and infrastructure equivalent to a dispersed ocean observing network for a commercial scale MRE site.

It is also important to state that autonomous deployment of any instrument includes risk. The deployment and retrieval of autonomous Sea Spider tripods was successful, in part, due to previous experience and modifications to the tripods and launch/recovery procedures. Partnering with equipment manufacturers was intended to minimize equipment failure risk and to maximize data acquisition quality. Any instrument package may collect no data, limited data, or poor data quality in non-traditional deployments. Partnering with equipment manufacturers and those with specific application experience remains the preferred operational strategy until integrated monitoring systems become commercially available.

Environmental monitoring of biological and physical variables will extend through the life cycle of any MRE site from site inspection to de-commissioning. An integrated characterization and monitoring plan is needed to ensure that biological effects and impacts can be detected, and to maximize the cost-effectiveness of all monitoring activities. The lack of definitions on what constitutes biological change, effect, and impact is a deficiency that impedes the development of standards and procedures for assessing and monitoring MRE sites and operations.

6. RECOMMENDATIONS

Baseline site characterization and monitoring appears to be inconsistent. Development of an assessment standard and definitions of what constitutes an impact, with corresponding metrics to monitor potential impacts, will clarify technological needs when designing MRE site characterization and monitoring plans. The absence of standardized assessment protocols also impedes comparison of environmental variability and potential impacts among sites. Monitoring requirements must be better defined before technology gaps for environmental characterization can be addressed. Development of baseline and monitoring standards are expected to continue as biological variability at sites is quantified. Only then can appropriate sampling technologies and corresponding survey designs be determined.

Baseline environmental characterization and monitoring MRE devices at pilot or commercial sites over the full range of relevant spatial and temporal scales will require a combination of long- (e.g. echosounder), medium- (e.g. multibeam sonar), and short- (e.g. acoustic camera) range acoustic technologies. Instrument integration will enable continuous monitoring to detect biological effects and impacts, and the ability to track trajectories of single or aggregate targets based on speed and direction (e.g. alpha-beta tracker, Blackman 1986). Integration of target tracking across technologies in real time has not been addressed nor implemented in MRE installations. Irrespective of target tracking, instrument integration will enable adaptive monitoring that can be used to reduce power consumption, data storage volumes, and reduce data processing as only defined events would be recorded. An example is the triggering of cameras or video systems by acoustic instruments when a target is within the optical field of view.

A turnkey system to track targets as they approach a device, with the ability to transfer target coordinates among technologies, does not exist. Filling this gap would provide encounter rates of animals with devices and provide the data to develop a warning or shutdown mechanism if approaching targets are identified as endangered/listed species, or are large enough to pose a threat to the device (e.g. marine mammal or large fish school). A software interface would link devices and either transfer target coordinates among devices, or independently track targets using data from each instrument. Depending on the location, velocity, and size of the target(s) a warning from the software interface could be sent to a monitoring station to enable an automatic or manual operational mitigation measure (e.g. modify operation of device to reduce or eliminate an interaction).

If MRE monitoring regulations specify protection of specific endangered species, then baseline surveys and monitoring programs are forced to measure all aquatic organisms at the same taxonomic resolution. Choices of monitoring technologies for species identification are currently limited to acoustic cameras and optical instruments that are both limited in range (maximum 10 to 15 m). A short monitoring range limits the response time for adaptive monitoring and/or mitigation actions. If a one meter animal (e.g. salmon, seal, porpoise) is swimming at one body length per second (i.e. 1 m/s), then the time from optical recognition to potential interaction with a device would range from 10 to 15 seconds. Quantifying encounter probabilities of aquatic organisms with turbines at real world current speeds and encounter consequences are needed to determine whether mitigation measures are necessary. Extending the range of species identification over 10s or 100s of meters would necessitate additional cabled instruments and increase the complexity of instrument integration, tracking, and costs of monitoring. Standardizing the resolution of species nekton identification would accelerate development of turnkey packages for MRE site monitoring.

Supporting the MRE lifecycle of site characterization, operational monitoring, and decommissioning will require clear definitions of quantities and thresholds, spatially- and temporally-indexed sampling, and the development of two critical analytic tools. Change is defined as a statistically significant difference in a variable or variable attribute. The transition from change to an effect to an impact occurs when a threshold or deviation from an empirical measurement or model output is exceeded. Changes to a variable can be negative, neutral, or positive and it is not known whether thresholds represent instantaneous, additive, multiplicative, or exponential set points. To ensure adequate baseline and cost-effective operational monitoring, both mobile and stationary measurements are required during site characterizations. For monitoring programs it is assumed that autonomous instrument packages will be more economical than vessel-based surveys. Cabled infrastructure is advocated for both device and site operational monitoring. The use of frequency (e.g. wavelet analysis) or time (e.g. Generalized Autoregressive Conditional Heteroscedasticity (GARCH) Process, Multivariate Autoregressive State Space (MARSS) models) domain statistical tools will enable variables or derived metric values to be tracked over time and trigger alerts when threshold(s) are exceeded. To determine the spatial area of point samples (i.e. spatial representativeness; Erkkilä and Kalliola 2007, Evans 1997, Janis and Robeson 2004) quantitative tools are needed to match scales of concentrated variability (e.g. semi-variograms) and to quantify rates of change in variance (e.g. power spectra) between temporally- and spatially-indexed data from baseline

measurements. Quantifying the translation between temporally- and spatially-indexed variance enables the determination of instrument package density within a monitoring domain, given an arbitrary probability to detect change. The second analytic tool needed is a procedure to scale observed effects at pilot to commercial scale sites. There is no current method to 'scale up' effects for mobile aquatic organisms. Until a pilot tidal turbine project is built out to a commercial MRE operation, there is no opportunity to collect empirical data that will enable development of a statistical technique or to test predictions from theoretical scaling(s). At present, commercial scale offshore wind farms may serve as analogues for tidal turbine or surface wave energy sites for technique development.


7. LITERATURE CITED

- Bassett, C., J. Thomson, and B. Polagye. 2013. Sediment-generated noise and bed stress in a tidal channel. *Journal of Geophysical Research* 118: 2249-2265.
- Blackman, S. S. 1986. Multiple-target tracking with radar applications. Artech House. pp. 449.
- Blaxter, J. H. S. 1975. The role of light in the vertical migration of fish – a review. In: *Light as an ecological factor*. G. C. Evans, R. Bainbridge, and O Racham. (eds.) Blackwell Scientific Publications, Oxford, UK. Pp. 189-210.
- Brierley, A., M. Brandon, and J. Watkins. 1998. An assessment of the utility of an acoustic Doppler current profiler for biomass estimation. *Deep Sea Research I* 45: 1555–1573.
- Brierley, A., R. Saunders, D. Bone, E. Murphy, P. Enderlein, S. Conti, and D. Demer. 2006. Use of moored acoustic instruments to measure short-term variability in abundance of Antarctic krill. *Limnology and Oceanography: Methods* 4: 18–29.
- Burgos, J. M. and J. K. Horne. 2008. Characterization and classification of acoustically detected fish spatial distributions. *ICES Journal of Marine Science* 65: 1235-1247.
- Burwen, D. L., S. J. Fleischman, and J. D. Miller. 2010. Accuracy and precision of salmon length estimates taken from DIDSON sonar images. *Transactions of the American Fisheries Society* 139: 1306–1314.
- Chambers, J. M., W. S. Cleveland, B. Kleiner, and P. A. Tukey. 1983. *Graphical Methods for Data Analysis*. Belmont: Wadsworth International Press. Pp. 395.
- Cleveland, W. S. 1981. LOWESS: A Program for Smoothing Scatterplots by Robust Locally Weighted Regression. *American Statistician* 35: 54-54.
- Cochrane, N., D. Sameoto, and D. Belliveau. 1994. Temporal variability of euphausiid concentrations in a Nova Scotia shelf basin using a bottom-mounted acoustic Doppler current profiler. *Marine Ecology Progress Series* 107: 55–66.
- Erkkilä, A., and R. Kalliola. 2007. Spatial and temporal representativeness of water monitoring efforts in the Baltic Sea coast of SW Finland. *Fennia - International Journal of Geography* 185: 107–132.
- Evans, M. 1997. Temporal and spatial representativeness of alpine sediment yields: Cascade Mountains, British Columbia. *Earth Surface Processes and Landforms* 22: 287 – 295.
- Flagg, C., C. Wirick, and S. Smith. 1994. The interaction of phytoplankton, zooplankton, and currents from 15 months of continuous data in the Mid-Atlantic Bight. *Deep Sea Research II* 41: 411–435.

- Foote, K. G. 1983. Linearity of fisheries acoustics with addition theorems. *Journal of Acoustical Society of America* 73: 1932-40.
- Foote, K.G., H. P. Knudsen, G. Vestnes, D. N. MacLennan, and E. J. Simmonds. 1987. Calibration of acoustic instruments for fish density estimation: a practical guide. ICES Cooperative Research Report Number 144.
- Gerlotto, F., P. Fréon, M. Soria, P. H. Cottais, and L. Ronzier. 1994 Exhaustive observation of 3D schools structure using multibeam side scan sonar: potential use for school classification, biomass estimation and behaviour studies. *ICES CM B*: 26.
- Helfman, G. S. 1993. Fish behaviour by day, night and twilight. In: *Behaviour of teleost fishes*. T. J. Pitcher. (ed.) Chapman and Hall, London, UK. Pp. 479-512.
- Janis, M., and S. Robeson. 2004. Determining the spatial representativeness of air-temperature records using variogram-nugget time series. *Physical Geography* 25: 513–530.
- Korneliussen, R. J., Y. Heggelund, I. K. Eliassen, and G. O. Johansen. 2009. Acoustic species identification of schooling fish. *ICES Journal of Marine Science* 66: 1111–1118.
- Legendre, P., and L. Legendre. 1998. *Numerical ecology*, 2nd English edn. Elsevier, Amsterdam
- Lohrmann, A., 2001. Monitoring sediment concentration with acoustic backscattering instruments. Nortek Tech. Note. N4000-712, Pp. 5.
- MacLennan, D., P. G. Fernandes, and J. Dalen. 2002. A consistent approach to definitions and symbols in fisheries acoustics. *ICES Journal of Marine Science* 59: 365-369.
- Pitcher, T. J. and J. K. Parrish. 1993. Functions of shoaling in teleost fishes. In: *Behaviour of teleost fishes*. T. J. Pitcher. (ed.) Chapman and Hall, London, UK. Pp. 363-439.
- Radenac, M. H., P. E. Plimpton, A. Lebourges-D'haussy, L. Commiena, and M. J. McPhaden. 2010. Impact of environmental forcing on the acoustic backscattering strength in the equatorial Pacific: Diurnal, lunar, intraseasonal, and interannual variability. *Deep Sea Research Part I* 57: 1314–1328.
- R Development Core Team. 2011. *R: a Language and Environment for Statistical Computing*. R Foundation for Statistical Computing, Vienna, Austria.
- Rivoirard, J., J. Simmonds, K. G. Foote, P. Fernandes, and N. Bez. 2000. *Geostatistics for Estimating Fish Abundance*. Blackwell Science, Oxford. Pp. 206.
- Simmonds, J. and D. MacLennan. 2005. *Fisheries Acoustics: Theory and Practice*. 2nd ed. Oxford: Blackwell Science. Pp. 437.

- Urmy, S. S., J. K. Horne, and D. H. Barbee. 2012. Measuring the vertical distributional variability of pelagic fauna in Monterey Bay. *ICES Journal of Marine Science* 69: 184-196.
- Verdant Power New York, LLC. 2011. Roosevelt Island Tidal Energy (RITE) Environmental Assessment Project. New York State Energy Research and Development Authority. Pp. 31.
- Viehman, H.A. 2012. Fish in a tidally dynamic region in Maine: Hydroacoustic assessments in relation to tidal power development. University of Maine MSc. Thesis. Pp. 100.
- Vogel, S. 1981. *Life in moving fluids: the physical biology of flow*. W. Grant Press, Boston MA. pp. 352.
- Winslade, P. 1974. Behavioural studies on lesser sandeel *Ammodytes marinus* (Raitt). II. The effect of light intensity on activity. *Journal of Fish Biology* 6: 577-586.

APPENDIX A: RESON FINAL REPORT:

	RESON, Inc. Goleta, CA 93117	Document Number:	XXXXXX	Rev:	A
		Document Title:	NOPP AMOS-I Final Report		
FINAL REPORT AMOS-I DEPLOYMENT IN ADMIRALTY INLET					

Notice of Proprietary Rights

This document contains proprietary information. The contents of this document are current as of the time of publication but are subject to change without notice. This document confers upon the recipient no right or license to make, have made, use, sell, or practice any technology or inventions described herein

Autonomous Marine Observation System (AMOS-I)



**Deployment in Admiralty Inlet, Washington, USA
for NOPP/NNMREC Fisheries Observation Project**



RESON, Inc. || 100 Lopez Road || Goleta, California 93117 USA



TABLE OF CONTENTS

1	EXECUTIVE SUMMARY	5
2	THE AMOS-I SYSTEM.....	5
2.1	SeaBat 7218-AUV System	5
2.1.1	7128-AUV System Projector	6
2.1.2	7128-AUV System Receiver	7
2.1.3	7128-AUV Integrated Control and Processing Unit (ICPU)	8
2.2	Submersible Battery Banks	10
2.3	AMOS-I Timing/Control System	11
2.4	AMOS-I Frame	11
3	SYSTEM PREPARATION	13
3.1	Deployment Issues.....	13
3.2	Mechanical Configuration.....	14
3.3	Timing/Control System Configuration.....	15
3.4	Testing Issues	17
4	SYSTEM DEPLOYMENT	18
5	RESULTS.....	20

LIST OF FIGURES

Figure 1 The 7128-AUV System and its interfaces to an Autonomous Underwater Vehicle (AUV).	5
Figure 2 The TC2162 Projector used in the 7128-AUV System.	6
Figure 3: EM 7216 Receiver Unit used in the 7128-AUV System.....	7
Figure 4 7128-AUV Integrated Control and Processing Unit (ICPU) front oblique view - the Single Board Computer and beamformer FPGA board are located inside the enclosure - the sonar power supplies and input/output controllers are mounted on the long side of the enclosure.	9
Figure 5 7128-AUV Integrated Control and Processing Unit (ICPU) rear oblique view - the sonar transmitter and its power supply are mounted on the long side of the enclosure - the computer power supply is mounted over the cooling fan on the end of the enclosure.....	9
Figure 6 The AMOS-I battery banks inside the battery chamber. Before deployment, the battery chamber is filled with light mineral oil and topped with a sheet of flexible rubber.....	10
Figure 7 A detailed block diagram of the 7128-AUV Sonar System and the AMOS-I Timing/Control System	11
Figure 8 The AMOS-I System, viewed from the front end.	12
Figure 9 The AMOS-I System, viewed from the side.....	12
Figure 10 Predicted tidal flows (in knots) for Admiralty Inlet, Washington, during mid-May, 2011. Green rectangles indicate periods of an hour or more with tidal flow less than 0.5 knot.	13
Figure 11 The AMOS-I System as deployed in Admiralty Inlet, equipped with two recovery floats, two recovery lines and two acoustic transponder/releases. The system is hanging from a third acoustic transponding release at the end of the line that will lower the system to the seabed.	14
Figure 12 The AMOS-I Timing/Control System, as originally configured.....	15
Figure 13 The AMOS-I Data Acquisition Schedule, as originally implemented in the Timing/Control System.	16
Figure 14 The AMOS-I System as deployed, with the power control relay bypassed so that 48-volt power to the 7128-AUV system is permanently on.	19
Figure 15 The full operator display produced by the 7128-AUV system.....	20
Figure 16 The sonar display during the descent of AMOS-I to the seabed.	21
Figure 17 The Acoustic Release and its floats, just after the release has opened.	22
Figure 18 The Acoustic Release and its floats, about 20 meters above the sonar head.	22
Figure 19 The Acoustic Release and its floats, about 40 meters above the sonar head.	23

Figure 20 The Acoustic Release (with its release hook open) being lifted back aboard the vessel. The floats are sitting in the water, waiting to be pulled aboard..... 23

LIST OF TABLES

Table 1: TC 2162 Projector Acoustic Characteristics	6
Table 2: TC 2162 Projector Unit Physical Specifications	7
Table 3: EM 7216 Beamforming Characteristics	8
Table 4: EM 7216 Receiver Unit Physical Specifications	8

1 EXECUTIVE SUMMARY

The RESON Autonomous Marine Observation System One (AMOS-I) was deployed successfully in Admiralty Inlet, Washington, USA on 25 May 2011 and recovered successfully two weeks later. The RESON SeaBat 7128-AUV sonar system functioned well at the time of deployment but shut down almost immediately because of an error made when the system was configured for deployment. The AMOS-I deployment failed to contribute any useful data toward the stated objectives of the project.

2 THE AMOS-I SYSTEM

The RESON Autonomous Marine Observation System One (AMOS-I) is designed for installation on the seabed and is capable of totally independent operation, recording up to 100 hours of sonar observations according to a pre-programmed schedule. The AMOS-I system consists of a RESON SeaBat 7128-AUV sonar system, submersible battery banks, a rugged frame and the AMOS timing/control system.

2.1 SeaBat 7218-AUV System

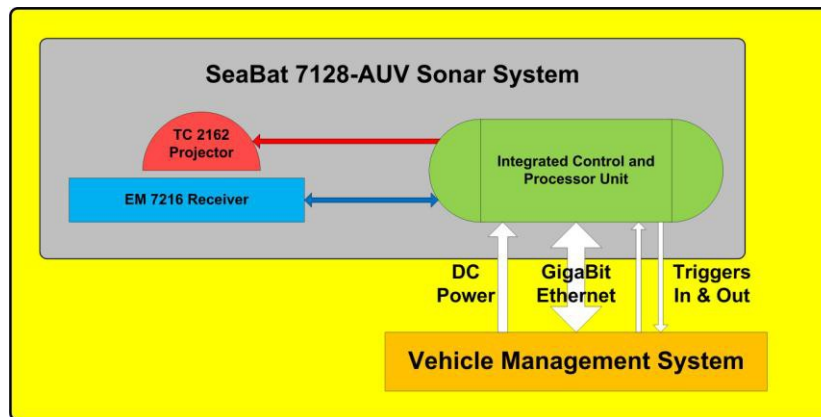


Figure 1 The 7128-AUV System and its interfaces to an Autonomous Underwater Vehicle (AUV).

The RESON SeaBat 7128 system is a 200 kHz / 400 kHz multibeam sonar system that provides a sonar view of a 120° sector to a maximum range of 500

meters from its sonar head. The SeaBat 7128-AUV is a version of the 7128 with an Integrated Control and Processor Unit (ICPU) that can be installed in a pressure housing, powered by a single-voltage battery supply and operated 1) by a remotely-located human operator, 2) under the control of a local vehicle control computer or 3) in a totally autonomous mode.

2.1.1 7128-AUV System Projector



Figure 2 The TC2162 Projector used in the 7128-AUV System.

The 7128-AUV system uses a TC2162 projector that can operate at either 200 kHz or 400 kHz and has a maximum operating depth of 6,000 meters. It broadcasts a fan-shaped sonar beam that is 26 degrees wide in one direction and more than 120 degrees wide in the other. The acoustic and physical characteristics of the TC2162 are shown in *Table 1: TC 2162 Projector Acoustic Characteristics* and *Table 2: TC 2162 Projector Unit Physical Specifications*.

Table 1: TC 2162 Projector Acoustic Characteristics

Characteristic	200 kHz mode	400 kHz mode
Bandwidth	30 kHz	62 kHz
Along-Track Beamwidth	27°	31°
Swath Coverage	130°	130°
Maximum Sound Pressure Level	205 dB re 1µPa at 1 meter	205 dB re 1µPa at 1 meter

Table 2: TC 2162 Projector Unit Physical Specifications

Specification	Value
Dimensions	Height: 86 mm
	Width: 240 mm
	Depth: 100 mm
Weight	Air: 3.0 kg (± 0.5 kg)
	Seawater: 1.7 kg (± 0.5 kg)

2.1.2 7128-AUV System Receiver

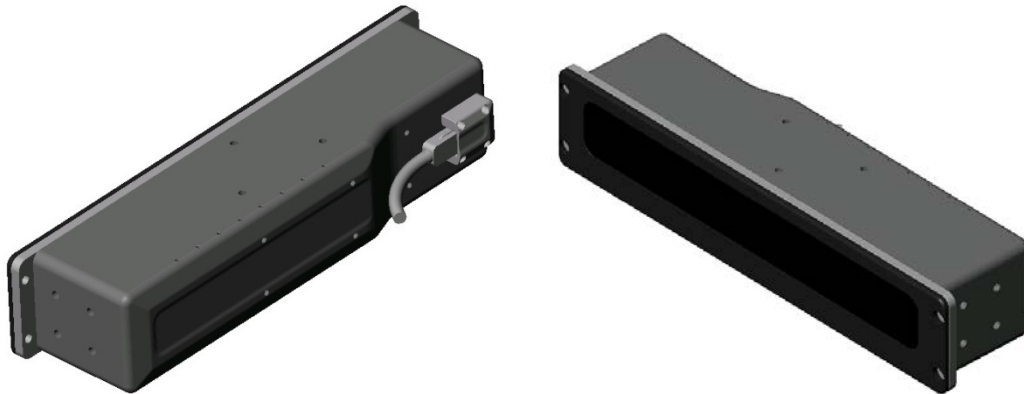


Figure 3: EM 7216 Receiver Unit used in the 7128-AUV System

The 7128-AUV system uses an EM7216 receiver that can operate at either 200 kHz or 400 kHz and has a maximum operating depth of 6,000 meters. It is sensitive to sonar energy arriving in a fan-shaped set of sonar beams that is 27 degrees wide in one direction and more than 120 degrees wide in the other. The EM 7216 receives acoustic signals from the water in front of the transducer; filters, amplifies, and digitizes the electrical signals from the transducer elements; then sends them to the ICPU for beam forming. The formed beams have the characteristics presented in *Table 3: EM 7216 Beamforming Characteristics*. The acoustic and physical characteristics of the EM7216 are shown in the *Table 4: EM 7216 Receiver Unit Physical Specifications*.

Table 3: EM 7216 Beamforming Characteristics

Characteristic	200 kHz	400 kHz
Number of beams across-track	256	512
Vertical beam width (-3 dB) Across-track	27°	27°
Coverage Horizontal beam width (-3 dB)	120°	120°
	1.0°	0.5°
	0.94°	0.47°

Table 4: EM 7216 Receiver Unit Physical Specifications

Specification	Value
Dimensions	Width: 496 mm
	Height: 102 mm
	Depth: 138 mm
Weight	Air: 10.7 kg (±1.0 kg)
	Seawater: 5.7 kg (±0.5 kg)

2.1.3 7128-AUV Integrated Control and Processing Unit (ICPU)

The Integrated Control and Processor Unit (ICPU) contains the hardware, firmware and software necessary to control the transmitter and receiver, drive the projector, accept the data from the receiver, process the raw sonar data to produce sonar beam data, record the various sonar data sets and communicate with external devices and systems.

The ICPU can be operated in a completely autonomous mode, in which the ICPU control files are configured to preset the sonar operating parameters. When the DC power is turned on, the single board computer boots up, loads the sonar software and starts the operation of the sonar using the preset parameters. These parameters can direct the ICPU to initiate the recording of specified types of sonar data records.

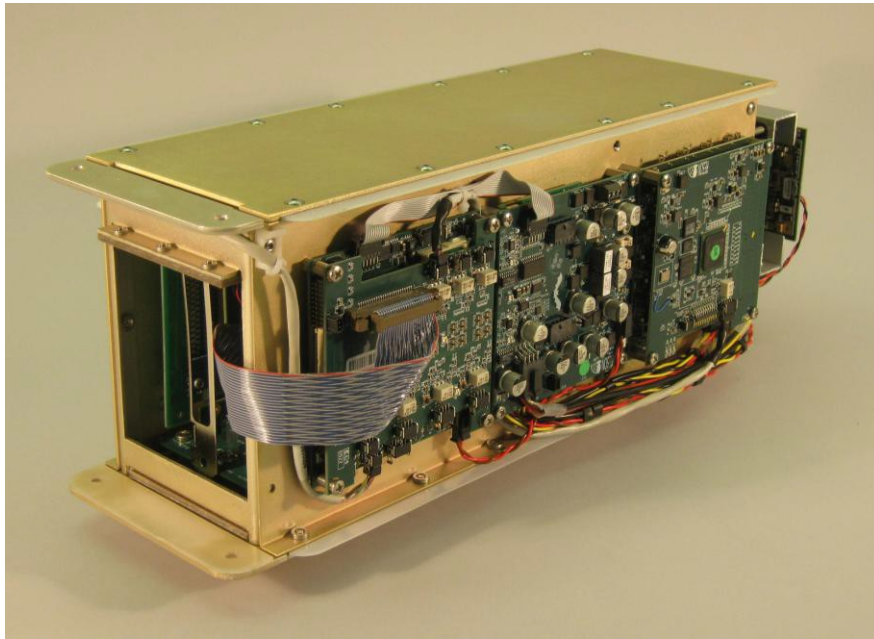


Figure 4 7128-AUV Integrated Control and Processing Unit (ICPU) front oblique view - the Single Board Computer and beamformer FPGA board are located inside the enclosure - the sonar power supplies and input/output controllers are mounted on the long side of the enclosure.

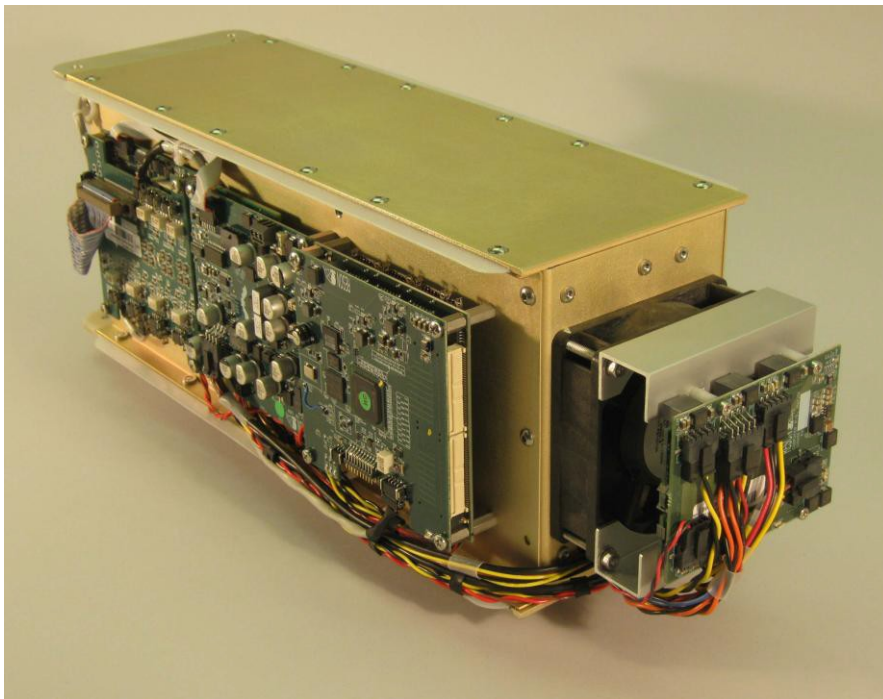


Figure 5 7128-AUV Integrated Control and Processing Unit (ICPU) rear oblique view - the sonar transmitter and its power supply are mounted on the long side of the enclosure - the computer power supply is mounted over the cooling fan on the end of the enclosure.

The ICPU can be installed in pressure housings with various depth ratings. The standard deep-water ICPU housing is manufactured from grade 5 titanium and has a maximum design depth of 6,000 meters. Housings manufactured from aluminum or stainless steel are available for installations at shallower depths.

A detailed block diagram of the ICPU is shown below in *Figure 7* A detailed block diagram of the 7128-AUV Sonar System and the AMOS-I Timing/Control System

2.2 Submersible Battery Banks

The AMOS-I System can be operated autonomously because it incorporates two 48-volt 5 kilowatt-hour battery banks that are capable of operating the 7128-AUV sonar for a total of about 100 hours. A third battery bank, consisting of a single 12-volt battery is capable of running the timing/control system for 30 days, including 100 hours of operation of the 7128-AUV sonar.

The battery banks are composed of 12-volt 115 Amp-hour marine deep-discharge lead acid batteries packaged in a pressure-compensated chamber that is fully flooded with light mineral oil. The mineral oil is immiscible with water and less dense than water so, in the flooded battery chamber, it forms a stable layer over the battery electrolyte and displaces any air inside or around the batteries.

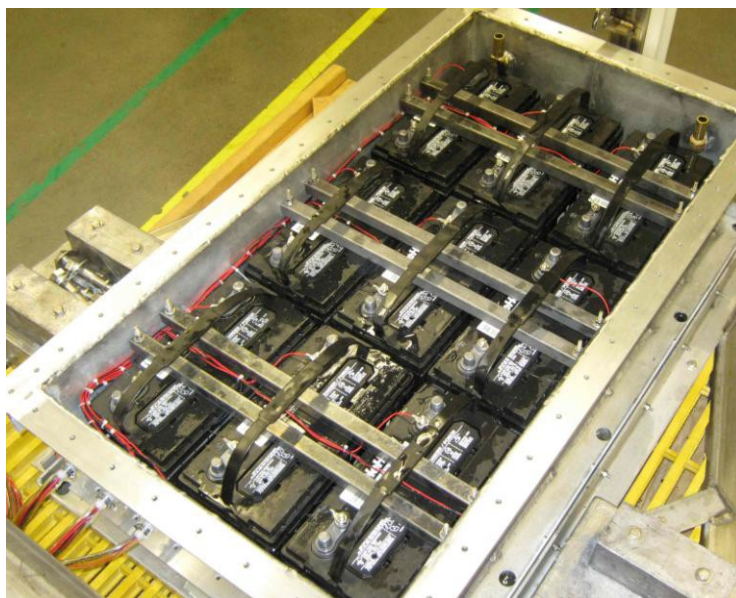


Figure 6 The AMOS-I battery banks inside the battery chamber. Before deployment, the battery chamber is filled with light mineral oil and topped with a sheet of flexible rubber.

2.3 AMOS-I Timing/Control System

The AMOS-I Timing/Control System controls the schedule of operations for the 7128-AUV system. It contains a small low-power microcontroller that is able to read the time and date from a precision clock/calendar circuit, switch a power relay to control the DC power to the 7128-AUV system and generate serial character messages that are converted to Ethernet message packets in order to control the activity of the ICPU.

A detailed block diagram of the ICPU and Timing/Control System is shown in Figure 7.

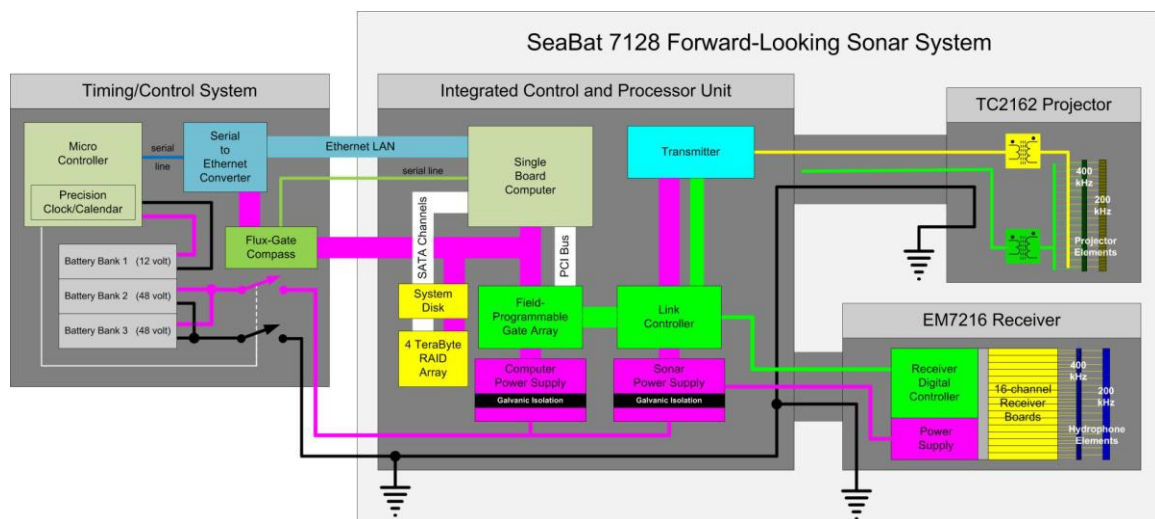


Figure 7 A detailed block diagram of the 7128-AUV Sonar System and the AMOS-I Timing/Control System

2.4 AMOS-I Frame

The AMOS-I frame provides structural support for the system components, protects the components from rocky material on the seabed, aims the sonar head upward and provides attachment points for lifting the system. In order to offer high structural integrity along with good corrosion resistance, the metal portions of the frame have been constructed from heavy wall Type 316 (A4) stainless steel. The protective grating on the floor of the AMOS-I frame is made of fiberglass and some smaller components are manufactured from plastic or sheet

rubber. The walls and floor of the battery housing were formed from aluminum sheet and are galvanically isolated from the AMOS-I frame.

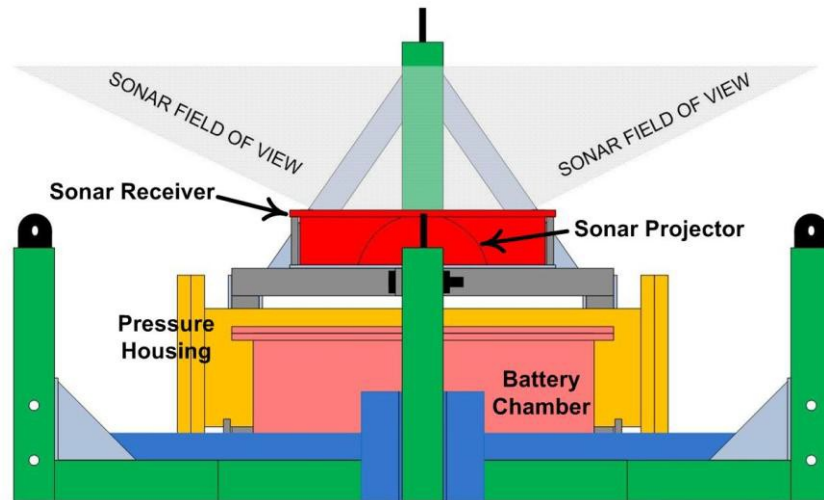


Figure 8 The AMOS-I System, viewed from the front end.

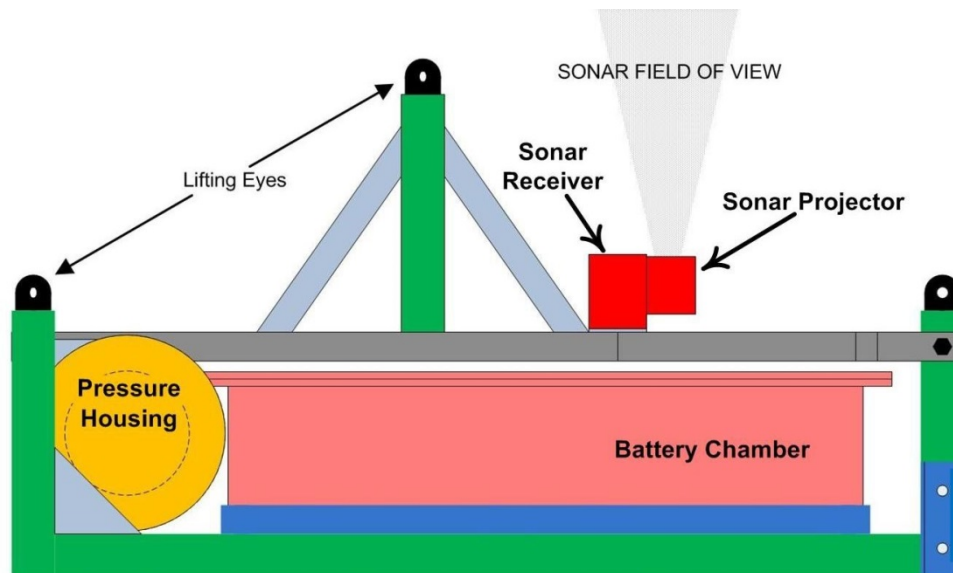


Figure 9 The AMOS-I System, viewed from the side.

The ICPU and the AMOS-I Timing/Control System are installed inside the Pressure Housing. This housing and its end-caps are composed of Type 316 (A4) stainless steel

3 SYSTEM PREPARATION

3.1 Deployment Issues

In the Admiralty Inlet deployment, three separate sonar systems, including the AMOS-I system, were to be deployed near one another on the seabed so that data could be collected simultaneously by all three. A major goal of the project was to compare the information gathered by each of the sonar systems while they observed exactly the same biological situations and events.

Admiralty Inlet is a constricted area that channels the substantial tidal flow into and out of Puget Sound. The rapid water motion through Admiralty Inlet has scoured the seabed clean of any sediment smaller than rock cobbles, giving a seabed that is uneven, hard and slick. Experience with instrument packages deployed in this area shows that the currents easily move and/or reorient packages unless the packages incorporate some means to grip the seabed.

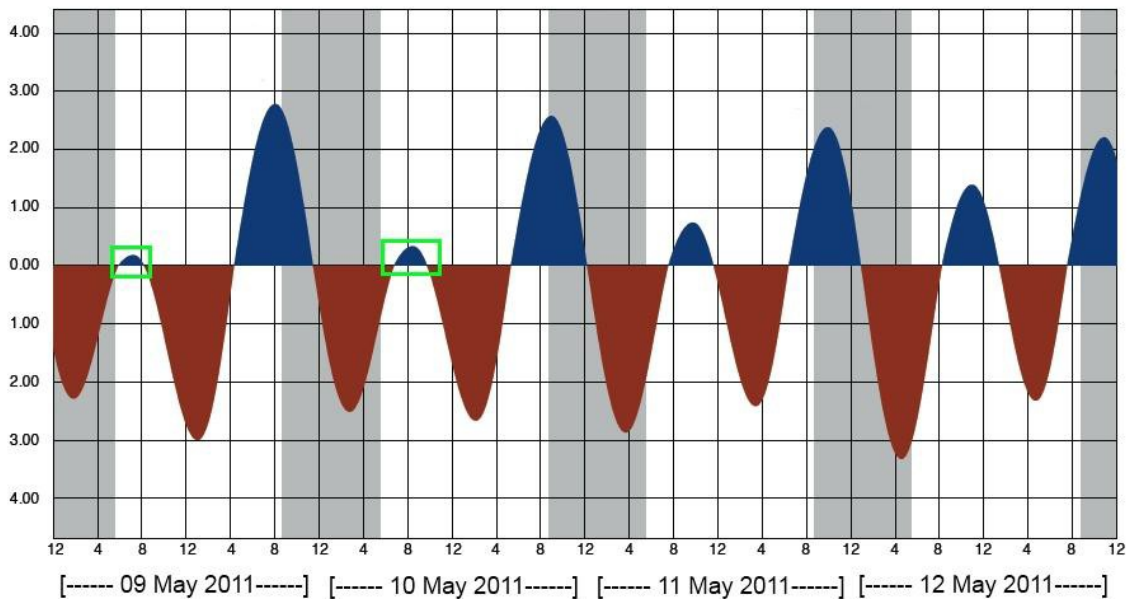


Figure 10 Predicted tidal flows (in knots) for Admiralty Inlet, Washington, during mid-May, 2011. Green rectangles indicate periods of an hour or more with tidal flow less than 0.5 knot.

The heavy tidal flow means that there are only two or three time windows in each half of the tidal cycle when the tidal motion is below 0.5 knot for two to three hours. These limited time windows are the optimum time to deploy and recover instrument packages that must be lowered to or lifted off of the seabed.

3.2 Mechanical Configuration

Since the water depth at the Admiralty Inlet deployment site did not exceed 100 meters, the AMOS-I System could be equipped with a relatively thin-walled pressure housing. The pressure housing was fabricated using standard schedule 40 pipe and ANSI flat pipe flanges made from Type 316 stainless steel.

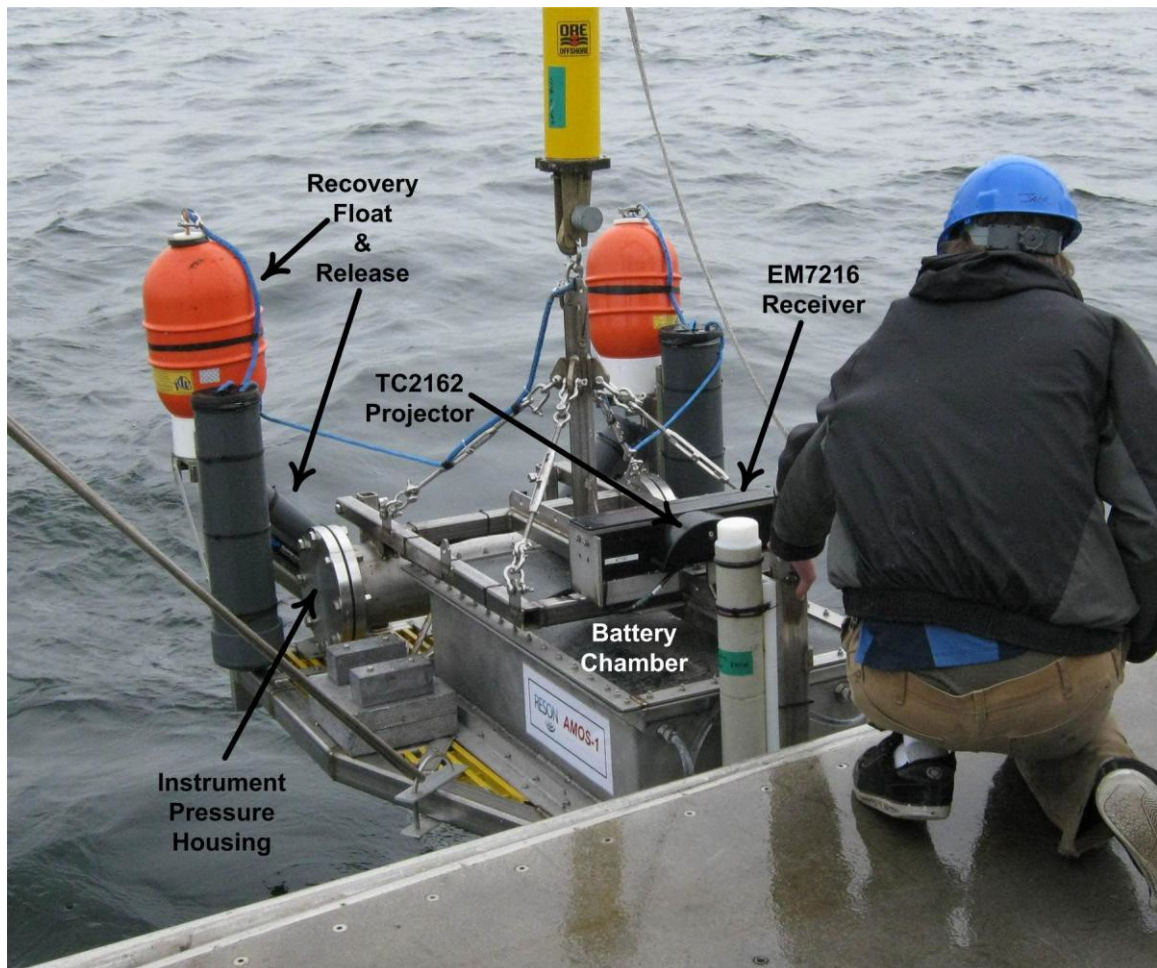


Figure 11 The AMOS-I System as deployed in Admiralty Inlet, equipped with two recovery floats, two recovery lines and two acoustic transponder/releases. The system is hanging from a third acoustic transponding release at the end of the line that will lower the system to the seabed.

In preparation for deployment, the central lifting point was installed on the top of the AMOS-I frame to provide an attachment point well above the center of gravity that would allow the frame to hang level. This would be the attachment point for the acoustic transponding release at the end of the line that would be used to lower AMOS-I to the seabed and then let go of the lifting point.

Also attached to the central lifting point were two recovery lines housed in canisters that were secured to the corner posts at the rear of the AMOS-I frame. The free ends of the recovery lines were attached to floats that were held by small acoustic transponding releases. In the recovery operation, an acoustic command issued from the recovery vessel would cause a recovery float to be released, allowing it to pull the free end of one of the recovery lines to the surface. The recovery line would then be used to lift AMOS-I from the seabed and back aboard the vessel.

3.3 Timing/Control System Configuration

As originally configured for the Admiralty Inlet deployment, the AMOS-I Timing/Control System followed a pre-programmed schedule to turn on the DC power for the SeaBat 7128-AUV system and send it control messages via Ethernet and magnetic compass heading data via a serial line.

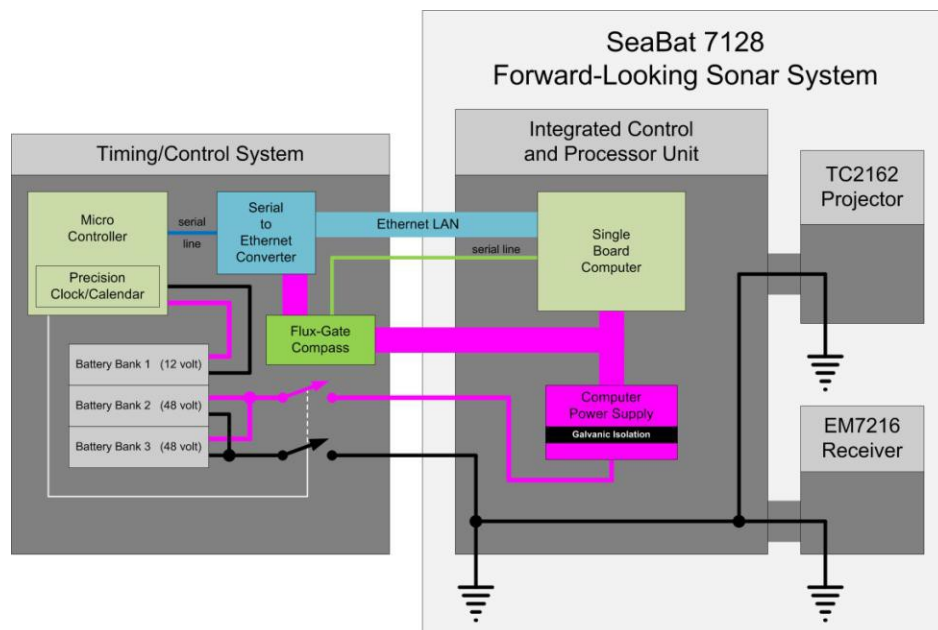


Figure 12 The AMOS-I Timing/Control System, as originally configured.

All of the instrument packages that were to be deployed during the experiment had operational durations that were limited by the capacity of their battery banks. In order to collect the most useful data set, it was agreed that each instrument package would operate about 10 percent of the time, for 12 minutes beginning at the start of every even-numbered hour, throughout a full 28-day tidal cycle. The Micro-Controller in the Timing/Control System was set up to do this, as shown in *Figure 13*.

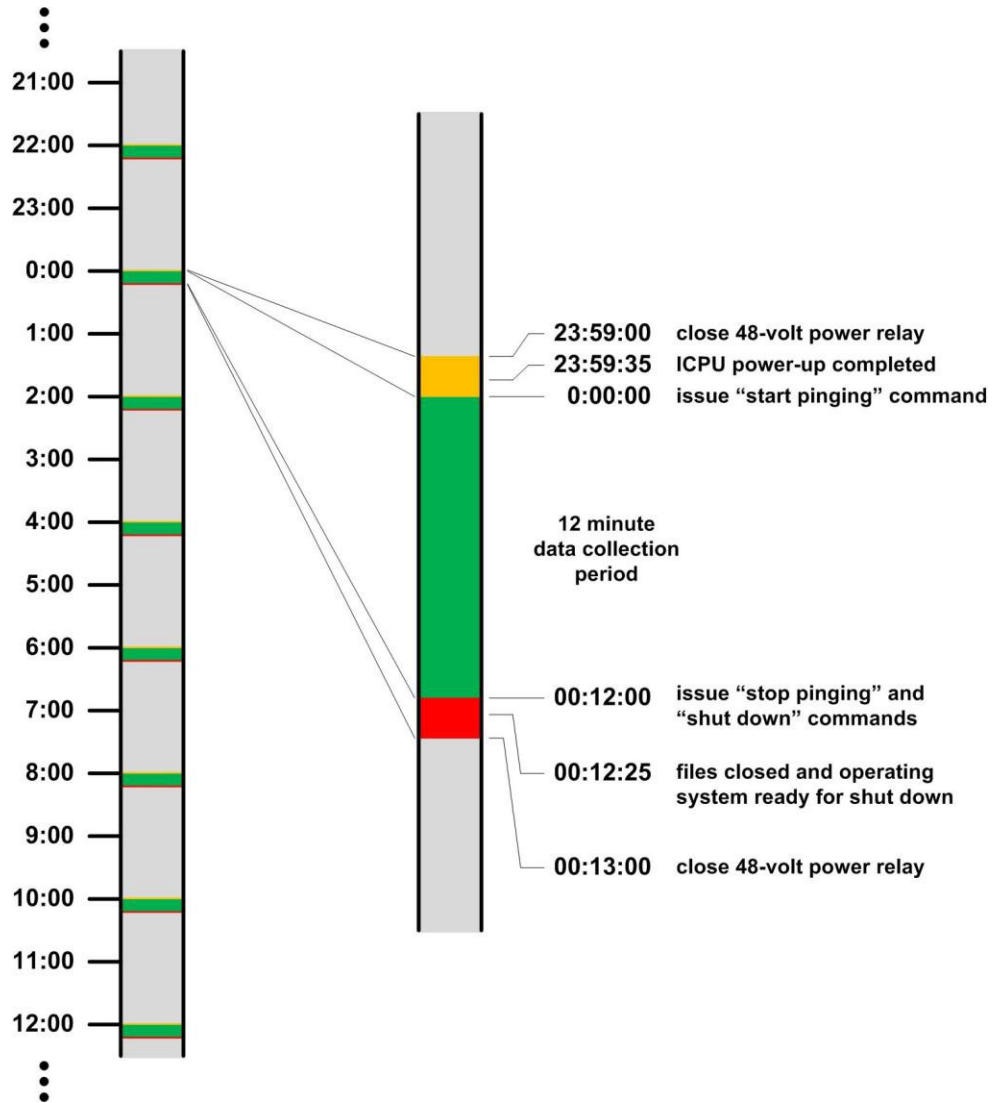


Figure 13 The AMOS-I Data Acquisition Schedule, as originally implemented in the Timing/Control System.

After the Micro-Controller closes the 48-volt power relay and sends DC power to the 7128-AUV system, it takes about 35 seconds for the Single Board Computer in the ICPU to perform its internal self-tests, load the operating system and sonar program, initiate the operation of the sonar and enable the data logging process. One minute after power-on, the Micro-Controller generates a message to tell the 7128-AUV system to begin pinging. Since the experiment requires that the sonar collect data during a time window that begins at the start of the hour, the power-on sequence is begun one minute before the start of the hour.

At the end of the 12-minute data acquisition window, the micro controller issues two commands: one to tell the 7128-AUV system to stop pinging and a second to tell the operating system in the ICPU to close the sonar program and any data files in preparation for a power shutdown. This process, which usually takes about 25 seconds, is followed by the opening of the 48 volt power relay one minute after the end of the data acquisition period.

3.4 Testing Issues

The core of the AMOS-I system is the 7128-AUV sonar system, which is a completely standard, commercial off-the-shelf product. The only customization done on the 7128-AUV system was to expand its data storage capacity to 4.5 TeraBytes (4,500 GigaBytes) so that full-resolution sonar image data could be recorded for the entire 100 hours of data acquisition.

The Timing/Control System, the submersible battery banks and the frame were custom designed for the AMOS-I system, specifically for the deployment in Admiralty Inlet.

Following the resolution of the last of the mechanical issues, the system development effort was centered on debugging the scheduling system and insuring that the sonar power control and command sequences were properly implemented. Toward the end, the testing consisted of allowing the AMOS-I system to cycle (according to the two-hour data acquisition schedule) on the test bench and then checking the sonar data files to confirm that they started and ended at the prescribed times and that they contained the specified types of data records.

In any given test run, we repeatedly discovered that data files were missing for some of the data acquisition periods but could not find a clear explanation for why this was occurring. Shortly before the AMOS-I deployment, it was discovered that there was an electrical intermittent inside the hardware module used to convert the serial messages from the Micro-Controller to the Ethernet messages accepted by the ICPU. This was a sobering prospect. If the ICPU did

not receive a “start pinging” message then the sonar would not be cycling during the data acquisition period and no data files would be recorded. If the ICPU did not receive a “shutdown” command prior to the turning off of the DC power, then it was possible for disk files to be corrupted resulting in unreadable data files or, worse, damaged system files that would prevent the single board computer from booting up the next time that DC power was turned on.

4 SYSTEM DEPLOYMENT

The bench testing of the AMOS-I system continued on board the deployment/recovery vessel until a few hours before the start of the 09 May 2011 deployment window. The behavior of the system had not stabilized sufficiently so the deployment schedule of the other instrument packages was adjusted so that the AMOS-I system would be deployed during the 10 May 2011 window.

After an additional day of bench tests, the system still displayed signs of instability and the deployment of AMOS-I was scratched from the schedule.

The Principal Investigator for the project graciously gathered the resources to schedule the deployment of the AMOS-I system 14 days later, the next time in which the tidal motion would be low enough to allow the system to be safely lowered to the seabed. It was stipulated, however, that a dockside overnight wet test of the AMOS-I system would have to be successfully performed prior to the departure of the deployment vessel.

In order to eliminate one source of problems, the software running on the Micro-Controller was modified so that it did not issue “start pinging” and “stop pinging” commands. Instead, the ICPU configuration file was changed so that the sonar began pinging as soon as the sonar program was loaded and initiated. The “shutdown” command was still used to insure that the programs and data files were closed in an orderly fashion.

The overnight dockside test produced many records of good sonar data and the clearance was given to load AMOS-I aboard the deployment vessel and begin the transit to the deployment site. However, closer scrutiny of the data records showed that, once again, some data records were missing.

During final system configuration efforts on the bench during the transit, it was confirmed that the serial/Ethernet converter module was behaving erratically.

The thought of having the power to the ICPU turned off every two hours without a warning message to the operating system raised the fear that, at some point, the ability of the AMOS-I system to collect sonar data would end when a corrupted disk file would prevent the operating system from booting up properly or would cause the operating system to generate a message that required the attention of the system user, who was not present.

Following a discussion on board the vessel, it was decided to avoid the risk of having the system lose its ability to power up/acquire data in favor of a sure thing: collecting data continuously for the 100 hours that the system would run once it was turned on.

This was implemented by bypassing the 48-volt power control relay. Once the 48-volt power from the battery banks was connected, the 7128-AUV system would run and collect data until the bus voltages on the battery banks dropped below the minimum voltages required by the power converter modules in the ICPU.

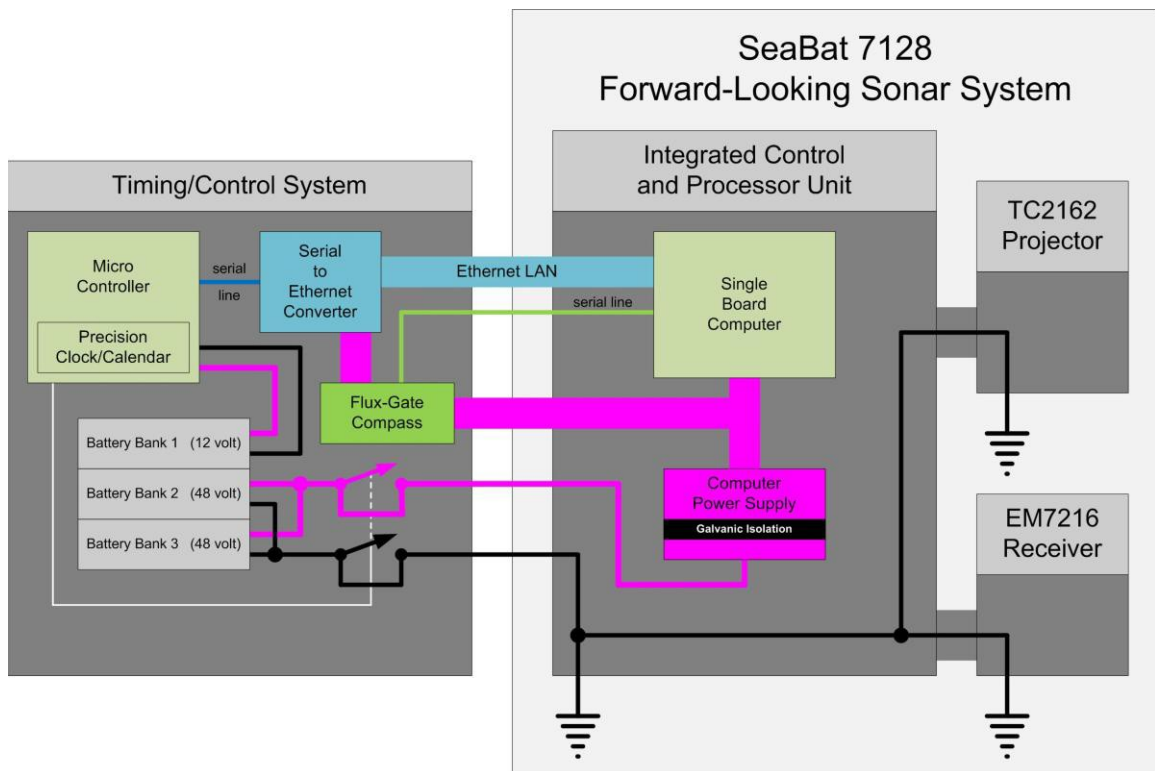


Figure 14 The AMOS-I System as deployed, with the power control relay bypassed so that 48-volt power to the 7128-AUV system is permanently on.

5 RESULTS

The change to keep the 48-volt power for the 7128-AUV system permanently on would have accomplished its purpose if the power to the Micro-Controller had been turned off or if the Ethernet line to the single board computer had been disconnected. Neither of these was done so the Timing/Control System continued to monitor the Clock/Calendar and generate Ethernet messages.

When the 48-volt battery bank cable was connected to the ICPU pressure housing, the ICPU booted up and the 7128-AUV system began to cycle and record data. At this time, the AMOS-I system was sitting on deck in the final minutes of transit, just before the deployment in Admiralty Inlet. We can confirm this by examining the sonar data records, which are present but show no sonar reflections because the system was running in air.

When the 7128-AUV system is running, it generates an operator display like the one shown in *Figure 15*. In this screen shot, the sonar head is at the bottom of the screen looking upward at the sea surface about 65 meters above.

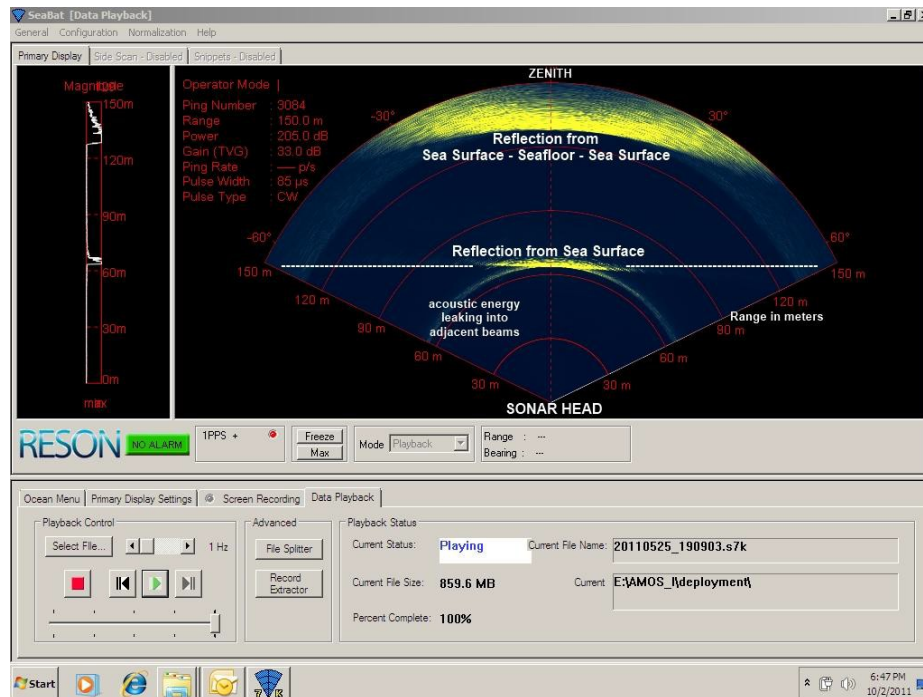


Figure 15 The full operator display produced by the 7128-AUV system.

When the AMOS-I system had been lifted off of the deck, into the water and was being lowered to the seabed, the sonar display indicated the distance from the sonar head to the sea surface. In *Figure 16*, the sonar head was 30 meters below the sea surface.

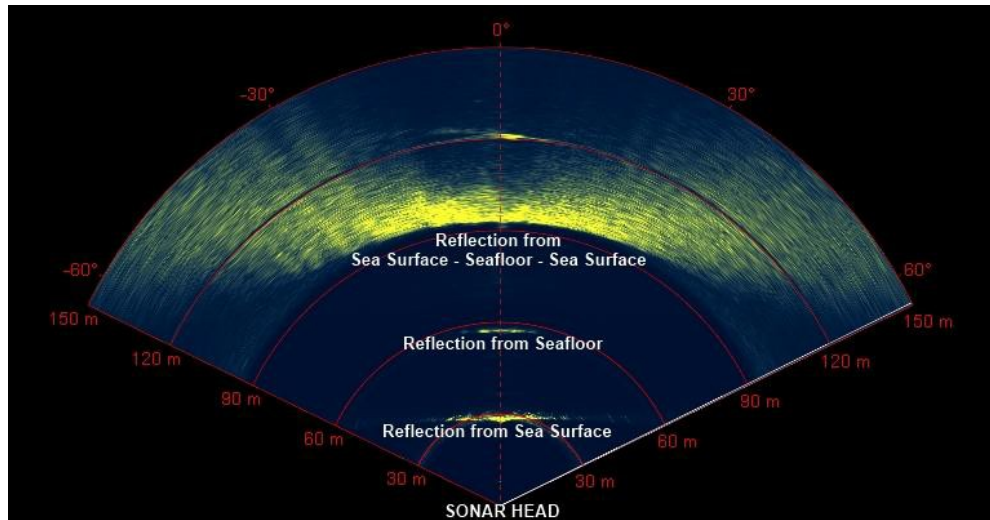


Figure 16 The sonar display during the descent of AMOS-I to the seabed.

At about this time, the local time was approaching 1200PDT, an even hour, so the Timing/Control System closed the 48-volt power relay. This made no difference because the relay had been bypassed and the 7128-AUV system was already running and recording data.

As the tidal motion stopped (as monitored by the vessel's acoustic Doppler current profiler (ADCP)), the AMOS-I frame was set on the seabed, the acoustic release was commanded to open and the release and its buoys were hauled back to the sea surface. The progress of the release and floats can be monitored in the figures below.

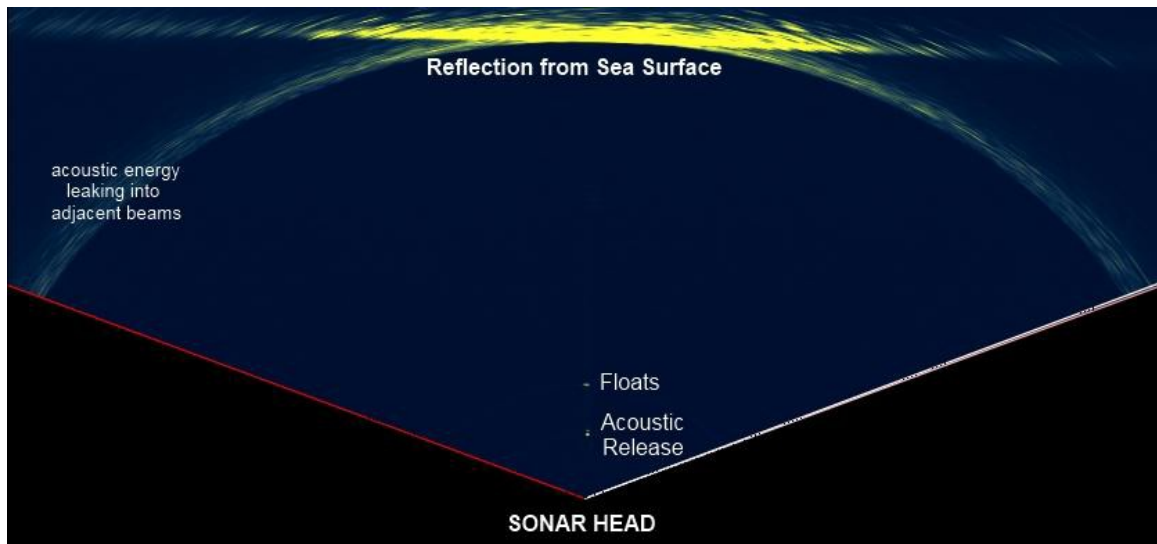


Figure 17 The Acoustic Release and its floats, just after the release has opened.

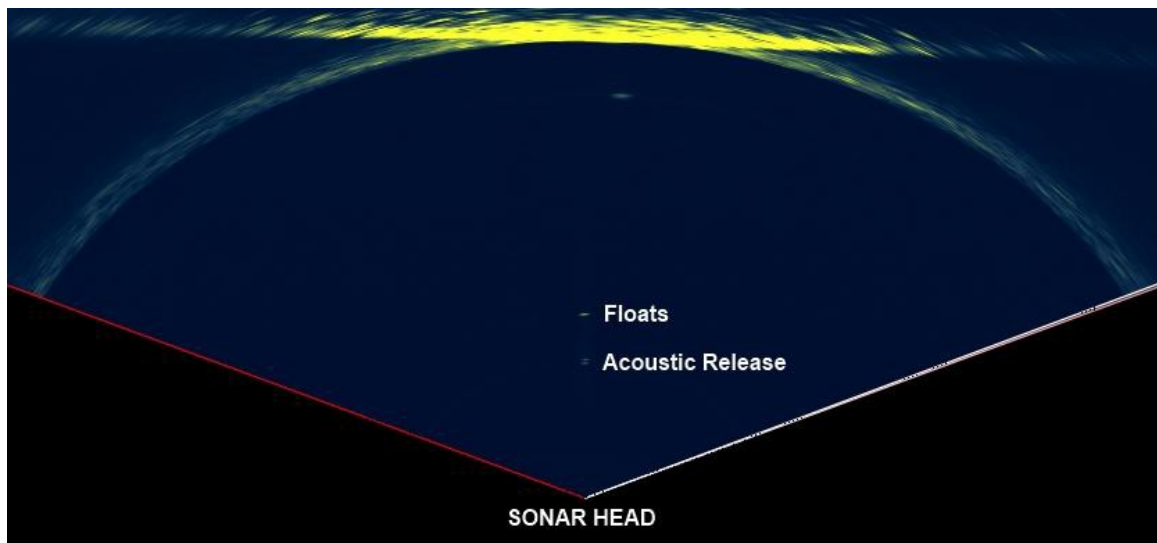


Figure 18 The Acoustic Release and its floats, about 20 meters above the sonar head.

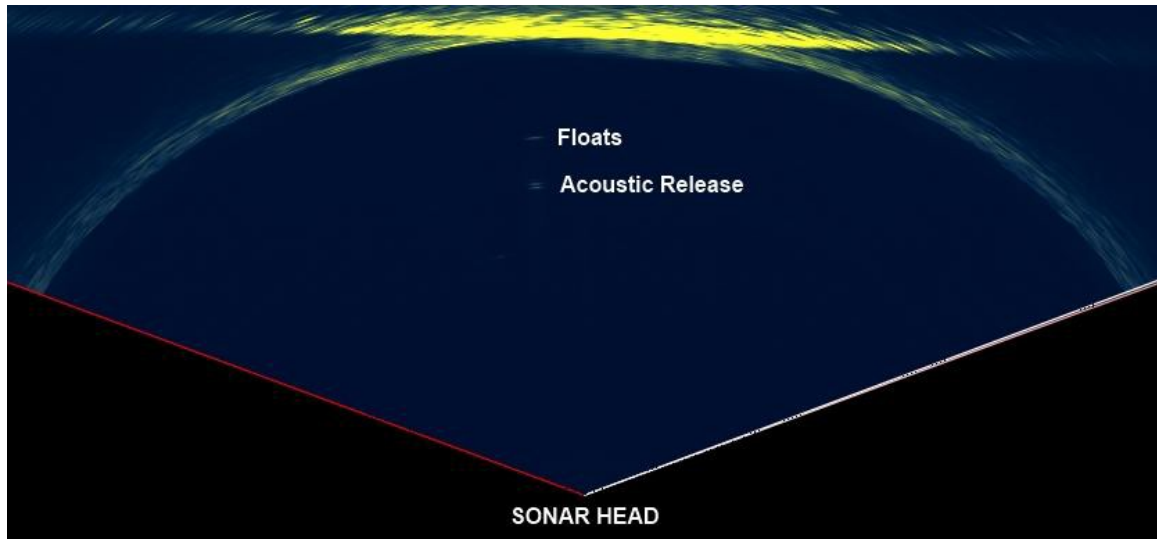


Figure 19 The Acoustic Release and its floats, about 40 meters above the sonar head.

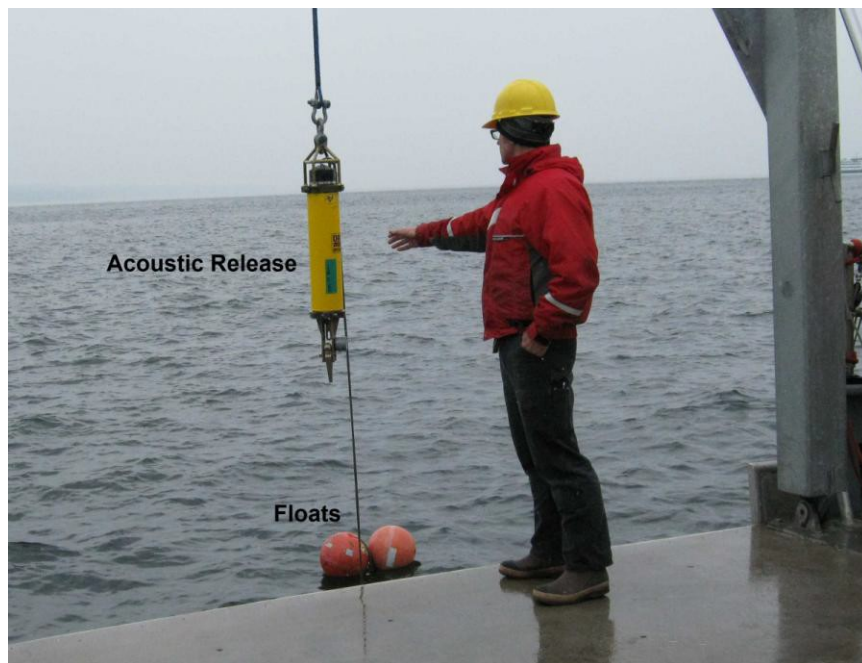


Figure 20 The Acoustic Release (with its release hook open) being lifted back aboard the vessel. The floats are sitting in the water, waiting to be pulled aboard.

The Acoustic Release was retrieved at about 1212 PDT, the time at which the Timing/Control System sent a “shutdown” command to the ICPU. The ICPU responded to this command by closing the sonar program, closing the data files and entering an idle state in anticipation of the loss of the 48-volt power. At 1213



PDT, the Timing/Control System opened the 48-volt power relay but, because the relay had been bypassed, the power to the ICPU was not turned off.

The AMOS-I system was now in a failure state. The Timing/Control System would close the 48-volt power relay at 1400 but the ICPU would not restart because the 48-volt ICPU power had never been turned off.

The AMOS-I system did not record any data after the recovery of the acoustic release.

**APPENDIX B: NORTHWEST FISHERIES SCIENCE
CENTER FINAL REPORT**

Report for Interagency Agreement Number M10PG00019 Between BOEMRE and NOAA

Report Prepared by NOAA, Northwest Fisheries Science Center
May 24, 2012

Background

The University of Washington (UW) partnered with NOAA's Northwest Fisheries Science Center (NWFSC), the Snohomish Public Utility District (PUD), and three technology vendors to evaluate the ability of three classes of active acoustic technologies (echo-sounders, multi-beam sonar, and acoustic camera) to characterize and monitor animal densities and distributions at a proposed tidal energy site in Puget Sound, Washington. The site is located off of Admiralty Head, Whidbey Island.

The specific objectives of this work were to:

1. Collect stationary acoustic data at the proposed Admiralty Head hydrokinetic site.
2. Perform a mobile acoustic and midwater trawling survey to characterize macro-invertebrate, fish, birds, and marine mammal spatial-temporal distributions at the study site.
3. Compare and contrast stationary instrument and mobile acoustic survey data
4. Evaluate abilities and weaknesses of each instrument type
5. Provide recommendations for future deployment and data acquisition

Stationary instrument deployments, mobile acoustic surveys, and mid-water trawling were conducted during a two week period in May, 2011 and a two week period in June, 2011. The mobile acoustic surveys and mid-water trawling work generally occurred over a 12 hour interval beginning each day at about 1400 hr and included flood, ebb and slack tidal periods. A sampling grid was laid out on an axis extending northwest and southeast of the proposed location of the tidal energy turbines (Figure 1). Transects were more closely spaced near the proposed turbine locations. The grid was constrained by water depth and the need to avoid the nearby shipping lanes for large vessels and Washington State ferries.

The NWFSC received funding to provide support for the mobile acoustic and mid water trawl work (e.g., catch processing) and to conduct bird and marine mammal observations. The NWFSC also evaluated detections of acoustically tagged fish associated with the proposed tidal energy site at Admiralty Head and examined detections of acoustically tagged fish on receivers located in the vicinity of the tidal energy site. The following is a report summarizing marine mammal and seabird surveys made during mobile acoustic and midwater trawl surveys and receiver detections.

Marine Mammal and Seabird Surveys

To assess distribution and abundance patterns, counts of birds and marine mammals were made during daytime surveys (Figure 2). Nine species of seabirds were identified during surveys, of which marbled murrelet is the only species listed under the Endangered Species Act. Rhinoceros

auklets (*Cerorhinca monocerata*) and pigeon guillemots (*Cepphus columba*) were the most abundant, followed by marbled murrelets (*Brachyramphus marmoratus*), common murrelets (*Uria aalge*), pelagic cormorants (*Phalacrocorax pelagicus*), western grebe (*Aechmophorus occidentalis*), common merganser (*Mergus merganser*), common loon (*Gavia immer*), and ancient murrelet (*Synthliboramphus antiquus*). Greater overall densities were observed in the northern grid primarily due to rhinoceros auklets (Figure 3). In the southern grid, pigeon guillemots were more abundant, along with pelagic cormorants and marbled murrelets. Four species of marine mammals were identified -- harbor porpoises (*Phocoena phocoena*) and harbor seals (*Phoca vitulina*) being the most abundant, followed by Steller sea lions (*Eumetopias jubatus*) and California sea lions (*Zalophus californianus*). The north grid also contained greater densities of marine mammals. June surveys averaged greater overall densities of both seabirds and marine mammals (Figure 4). Pigeon guillemots, pelagic cormorants, common mergansers, and western grebes were more abundant in May.

Detections by Acoustic Receivers

Since 2010, instrument packages have been deployed in the vicinity of the proposed Snohomish PUD tidal energy site to collect baseline data and characterize site conditions. These instrument packages often included VR2 acoustic receivers that scan the area for fish with Vemco transmitters; depending on conditions, receivers can have a range of up to 500m. Data from these receivers are uploaded to a regional data base system called HYDRA where the detection data can be accessed. All fish that could be detected at the tidal energy site were tagged as part of other studies within or outside Puget Sound; no fish were tagged specifically to evaluate their behavior around the proposed tidal energy site. The species, size at tagging, tagging location, and so on of the detected fish can only be determined if the investigator can be identified and they are willing to share this data.

Although receivers have been used periodically since 2008, we looked at receiver records between November 2010 and November 2011 (there is a receiver located at the site that will not be retrieved until June 2012) at the PUD tidal energy site in order to bracket the mobile and stationary hydro acoustic tests (Table 1). We also looked at detections on a line of receivers that NOAA maintains with POST (Pacific Ocean Shelf Tracking) that runs from Nodule Pt. to Bush Pt. This receiver array fully spans Puget Sound at this point and is about 6 miles south of the tidal energy site. It has been operational since fall 2009 and detections are uploaded in the spring and fall.

Few fish have been detected at the tidal energy site since instrument deployments began. Since November, 2010, the only fish for which we have meta data is a hatchery Chinook detected in late January, 2011 at the PUD site that had been tagged and released in early January near Bainbridge Island. The lack of fish is most likely due to few tagged fish being available to be detected in Puget Sound during this time period.

Detections on the Admiralty Inlet line since September 2009, for which we could obtain meta data (there are a number of fish that we could not obtain meta data) are summarized in Table 2. Again, the number of fish tagged is a major factor affecting what has been detected on this line.

In general, most fish that have been detected on the Admiralty Inlet line were on the east side of the channel (where the tidal energy site is location) and close to shore. The spiny dogfish was detected for an extended period on the Admiralty Inlet line indicating it was resident in the area.

Table 1. Deployments of acoustic receivers in the vicinity of the proposed tidal energy site in Admiralty Inlet. Most deployments did not detect fish.

Date Deployed	Turbine Location	Ferry Lane	Admiralty Inlet
11/10-2/11	1	1	
2/11-5/11	1		1
5/11-8/11	2		
6/11-8/11	3		
8/11-11/11	2		
11/11-6/12	1		

Table 2. Detections of fish that could be identified on the Admiralty Inlet line between September 2009 and April 2012.

Scientific Name	Common Name	Number of Individuals
<i>Oncorhynchus tshawytscha</i>	Chinook salmon (hatchery)	3
<i>Oncorhynchus kistuch</i>	Coho salmon (hatchery)	1
<i>Squalus acanthias</i>	Spiny dogfish	1
<i>Hexanchus griseus</i>	Six gill shark	2
<i>Ophiodon elongatus</i>	Lingcod	1

Figure 2. Number of birds (10 species on the left of the plot) and marine mammals (6 species on the right) observed per km during daytime acoustic surveys conducted in the Admiralty Inlet study area, Washington. May and June observations were combined as well as data from both north and south survey sections.

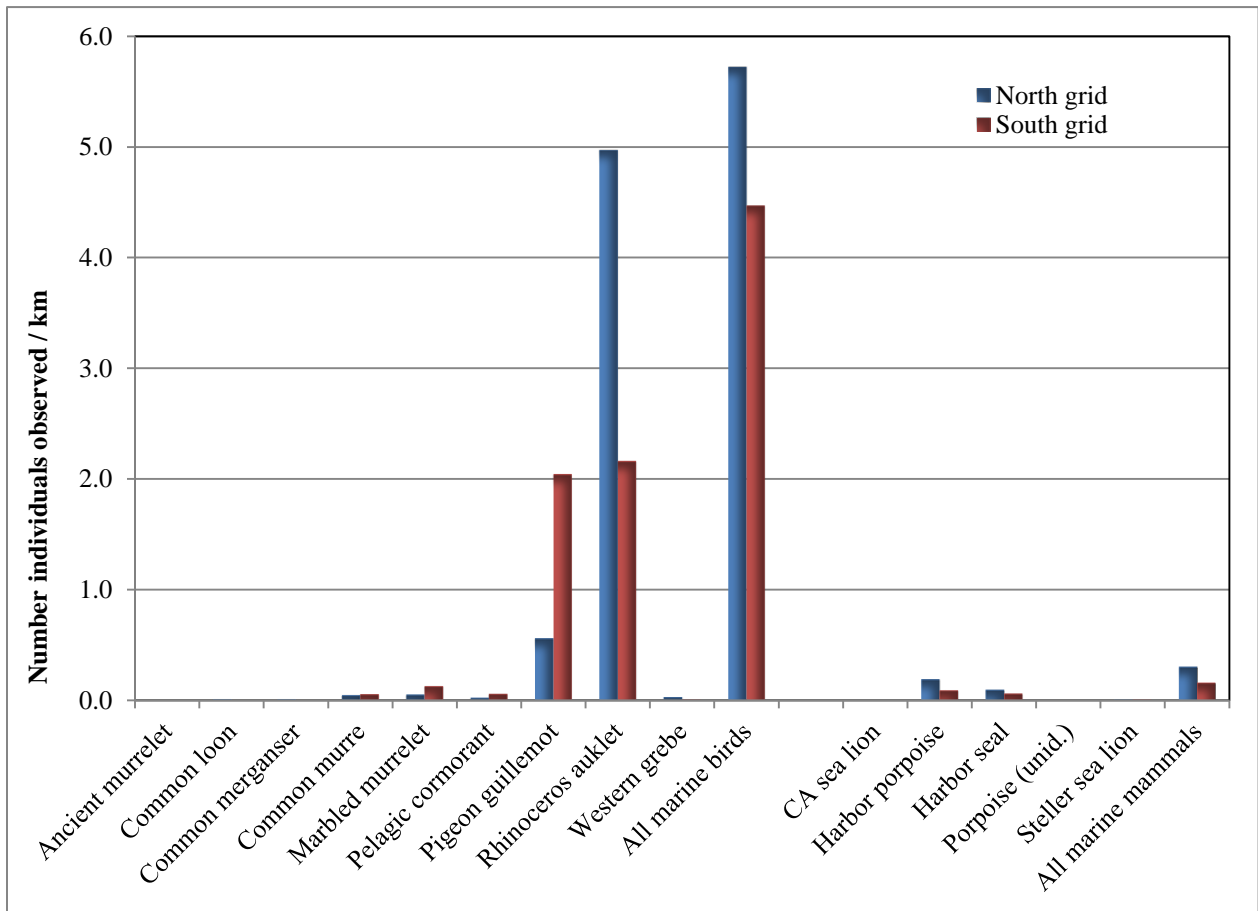


Figure 3. Number of birds (10 species on the left of the plot) and marine mammals (6 species on the right) observed per km during daytime acoustic surveys conducted in the north (blue bars) and south (red bars) survey sections of the Admiralty Inlet study area, Washington. May and June observations were combined.

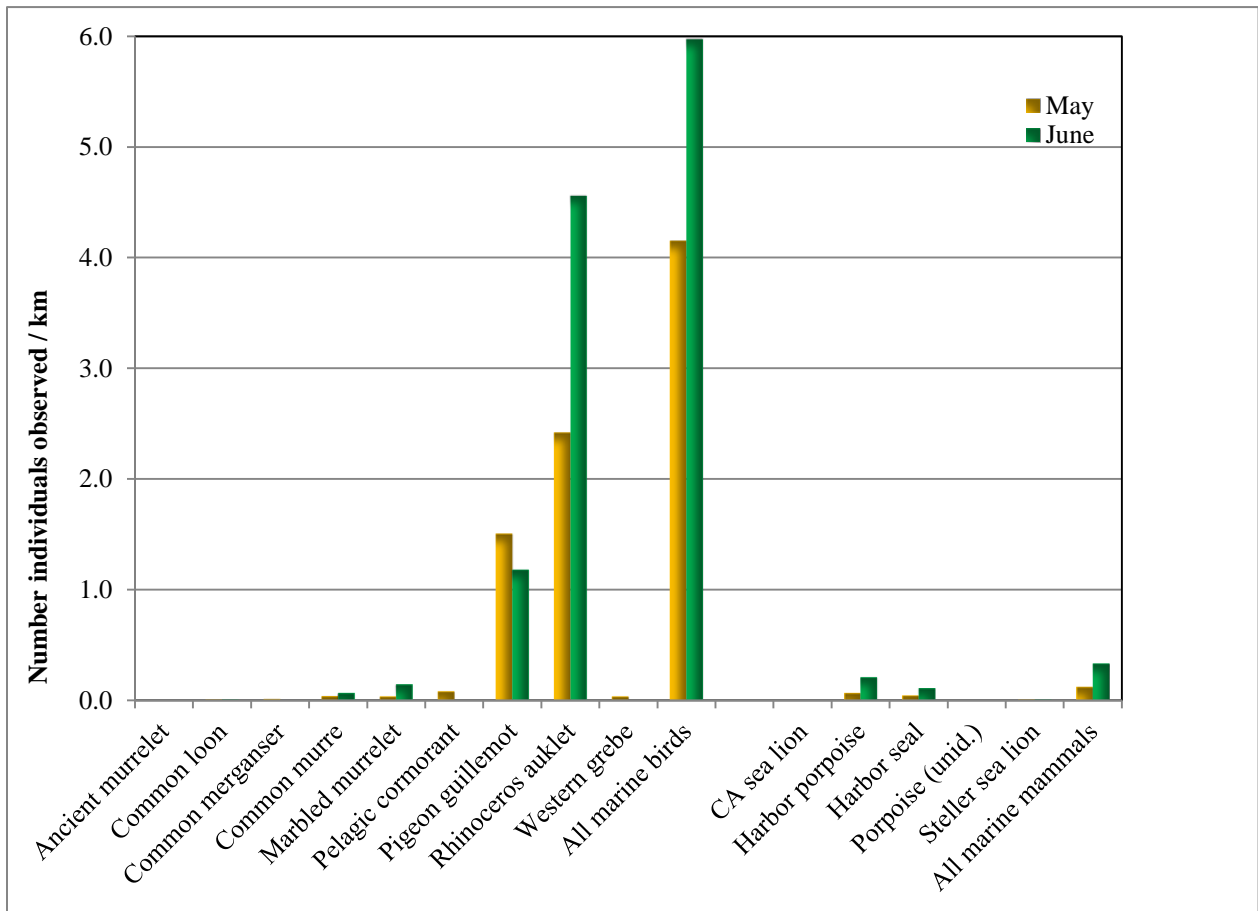


Figure 4. Number of birds (10 species on the left of the plot) and marine mammals (6 species on the right) observed per km during daytime acoustic surveys conducted in May (gold bars) and June (green bars) in the Admiralty Inlet study area, Washington. Data from the north and south survey sections were combined.



The Department of the Interior Mission

As the Nation's principal conservation agency, the Department of the Interior has responsibility for most of our nationally owned public lands and natural resources. This includes fostering sound use of our land and water resources; protecting our fish, wildlife, and biological diversity; preserving the environmental and cultural values of our national parks and historical places; and providing for the enjoyment of life through outdoor recreation. The Department assesses our energy and mineral resources and works to ensure that their development is in the best interests of all our people by encouraging stewardship and citizen participation in their care. The Department also has a major responsibility for American Indian reservation communities and for people who live in island territories under US administration.



The Bureau of Ocean Energy Management

The Bureau of Ocean Energy Management (BOEM) promotes energy independence, environmental protection, and economic development through responsible, science-based management of offshore conventional and renewable energy resources.

The BOEM Environmental Studies Program

The mission of the Environmental Studies Program (ESP) is to provide the information needed to predict, assess, and manage impacts from offshore energy and marine mineral exploration, development, and production activities on human, marine, and coastal environments.